UNIVERSIDAD COMPLUTENSE DE MADRID

FACULTAD DE CIENCIAS QUÍMICAS

Departamento de Bioquímica y Biología Molecular

TESIS DOCTORAL

Biochemical organization of FtsZ in minimal membrane systems and cytomimetic crowded environments

Organización bioquímica de FtsZ en sistemas mínimos de membrana y entornos citomiméticos aglomerados

MEMORIA PARA OPTAR AL GRADO DE DOCTORA

PRESENTADA POR

Marta Sobrinos Sanguino

Directores

Germán Rivas Caballero
Silvia Zorrilla López

Madrid, 2019

UNIVERSIDAD COMPLUTENSE DE MADRID

FACULTAD DE CIENCIAS QUÍMICAS

TESIS DOCTORAL

Organización bioquímica de FtsZ en sistemas mínimos de membrana y entornos citomiméticos aglomerados

Biochemical organization of FtsZ in minimal membrane systems and cytomimetic crowded environments

MEMORIA PARA OPTAR AL GRADO DE DOCTOR

PRESENTADA POR

Marta Sobrinos Sanguino

Bajo la dirección de:

Prof. Germán Rivas Caballero

Dra. Silvia Zorrilla López

Madrid, 2018

ORGANIZACIÓN BIOQUÍMICA DE FtsZ EN SISTEMAS MÍNIMOS DE MEMBRANA Y ENTORNOS CITOMIMÉTICOS AGLOMERADOS

BIOCHEMICAL ORGANIZATION OF FtsZ IN MINIMAL MEMBRANE SYSTEMS AND CYTOMIMETIC CROWDED ENVIRONMENTS

Memoria presentada por
MARTA SOBRINOS SANGUINO
para optar al grado de Doctor en Bioquímica, Biología Molecular y Biomedicina

UNIVERSIDAD COMPLUTENSE DE MADRID
FACULTAD DE CIENCIAS QUÍMICAS

Trabajo realizado en el
Centro de Investigaciones Biológicas
Consejo Superior de Investigaciones Científicas

Bajo la dirección de:
Prof. Germán Rivas Caballero
Dra. Silvia Zorrilla López

CSIC
CONSEJO SUPERIOR DE INVESTIGACIONES CIENTÍFICAS

La presente Tesis Doctoral titulada “Organización bioquímica de FtsZ en sistemas mínimos de membrana y entornos citomiméticos aglomerados” ha sido realizada por Marta Sobrinos Sanguino, bajo la dirección del Prof. Germán Rivas Caballero y la Dra. Silvia Zorrilla López, en el Departamento de Biología Química y Estructural del Centro de Investigaciones Biológicas del Consejo Superior de Investigaciones Científicas (CSIC).

Opta al Grado de Doctor:

Marta Sobrinos Sanguino

VºBº de los directores:

Prof. Germán Rivas Caballero

Dra. Silvia Zorrilla López

VºBº del tutor académico:

Prof. Francisco Gavilanes Franco

A mi familia

Ten siempre en tu mente a Ítaca.
La llegada allí es tu destino.
Mas no apresures tu viaje en absoluto.
Mejor que dure muchos años,
y ya anciano recales en la isla,
rico con cuanto ganaste en el camino,
sin esperar que te de riquezas Ítaca.

Ítaca te dio el bello viaje.
Sin ella no habrías emprendido el camino.
Pero no tiene más que darte.

Y si pobre la encuentras, Ítaca no te engañó.
Así sabio como te hiciste, con tanta experiencia,
comprenderás ya qué significan las Ítacas.

Constantino Cavafis. Extracto del poema *Ítaca.*

AGRADECIMIENTOS

Durante estos años he tenido la enorme suerte de recibir el cariño y guía de personas maravillosas, sin cuyo apoyo, no hubiera logrado llegar al final. Es por ello que me gustaría reservar este espacio para agradecérselo.

En primer lugar, me gustaría agradecer muy sinceramente a Germán Rivas todo el apoyo y consejo que me ha brindado durante estos años. Gracias por la confianza depositada en mí y por descubrirme que puedo conseguir grandes retos si confío en mí misma, que es la mejor lección que me llevo.

A Silvia y Begoña, ambas supervisoras y directoras de esta tesis. Sin duda, esta tesis no hubiera sido posible sin vuestra guía, consejo y paciencia. Gracias por hacerme sentir que formo parte de un equipo. Gran parte de mi crecimiento profesional y personal en los últimos años os lo debo a vosotras, algo por lo que estaré siempre agradecida.

A Mercedes y Carlos, por estar siempre disponibles para brindarme consejos y experiencias, siempre de esa manera tan contagiosamente cercana y optimista.

A Noe y Ana, que han sido un apoyo esencial durante estos años. Jamás tendría espacio aquí para enumerar los momentos tan geniales que hemos pasado como comando. Y aunque esto se acabe… Siempre nos quedará Sia y sus canciones.

Gracias también a Adrián y Míchel, con los que me hubiera encantado compartir muchas más horas de laboratorio. Pero este tiempo ha sido suficiente para saber que ya sois “Increíbles”. Os deseo que seáis tan felices como yo trabajando en el B09, os quedáis en buenísimas manos.

Y gracias también a Marina, Sara, Conchi, Pablo, Elisa, Víctor y a todas las personas que han pasado por el laboratorio y ya no están. Sin duda, todos son grandes científicos, y mejores personas.

A los doctores Allen Minton y Ralf Richter, porque también han sido una parte de esencial de mi aprendizaje durante estos años. At this point, I would like to thank to Dr. Ralf Richter and his groups, in San Sebastián and Leeds that made me feel at home during my stays. I want to thank Dr. Ralf Richter for showing great interest on my work and his wise advice. Especial thanks go to Rickard, Lewis and Fouzia for their kindness and support. Fozi, thank you for being the best housemate, together with Freddie and Amanda. ¡Os espero en Madrid!

No puedo olvidarme de las personas con las que he compartido horas de café (e infusiones). A Luque, Ruth, Alicia, Aída, Mariano, Paco, Juan, Albert, Hugo y todos los que se han unido a nuestra pequeña desconexión matutina. Siempre recordaré las nuestros banquetes a la hora del desayuno y los buenísimos momentos de cada fiesta de la primavera. Sois geniales.

Gracias también al personal de los servicios del CIB, pasando por microscopía confocal, microscopía electrónica, ultracentrifugación analítica, cafetería, conserjería, limpieza, y un interminable etcétera. Todos ellos hacen de un centro como el CIB un lugar especial en el que pasar las horas.

Estoy en deuda también con las personas que, más allá de la ciencia, sabiéndolo o no, me han dado fuerza y apoyo para continuar. Entre ellos están mis amigos de toda la vida, que también forman parte de mi familia: Mario, García, Marina, Nacho, gracias por vuestra amistad sincera, que sin duda es de lo más valioso que tengo.

Gracias a Lidia y Gema, que son auténticas vikingas luchando por lo que quieren. Sin duda lo vais a conseguir. Luis y Rubén, gracias por los buenos momentos… ¡y por todos los grandes viajes que aún estar por venir!

Y gracias, por supuesto, a las personas que el baile ha puesto en mi vida. Gracias por el cariño, por las risas y por cada lunes en el Montes o en el Fresno. Que no se pierdan las buenas costumbres.

Gracias a ti, Jose, por escucharme, aconsejarme y quererme. Por las risas, que es de lo más valioso que tenemos, y por la fuerza para reinventarte cuando ha sido necesario. Eres el mejor compañero de aventuras.

Por último, un agradecimiento muy especial va para mi familia. En especial, me gustaría dedicarte esta tesis a ti, abuelo, porque sé que te hubiera encantando saber que tu nieta al final va a ser “doctora”, entendido a tu manera.

Mención especial merecen mis padres y mi hermano. Por vuestro apoyo incondicional, que es el máximo responsable de que yo haya llegado hasta aquí. Mamá, gracias por el entusiasmo que pones en todo lo que hago, por la música y el baile, que tanto nos unen. Papá, gracias por tu predisposición siempre a ayudar y por cada ratito por la mañana que pasamos juntos. Víctor, tus abrazos y sonrisas me llenan de energía y felicidad. Eres genial y vas a conseguir lo que te propongas. Gracias a los tres por demostrarme que, esté donde esté, no estoy sola. Os quiero y admiro.

TABLE OF CONTENTS

RESUMEN / SUMMARY

RESUMEN

Organización bioquímica de FtsZ en sistemas mínimos de membrana y entornos citomiméticos aglomerados

La división bacteriana es un proceso esencial estrictamente regulado en el tiempo y el espacio. En la mayoría de las bacterias, FtsZ es el principal componente de la maquinaria molecular que efectúa la citocinesis, el divisoma. Esta proteína es una GTPasa homóloga de la tubulina eucariota con capacidad de autoensamblaje que interacciona con otros elementos que contribuyen a su función formando un anillo dinámico en el centro de la célula para constreñir la membrana. Este ciclo de ensamblaje y desensamblaje vinculado a GTP es un proceso clave en la formación del anillo de división. El primer complejo del divisoma es el proto-anillo que, en *E. coli,* está formado por FtsZ y sus proteínas de anclaje a la membrana, ZipA y FtsA, que interaccionan en la membrana citoplasmática formando una estructura esencial para la incorporación del resto de las proteínas de división.

Los sistemas mínimos de membrana, tales como nanodiscos, microesferas recubiertas de lípidos, bicapas lipídicas soportadas, microgotas y vesículas se han utilizado como soportes para reconstituir los elementos del proto-anillo con el fin de analizar sus propiedades funcionales en condiciones controladas. Recientemente, se ha demostrado que la densidad superficial de ZipA es un parámetro clave en el control del ensamblaje y la desestabilización de los polímeros FtsZ que produce polímeros curvos y da como resultado la aparición de patrones dinámicos quirales. También se ha demostrado que el colapso de vesículas que contienen ZipA, inducido por los filamentos dinámicos de FtsZ, sólo ocurre por encima de cierto umbral de densidad de ZipA. Estas transiciones dependientes de la densidad demuestran la importancia de la concentración superficial de los elementos del proto-anillo que se anclan a la membrana en la modulación del comportamiento de los polímeros de FtsZ.

La reconstitución de divisomas funcionales también necesita reproducir fielmente el entorno intracelular aglomerado en el que tiene lugar la división. Se ha descrito que la exclusión de volumen debida a la aglomeración macromolecular tiene un impacto notable en la energética de las reacciones macromoleculares. Por ejemplo, la condensación de FtsZ en estructuras supramoleculares se ve favorecida por la aglomeración macromolecular. Debido a que esta aglomeración puede conducir a fenómenos de separación de fases, el citoplasma puede contener microentornos y/o

compartimentos en los que las proteínas y otros metabolitos se acumulan y realizan funciones especializadas. Por ello, actualmente existe un gran interés en simular la compartimentación celular mediante la encapsulación de sistemas de separación de fases dentro de contenedores lipídicos.

El objetivo general de esta tesis es contribuir a la comprensión de la reactividad bioquímica y la organización de la proteína esencial de la división bacteriana FtsZ, y a estudiar cómo estas propiedades están moduladas por las interacciones moleculares específicas que ocurren en la membrana y por la aglomeración del entorno intracelular.

En los dos primeros capítulos de la tesis se describe la caracterización cuantitativa de la interacción entre FtsZ y ZipA en microesferas recubiertas de lípidos (**Capítulo 1**) y bicapas lipídicas soportadas (**Capítulo 2**). El uso de microesferas recubiertas de lípido permitió la inmovilización de ZipA en la bicapa lipídica y la caracterización de la formación del complejo FtsZ-ZipA en el entorno de la membrana, mediante ensayos de sedimentación diferencial combinados con espectroscopía de fluorescencia. Se observó que el equilibrio de unión de FtsZ-GTP con ZipA era saturable, mientras que la interacción de FtsZ-GDP no lo era. La diferencia entre los dos modos de unión podría atribuirse a la distinta composición de oligómeros de FtsZ-GDP libre y FtsZ-GTP libre formados en solución. Por otro lado, la reconstitución de la interacción ZipA-FtsZ en bicapas soportadas (**Capítulo 2**) y su análisis mediante aproximaciones biofísicas (QCM-D y SE) permitió demostrar que la densidad del receptor modula tanto la unión de FtsZ-GMPCPP a ZipA como la organización de los polímeros en la membrana. Estos estudios también determinaron que la unión de FtsZ-GMPCPP a las bicapas que contienen ZipA ocurre en dos fases que se corresponden con los diferentes modos de extensión del polímero: primero sobre la superficie y después hacia la solución. Tanto las propiedades de unión como la cinética de disociación de la membrana de los polímeros de FtsZ-GMPCPP fueron diferentes a las encontradas para la forma GDP. Los resultados de los **Capítulos 1 y 2** proporcionan información sobre el modo de interacción de los elementos del proto-anillo en sistemas mínimos de membrana y contribuyen a completar la comprensión de los primeros eventos de la división bacteriana.

A continuación, se estudió la influencia de los microcompartimentos sin membrana resultantes de la separación de fases, inducida por la aglomeración macromolecular sobre la organización espacial dinámica de FtsZ utilizando varios

sistemas de separación de fases (**Capítulo 3**). Se observó que FtsZ se acumulaba en una de las fases y/o en la interfaz, dependiendo de la composición del sistema y del estado de oligomerización de dicha proteína. Estos resultados se observaron tanto en sistemas de separación de fases en solución como en microgotas acuosas estabilizadas con lípidos que contenían fases separadas. La visualización de las microgotas reveló que la distribución y disposición estructural de los filamentos de FtsZ están determinadas por la naturaleza del sistema de fases. La redistribución de los filamentos dinámicos tras la despolimerización sugiere que la proteína puede desplazarse entre microentornos en respuesta a cambios en su estado de asociación. La existencia de estos compartimentos dinámicos inducidos por transiciones de fase puede alterar la composición local y la reactividad de FtsZ durante su ciclo de vida, actuando como un factor modulador inespecífico de la función celular. En el **Capítulo 4**, se describe la encapsulación por microfluídica de FtsZ y un sistema de separación de fases dentro de microgotas. Posteriormente, a partir de estas microgotas se prepararon vesículas gigantes permeables (que permiten la captación de ligandos), con mayor rendimiento, homogeneidad y compatibilidad biomolecular que otros métodos disponibles para la producción de este tipo de vesículas.

SUMMARY

Biochemical organization of FtsZ in minimal membrane systems and cytomimetic crowded environments

Bacterial division is an essential process highly regulated in time and space. In most bacteria, FtsZ is the major component of the divisome (molecular machinery effecting cytokinesis) which interacts with additional proteins that contribute to its function forming a dynamic ring at the midcell that is essential to constrict the membrane. FtsZ is a self-assembling GTPase, homolog of eukaryotic tubulin. The GTP-linked assembly and disassembly cycle of GTP is thought to be a key process in the formation of the division ring. The first molecular assembly of the divisome is the proto-ring, which in *E. coli* it is formed by FtsZ and the membrane tethering proteins ZipA, and FtsA. These proto-ring elements assemble at the cytoplasmic membrane forming a structure required for the incorporation of the remaining division proteins.

Minimal membrane systems, such as nanodiscs, lipid-coated microbeads, supported lipid bilayers, droplets and vesicles, have been used as scaffolds to reconstitute the proto-ring elements in order to test their functional properties under controlled conditions. Recently, it has been shown that the surface density of ZipA is a key parameter controlling the assembly and destabilization of FtsZ polymers rendering curved polymers, which results in the emergence of chiral dynamic patterns. Along these lines, it has also been shown that the shrinkage of ZipA-containing vesicles driven by dynamic FtsZ polymers only occurs above a certain threshold ZipA density. These density-dependent transitions highlight the relevance of surface concentration of proto-ring membrane-tethered elements on modulating the behaviour of FtsZ polymers.

Reconstitution of functional divisome assemblies needs also to faithfully reproduce the crowded intracellular environment in which division takes place. Excluded volume effects due to crowding are known to have a considerable impact on the functional energetics of macromolecular reactions. For example, FtsZ assembly into high-order structures is favoured by crowding. Because crowding leads to liquid/liquid phase separation (LLPS), the cytoplasm can contain microenvironments and/or compartments in which proteins and other metabolites accumulate and perform specialized functions. In this line, there is currently a growing interest in mimicking the cellular compartmentalization by encapsulation of phase-separated systems inside lipid containers.

The **general objective** of this thesis is to contribute to the understanding of the biochemical reactivity and organization of the essential bacterial division FtsZ protein, and how these properties are modulated by specific molecular interactions in membranes and by the crowded intracellular environment.

The first two chapters of the thesis describe the quantitative characterization of the interaction between FtsZ and ZipA reconstructed in lipid-coated microbeads (**Chapter 1**) and supported lipid bilayers (**Chapter 2**). Lipid-coated microbeads allowed the immobilization of ZipA in the lipid bilayer and the measurement of FtsZ-ZipA complex formation at the vicinity of the membrane by means of differential sedimentation assays combined with fluorescence spectroscopy. The equilibrium binding of FtsZ-GTP to ZipA was found to be saturable, whereas the interaction of the GDP form of FtsZ was not. The difference between the two modes of binding could be attributed to the difference between the composition of oligomers of free FtsZ-GDP and free FtsZ-GTP formed in solution. On the other hand, the reconstitution of ZipA-FtsZ interaction in supported bilayers (**Chapter 2**) allowed us to demonstrate that the receptor density modulates both the binding of FtsZ-GMPCPP to ZipA and the organization of the polymer film at the membrane, as revealed by biophysical approaches (QCM-D and SE). Our studies have also established that FtsZ-GMPCPP binding to ZipA-containing bilayers occurs in two phases, corresponding to the different modes of polymer extension on the surface or to the bulk solution. Both the equilibrium binding properties and the kinetics of dissociation from the membrane of FtsZ-GMPCPP polymers were different to the ones found for the GDP form of FtsZ. The results of **Chapters 1 and 2** provide insights on the mode of interaction of proto-ring elements in minimal membrane systems and contribute to complete our understanding of the initial events of bacterial division.

Next, the influence of membrane-free microcompartments resulting from crowding-induced liquid/liquid phase separation (LLPS) on the dynamic spatial organization of FtsZ was studied using several LLPS systems (**Chapter 3**). FtsZ was found to accumulate in one of the phases and/or at the interface, depending on the system composition and on the oligomerization state of the protein. These results were observed both in bulk LLPS and in lipid-stabilized, phase-separated aqueous microdroplets. The visualization of the droplets revealed that both the location and structural arrangement of FtsZ filaments is determined by the nature of the LLPS system. Relocation upon depolymerization of the dynamic filaments suggests the protein may shift among microenvironments in response to changes in its association

state. The existence of these dynamic compartments driven by phase transitions can alter the local composition and reactivity of FtsZ during its life cycle acting as a nonspecific modulating factor of cell function. In **Chapter 4**, the encapsulation by microfluidics of FtsZ and a LLPS system inside microdroplets is described. These droplets were then converted into permeable giant vesicles (allowing ligand uptake), with higher yield, homogeneity and biomolecular compatibility than previously described.

ABBREVIATIONS

Abbreviations

Alexa 488/647	Fluorescent dye Alexa Fluor 488 or 647
AFM	Atomic Force Microscopy
BSA	Bovine Serum Albumin
Dextran 500	Dextran with average weight of 500 kDa
Dextran T40	Dextran with average weight of 40 kDa
DGS-NTA	1,2-dioleoyl-sn-glycero-3-[(N-(5-amino-1-carboxypentyl)iminodiacetic acid)succinyl] (nickel salt)
DiIC18	Fluorescent dye (1,1'-dioctadecyl-3,3,3',3'-tetramethylindodicarbocyanine perchlorate)
DMPC	1,2-dimyristoyl-sn-glycero-3-phosphocholine
DMSO	Dimethyl sulfoxide
DNA	Deoxyribonucleic acid
DOPC	1,2-dioleoyl-*sn*-glycero-3-phosphocholine
E. coli	*Escherichia coli*
EcL	Ternary mixture of *E. coli* lipids
EDTA	Ethylenediaminetetraacetic acid
FRAP	Fluorescence Recovery After Photobleaching
FtsA	Filamenting temperature-sensitive mutant A
FtsZ	Filamenting temperature-sensitive mutant Z
FtsZ-GDP	FtsZ bound to GDP nucleotide (guanosine-5’-diphosphate)
FtsZ-GMPCPP	FtsZ bound to GMPCPP nucleotide (guanosine-5'-[(α,β)-methyleno]triphosphate)
FtsZ-GTP	FtsZ bound to GTP nucleotide (guanosine-5’-triphosphate)
FtsZ-mts	Membrane-targeted FtsZ mutant
GMPCPP	Slowly hydrolysable analogue of GTP (guanosine-5'-[(α,β)-methyleno]triphosphate)
GUV	Giant Unilamellar Vesicle
IPTG	Isopropyl-β-D-1-thiogalactopyranoside
LB	Luria-Bertani media

LLPS	Liquid-Liquid Phase Separation
MLV	Multilamellar Vesicle
Nd-ZipA	Nanodisc containing ZipA
NITSE	Non-Ideal Tracer Sedimentation Equilibrium
oriC	Origin of replication in *E. coli*
PDMS	Polydimethylsiloxane polymer
PEG 8	Polyethyleneglycol with average weight of 8 kDa
QCM-D	Quartz-Crystal Microbalance with Dissipation Monitoring
RNA	Ribonucleid acid
rpm	Revolutions Per Minute
RS	GTP Regeneration System
s1ZipA	s1ZipA-His_6. Soluble recombinant fragment of ZipA-His_6, lacking the transmembrane region of the wild type protein.
s2ZipA	s2ZipA-His_6. Soluble recombinant fragment of ZipA-His_6, consisting of the globular domain of the wild type protein.
SD	Standard Deviation
SDS-PAGE	Sodium Dodecyl Sulfate Polyacrylamide Gel Electrophoresis
SE	Spectroscopic Ellipsometry
SLB	Supported Lipid Bilayer
SUV	Small Unilamellar Vesicle
TIRFM	Total Internal Reflection Fluorescence Microscopy
Tris-NTA	Modified lipid with three NTA groups per molecule
ZipA	FtsZ interacting protein A
Z ring	Ring of FtsZ filaments formed at midcell
2D/3D	Two-dimensional/three-dimensional

INTRODUCTION

1. Bacterial division machinery

The cell division machinery in *Escherichia coli* is responsible for the constriction and separation of a mother cell into two daughter cells of nearly identical size. This process, known as cytokinesis, provides the force to split cells and is spatially regulated to faithfully partition the genetic material.

The bacterial cell cycle is traditionally divided into three stages: the period between division and the initiation of chromosome replication, the period required for replication, and the time between the end of replication and completion of division (Figure I.1). In *E. coli*, DNA replication begins at a single origin (*oriC*) on a single circular chromosome. Replication proceeds bidirectionally around the circumference of the chromosome, finishing at a region opposite *oriC*. During replication the chromosome remains in a condensed structure that is known as the nucleoid. Division is initiated near the end of chromosome segregation by the formation of a cytokinetic ring (Z ring) at the nascent division site (Wang and Levin 2009).

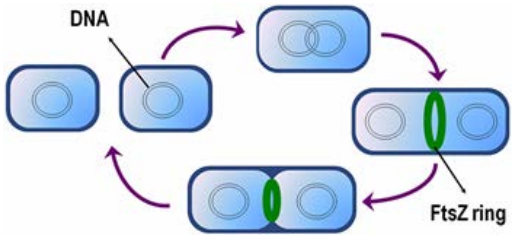

Figure I.1. Scheme of the bacterial cell cycle. The bacterial cells (in blue) are outlined in dark blue and contain schematic chromosomes (ovals). The earliest event in bacterial cytokinesis is the assembly of the essential FtsZ protein into a ring-like structure called the Z ring (in green). The Z ring recruits other accessory proteins to assemble the cell division machinery. Figure from www.warwick.ac.uk.

The recruitment of the division proteins follows a pathway involving both sequential and concerted stages. Biochemically, in *E. coli*, cytokinesis is carried out by a protein complex consisting of at least 15 proteins (cytoplasmic and membrane-bound) that assemble to form the mature division ring. At the beginning, three proteins (FtsZ, ZipA and FtsA) associate giving rise to a multiprotein complex called the proto-ring (Figure I.2), that later on recruits other proteins, constituting the division ring or divisome, anchored to the membrane (Adams and Errington 2009, Haeusser and Margolin 2016, Rico *et al.* 2013). The ring is initially formed at midcell by the polymers of the essential protein FtsZ. The proteins ZipA and FtsA interact with FtsZ, acting as membrane tethers for FtsZ filaments (Lowe and Amos 2017, Pichoff and Lutkenhaus 2002). The

next protein added is FtsK, followed by the FtsQ-FtsB-FtsL complex. Later, the FtsW-FtsI complex, involved in peptidoglycan synthesis, is recruited and finally FtsN, which completes the division ring (Margolin 2006, Vicente and Rico 2006).

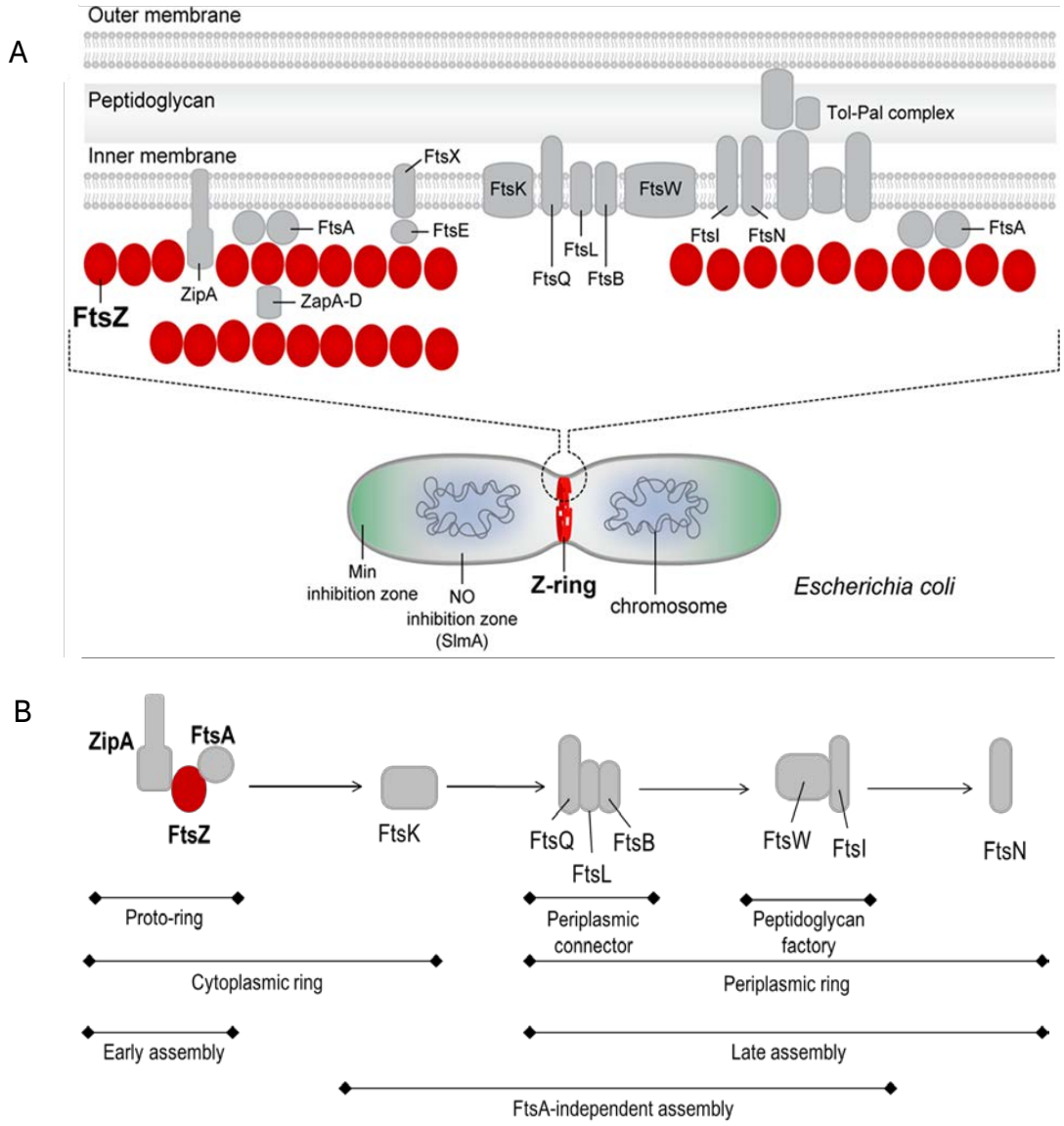

Figure I.2. *E. coli* division machinery. (A)The multiprotein complex assembles at the division site and triggers the constriction of the bacterial membrane. First, the proto-ring (FtsZ, ZipA and FtsA) assembles at midcell. Once the proto-ring is formed, other essential proteins are recruited to form the divisome. The process is spatio-temporally regulated by the Min system and the nucleoid occlusion. Scheme adapted from (Hurley *et al.* 2016). (B) The assembly of all the components occurs following a sequential and concerted pathway. Adapted from Martos *et al.* 2012.

To avoid aberrant division, cytokinesis needs to be precisely controlled, in time and space. In *E.coli* the main regulatory systems include the Min system and nucleoid occlusion (Ortiz *et al.* 2016). The Min system comprises MinC, MinD and MinE proteins that spatially regulate Z ring positioning by inhibiting FtsZ polymerization near the cell poles. FtsZ polymerization at the cell poles would result in the formation of anucleated minicells, emphasizing that the position of the ring dictates the site of cytokinesis (Bi and Lutkenhaus 1991). On the other side, nucleoid occlusion prevents Z ring assembly over the nucleoid through the action of its effector, the DNA-binding protein SlmA (Bernhardt and de Boer 2005). It is only when the two nucleoids segregate to opposite sites of the dividing cell when the midcell position becomes available to assemble a Z ring (Jaffe *et al.* 1990, Ortiz *et al.* 2016, Woldringh *et al.* 1991). It has been recently proposed that, in addition to these two canonical site-selection systems, the Ter-linkage (Mannik and Bailey 2015) participates in Z ring positioning and that, even in the absence of these three mechanisms, Z ring assembly mainly occurs next to midcell, suggesting that additional factors that remain to be determined may contribute to Z ring positioning (Bailey *et al.* 2014).

2. Initial steps of bacterial division in *E. coli*: the proto-ring assembly

FtsZ polymers require at least one membrane-associated factor to tether them to the inner surface of the cytoplasmic membrane. In *E. coli*, this task is achieved through a partnership between FtsA and ZipA, essential proteins for cytokinesis that simultaneously associate with the membrane and bind to the conserved carboxy-terminal tail of FtsZ (Rico *et al.* 2013). The complex formed by these three proteins at the membrane constitutes the proto-ring. The second most conserved division protein among bacterial species, FtsA, associates with the membrane through a C-terminal amphipathic helix (Pichoff and Lutkenhaus 2005), which constitutes an independently functioning membrane-targeting sequence. Conversely, ZipA is unique to the Gammaproteobacteria and contains an amino-terminal transmembrane domain that provides another potentially more permanent membrane tether for FtsZ than FtsA (Hale and de Boer 1997). The Z ring can still assemble when FtsA or ZipA are inactivated because only one of the two tethers is required for ring assembly, but cytokinesis is arrested at the proto-ring stage in these cases (Pichoff and Lutkenhaus 2002). In the absence of both membrane tethers, the Z ring fails to assemble. An FtsA mutant (R286W), called FtsA*, has been recently found to skip the requirement of ZipA in the cell (Geissler *et al.* 2003, Pichoff and Lutkenhaus 2005, Pichoff *et al.* 2012), and

allowing to form an active proto-ring attached to the membrane without ZipA. The equilibrium between the number of molecules of each proto-ring component seems to be crucial for cell division (Pla *et al.* 1991), since either overproduction or depletion of these proteins results in a defective Z ring (Pichoff and Lutkenhaus 2005).

2.1 FtsZ

FtsZ is the central protein in bacterial division (Erickson *et al.* 2010, Haeusser and Margolin 2016, Mingorance *et al.* 2010). It is a cytoplasmic soluble protein of 40.3 kDa, widely distributed in prokaryotic cells (Erickson 1995, Lowe 1998), and the first protein to be localised at the division site that triggers subsequent steps of the process. This tubulin homologue is a GTPase which binds and hydrolyses GTP (Mukherjee *et al.* 1993, Romberg and Levin 2003).

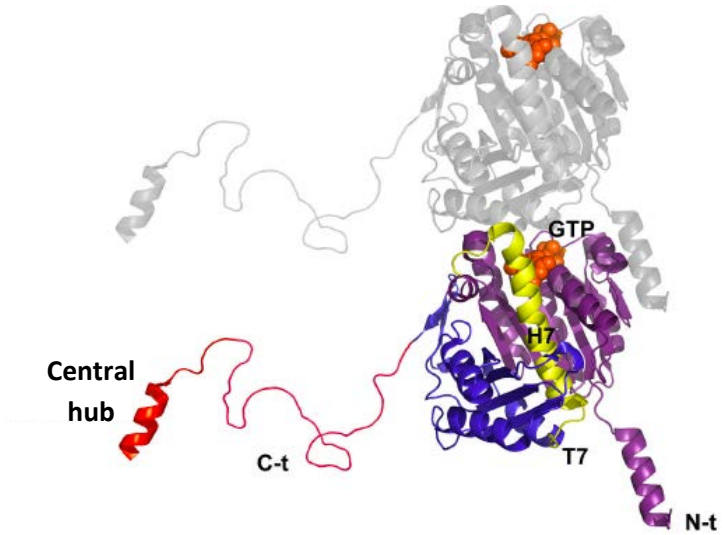

Figure I.3. FtsZ dimer modelled from the *Methanococcus jannaschii* crystal structure. The bottom monomer (adapted from the Protein Data Bank (PDB) entry 1W5A) shows the N-terminal domain (purple) and the carboxy-terminal domain (blue). Domains are connected by the catalytic H7 helix followed by the T7 loop (both in yellow). The C-terminal linker (red) is shown here as a free-drawn unstructured region since it is not fixed in the crystal. The structure of the central hub at the C-terminal end (red) is based on the structure of the interacting region of the *E. coli* FtsZ protein with the globular domain of ZipA (PDB entry 1F47). Image from Ortiz *et al.* 2016.

The 3D crystal structure of FtsZ has been resolved for four microorganisms: *Methanococcus jannaschii* (Figure I.3), *Thermotoga maritime*, *Pseudomonas aeruginosa* and *Mycobacterium tuberculosis* (Cordell *et al.* 2003, Leung *et al.* 2004, Lowe 1998, Oliva *et al.* 2004). According to these data and based on the sequence homology, a theoretical model for the structure of FtsZ from *E. coli* has been proposed.

Only residues 369-383, forming the central hub, correspond to the original *E. coli* structure. This model presents the FtsZ monomer as a globular protein formed by two closely packed domains. In addition, it has an N-terminal extension which contacts with the adjacent subunit in the polymers and a C-terminal extension that is considered as a central hub that integrates signals from a variety of proteins including, among others, FtsA, ZipA, MinC and SlmA (Figure I.4).

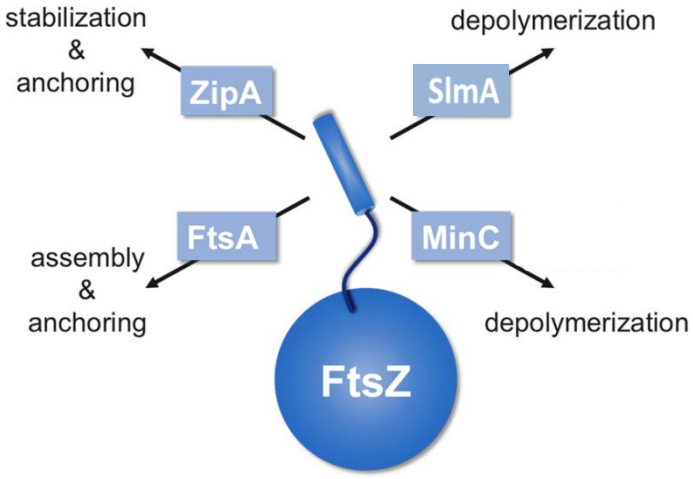

Figure I.4. Scheme of some interactions occurring through FtsZ C-terminal linker and their functional implications. The C-terminus of FtsZ is represented as a cylinder protruding from the globular domain of the protein. Image modified from Pazos *et al.* 2013.

· **Assembly of FtsZ.** The formation of FtsZ protofilaments is coupled to GTP hydrolysis (de Boer *et al.* 1992). FtsZ polymerizes in a cooperative manner to form single stranded protofilaments, whose basic structure is the linear protofilament of only one FtsZ subunit thickness (~5 nm) and between 40-150 subunits in length depending on the solution conditions. FtsZ polymerization occurs above the critical concentration of polymerization in solution (~1 µM (Mukherjee and Lutkenhaus 1998)) and the mode of association of FtsZ consists of a head-to-tail interaction between the subunits forming single-stranded dynamic protofilaments (Scheffers *et al.* 2002) (Figure I.3).

The protofilaments formed by FtsZ are very dynamic and they rapidly disassemble when the GDP:GTP ratio increases as a result of nucleotide hydrolysis. To keep the polymers in solution long enough for their analysis, strategies like the use of GMPCPP, a slowly hydrolysable analogue of GTP (Salvarelli *et al.* 2011) or the addition of an enzymatic GTP regeneration system are employed (González *et al.* 2003, Small and Addinall 2003). The GTP regeneration system allows continuous formation of GTP

from GDP by the addition of acetyl phosphate and, as catalyzer of the reaction, acetate kinase.

Depending upon solution and working conditions (buffer composition, temperature, protein density, surface effects, excluded volume and electrostatic non-specific effects of macromolecular additives, specific effects of other cell division proteins) FtsZ filaments can adopt a variety of supramolecular structures (Figure I.5), including filaments, ribbons, bundles, spirals or toroids (Erickson *et al.* 1996, González *et al.* 2003, González *et al.* 2005, Lowe and Amos 2000, Mingorance *et al.* 2005, Mukherjee and Lutkenhaus 1998, Oliva *et al.* 2003, Popp *et al.* 2009, Yu and Margolin 1997). In the presence of calcium (Yu and Margolin 1997) or crowding agents (Rivas *et al.* 2013), the protofilaments can assemble laterally to form bundles of filaments (see more detailed information in sections below).

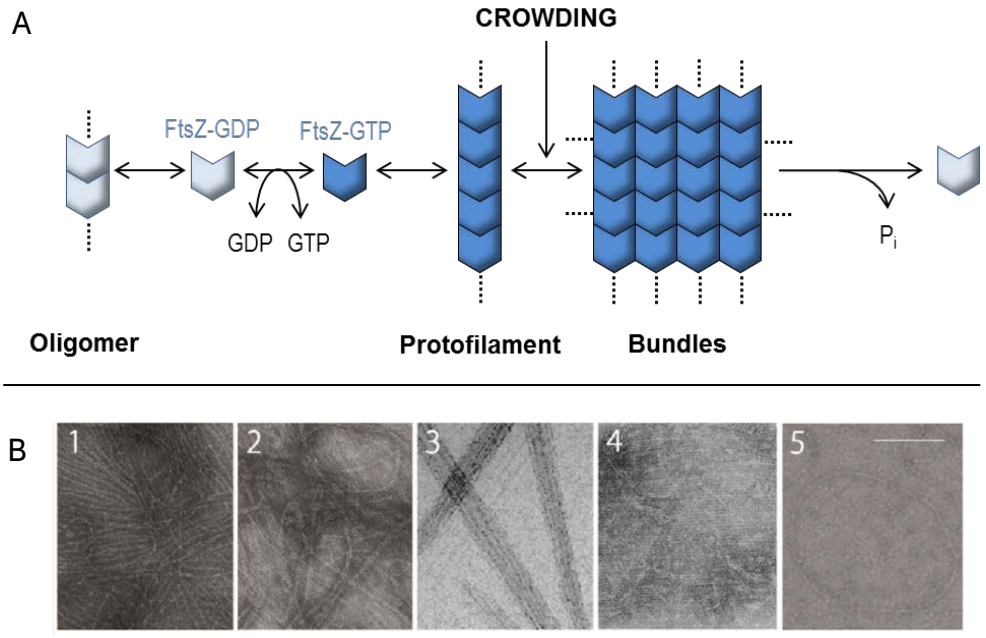

Figure I.5. Self-assembly of FtsZ under different conditions (A) Scheme of FtsZ assembly summarizing the FtsZ assembly reactions taking place in the absence (FtsZ-GDP) and presence of GTP (FtsZ-GTP) and in the presence of crowding agents. (B) The polymerization of FtsZ requires GTP, which allows the formation of filaments with different morphologies, depending on the conditions, such as protofilaments (1), ribbons (2), bundles (3), lamins (4) or toroids (5). Scale bar ~100 nm. Adapted from de Pereda *et al.* 1996, González *et al.* 2003, González *et al.* 2005, Popp *et al.* 2009, Yu and Margolin 1997.

In the absence of GTP, FtsZ oligomerizes following a Mg^{2+}-linked non-cooperative process (Rivas *et al.* 2000). The oligomer formation mechanism is best described as an indefinite self-association, with binding of an additional Mg^{2+} for each FtsZ monomer added to the growing oligomer, and a slight gradual decrease of the affinity of addition of a subunit with increasing oligomer size. The FtsZ oligomer species are compatible with a linear single-stranded arrangement of FtsZ monomers as determined by sedimentation velocity (Rivas *et al.* 2000). This oligomerization can be dismished by the increase of ionic strength and decrease of Mg^{2+} in the solution. Although the affinity for GTP is higher than for GDP, both nucleotides can compete, being this one of the mechanisms proposed as regulator of the polymer assembly (Fu *et al.* 2010).

2.2 ZipA

ZipA is a bitopic membrane-bound protein, essential for division in *E. coli*, although it is not particularly conserved in groups different from gammaproteobacteria. Its main function is anchoring the Z ring to the membrane and, together with FtsZ and FtsA, recruits other proteins for the formation of the divisome. ZipA is a required element for the proper formation of the Z ring (Hale and de Boer 1999). *In vivo*, ZipA is three times less abundant than FtsZ (Rueda *et al.* 2003) and only 30% of ZipA is finally localised at the division site (Stricker *et al.* 2002).

This protein of 36.4 kDa has a highly hydrophobic N-terminal helix of approximately 25 aminoacids that attaches to the inner membrane and an unstructured and flexible P/Q-enriched fragment (160 aminoacids) which includes a charged region (Erickson 2001) (Figure I.6). This fragment connects the transmembrane region with the C-terminal globular domain that interacts specifically with FtsZ (Hale and de Boer 1997, Ohashi *et al.* 2002).

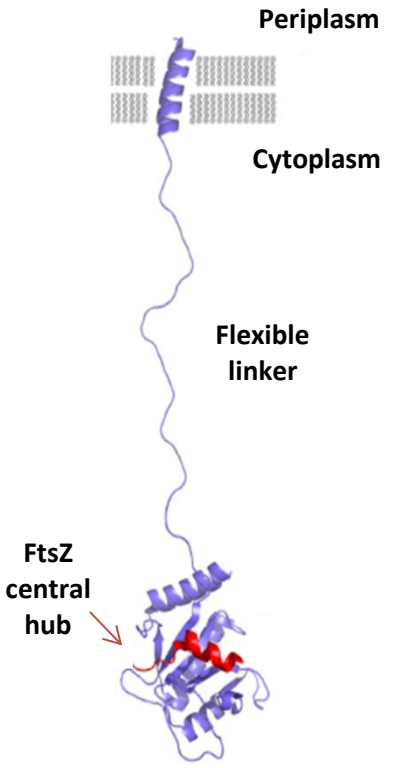

Figure I.6. Tridimensional model of the structure of ZipA from *T. maritima*. ZipA is shown with its C-terminal globular domain (in blue), bound to the FtsZ central hub (red). The flexible linker of ZipA is depicted here as a free-drawn unstructured peptide. The transmembrane segment (blue) is an alpha helix which anchors ZipA to the membrane. Image from Ortiz *et al.* 2016.

The wild type protein is monomeric (López Navajas 2007) and mutants without the transmembrane region behave also as monomers (Martos *et al.* 2010). It has been reported the presence of possible dimers of the protein in cellular extracts, using bidimensional native electrophoresis (Skoog and Daley 2012). The group of Mosyak (Mosyak *et al.* 2000) revealed by crystallography the structure of the complex formed by the C-terminal domain of ZipA and an FtsZ peptide corresponding to its C-terminal region (PDB entry 1F47). The structural data confirmed that the globular C-terminal domain of ZipA interacts directly with FtsZ (Mosyak *et al.* 2000).

3. Studying the proto-ring elements in membrane-like systems

The study of proto-ring interactions is essential, not only to understand the way the bacterial division machinery works, but also because bacterial division, and particularly the interactions of FtsZ, are considered emerging targets for the design of new antibiotics (Den Blaauwen *et al.* 2014). As for many cellular processes, in cell division, the lipid membrane does not only represent a passive physical barrier, but also provides a highly dynamic platform for the interplay between lipids, membrane binding proteins and cytoskeletal elements. Thus, in the initial steps of bacterial division, the Z ring is attached to the membrane through interaction with the other proto-ring elements: ZipA, a membrane-bound protein, and FtsA, an amphitropic protein. Even though many aspects of these interactions are known, their mutual interdependence appears to be highly complex and difficult to study in a living cell. Alternatively, the interactions and assembly properties of FtsZ are currently being studied through topologically restricted reconstructions of the proto-ring structured in biomimetic membrane systems. This type of bottom-up strategy allows the precise control of the biophysical and biochemical parameters involved in biological processes (Loose and Schwille 2009, Martos *et al.* 2012, Vogel and Schwille 2012). Among the main membrane-like systems, we find nanodiscs, lipid coated beads, supported lipid bilayers (SLBs), droplets and giant unilamellar vesicles (GUVs) (Figure I.7).

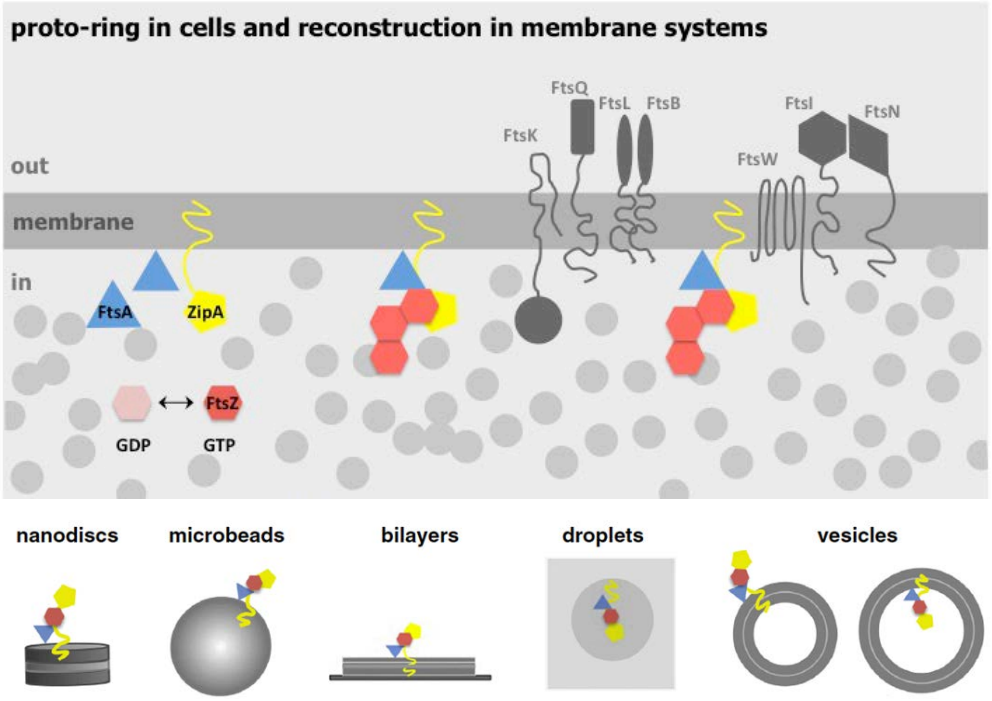

Figure I.7. Scheme illustrating the essential divisome elements in the living cell (upper panel) and reconstruction of proto-ring in biomimetic membrane systems: nanodiscs, lipid coated microbeads, supported lipid bilayers, droplets and vesicles (lower panel). Adapted from Martos *et al.* 2012.

· **Biochemical analysis of proto-ring elements in nanodiscs.** Nanodiscs consist of a ring formed by two copies of a membrane scaffold protein that encircles a phospholipid mixture, which can incorporate membrane proteins preserving their natural properties (Bayburt and Sligar 2010, Nath *et al.* 2007). They behave as soluble structures, allowing the quantitative analysis of the interactions of the proteins inserted with other elements in lipid environments by biochemical and biophysical techniques. Nanodiscs constitute a detergent-free approach for the solubilization of membrane proteins and offer access to both sides of the membrane. However, they are not suitable for the analysis of the effect of surface receptor density on the interactions under study.

Nanodiscs have been used to study ZipA-FtsZ interaction. A single copy of full-length ZipA was integrated in nanodiscs made of *E. coli* lipids as measured by analytical ultracentrifugation (Figure I.8). This finding was confirmed by EM and is compatible with fluorescence correlation spectroscopy measurements of the diffusion coefficient of ZipA-containing nanodiscs (Nd-ZipA), labeled with a trace amount of a fluorescent lipid (Hernández-Rocamora *et al.* 2012, Hernández-Rocamora *et al.* 2012) (Figure I.8).

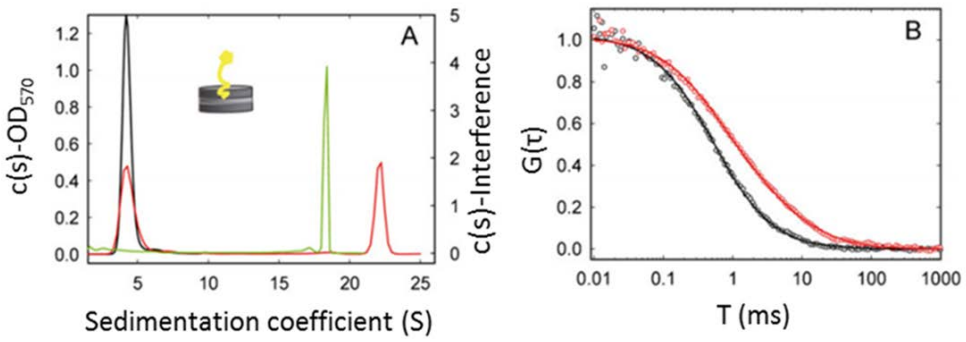

Figure I.8. Reconstruction of proto-ring elements in nanodiscs. (A) Sedimentation coefficient distributions of fluorescently labelled ZipA-containing nanodiscs (Nd-ZipA) in the absence (black) and presence (red) of FtsZ–GMPCPP obtained from absorbance data. Green curve corresponds to the sedimentation coefficient distribution of FtsZ–GMPCPP alone from interference data. Inset: Schematic representation of a nanodisc containing ZipA. (B) Normalized fluorescence correlation spectroscopy autocorrelation profiles of fluorescently labelled Nd-ZipA in the absence (black) and presence (red) of FtsZ– GMPCPP. Adapted from Hernández-Rocamora *et al.* 2012.

These biophysical techniques were used to determine the way that ZipA embedded in nanodiscs interacts with FtsZ in the presence of GDP, GTP, or GMPCPP. They also allowed verification that peptides comprising the FtsZ region of interaction with ZipA compete with FtsZ polymers for Nd-ZipA binding. The strength of the interactions between Nd-ZipA and FtsZ oligomers and polymers was found to be of the same moderate affinity as the binding of FtsZ to a soluble variant of ZipA lacking the transmembrane region (Martos *et al.* 2010), suggesting that neither the transmembrane region of ZipA nor FtsZ polymerization have a significant influence on the binding of FtsZ to ZipA. Moreover, they also support the dynamic nature of the anchoring of FtsZ to the membrane, facilitating the space and time modulation of FtsZ distribution during the cell cycle and its subsequent relocation to midcell when required for the assembly of a division ring.

· **Biochemical analysis of proto-ring elements in lipid-coated microbeads**. Micron-size beads coated with natural membranes or artificial proteolipid bilayers provide a robust system to generate lipid surfaces with uniform curvatures, in which both the lipid composition and the material of the bead can be modified in a controlled manner to obtain the desired properties of the system. It has been described the functionalization of these microbeads by coating them with different lipid composition (Ahmed and Wunder 2009, Gopalakrishnan *et al.* 2009, Lim *et al.* 2006, Linseisen *et al.* 1997, Tsuda *et al.* 2008). Functionalization of microbeads is based on the amphiphilic property of lipids. The spontaneous adsorption of material to the surface allows the

deposition of lipid vesicles on the surface of the microbeads. Phospholipid molecules organize then in a dynamic and fluid membrane (Nollert *et al.* 1995). Lipid coated microbeads can be used in pelleting experiments to identify and quantify lipid-protein and protein-protein interactions. Unlike assays based upon changes in optical properties (Du *et al.* 2015), this assay is a direct and unambiguous measurement of binding. However, their use for transmembrane proteins is limited due to their interaction with the support surface. Several approaches have been devised to circumvent this problem, such as the use of artificial membrane anchors or the use of hydrogels that increase the distance to the solid support.

The binding of FtsA to microbeads coated with inner membranes or phospholipids was quantified usingfluorescently labelled FtsA (Martos *et al.* 2012). The apparent affinity of FtsA binding to the inner membrane showed to be ten-fold higher than to the *E. coli* phospholipids mixture, suggesting that inner membrane proteins could modulate FtsA-membrane interactions.

The interaction between FtsZ and inner membranes (containing the full-length ZipA naturally incorporated) and between FtsZ and a soluble variant of ZipA attached to lipids adsorbed to silver-coated polystyrene microbeads was monitored by surface-enhanced Raman scattering sensing, a surface-sensitive technique based on the enhancement of Raman scattering by molecules adsorbed to metal surfaces (Ahijado-Guzmán *et al.* 2012). This strategy enabled structural changes arising from the binding of FtsZ polymers and oligomers to ZipA attached to the bead to be detected.

· **Structural studies of proto-ring elements on supported lipid bilayers (SLBs).** The formation of SLBs is based on the deposition of a lipid bilayer on a solid planar surface (Kiessling *et al.* 2008, Loose and Schwille 2009). From the different methods to form these bilayers, the one based on the fusion of lipid vesicles is the most commonly used (Brian and McConnell 1984). Vesicles merge with the hydrophilic surface, in the presence of calcium, forming a lipid bilayer separated from the surface by a thin layer of water. The presence of this spacer preserves some essential characteristics of the biological membranes such as fluidity and diffusion of molecules. Thanks to the adsorption on a solid support, changing physical conditions (*e.g.*, buffer) without disrupting the membrane is much easier in SLBs than in free-standing membranes. Additionally, supported membranes are not only accessible to all kinds of optical microscopy, but also to surface-sensitive techniques, such as atomic force microscopy (AFM), total internal reflection fluorescence microscopy (TIRFM), quartz-crystal

microbalance with dissipation monitoring (QCM-D) or spectroscopic ellipsometry (SE), allowing the study of the structural organization and dynamics of proteins and lipids on the membrane (Sezgin and Schwille 2012). Interactions between soluble and membrane-bound proteins can also be measured by acoustic and plasmonic sensing assays (Galush *et al.* 2009, Herrig *et al.* 2006). As mentioned for the lipid coated microbeads, the interaction of transmembrane proteins with the support can be a limitation of the method, but it can be solved with different strategies of protein anchoring.

SLBs have been widely employed for the characterization of the structural organization and interactions between proto-ring elements using biophysical techniques (Martos *et al.* 2015, Ramírez *et al.* 2016, Rivas *et al.* 2014, Vogel and Schwille 2012). FtsZ polymers anchored to lipid bilayers through a soluble variant of ZipA were found to form dynamic bidimensional networks which evolve and reorganize with time by fragmentation, annealing and lateral condensation, as revealed by AFM (Mateos-Gil *et al.* 2012). Co-polymers of wild-type FtsZ and a variant form containing a membrane targeting sequence were found to present an intrinsic curvature as their alignment on microstructured substrates supporting the lipid bilayers, visualized by AFM and TIRFM, depends largely on the curvature of the surface. They preferentially align themselves along curvatures that reproduce the ones found in the inner face of *E. coli* cells (Arumugam *et al.* 2012). Recruitment of FtsZ polymers by FtsA has also been analysed in SLBs, showing that both proteins self-organize into complex patterns, such as fast-moving filaments, bundles and chirally rotating rings (Loose and Mitchison 2014). A recent study has shown that FtsA is in fact dispensable to form dynamic chiral vortices, and that the phenomenon is an intrinsic property of FtsZ alone when supplemented with an artificial membrane anchor (Ramírez *et al.* 2016) (Figure I.9).

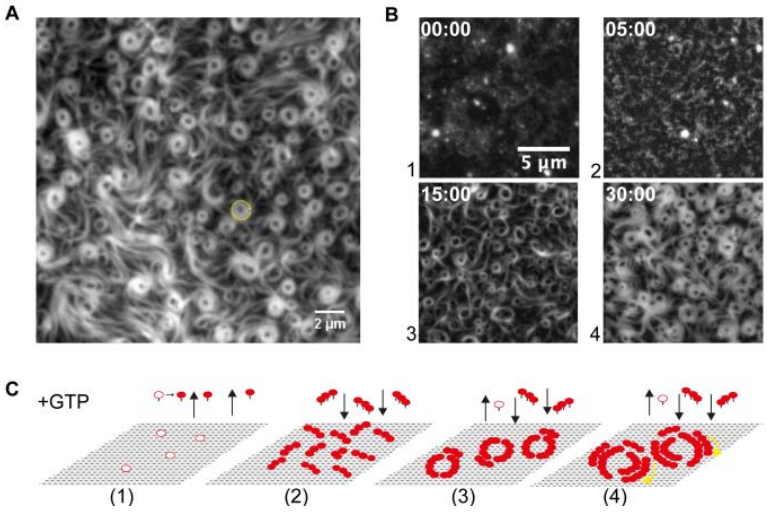

Figure I.9. Formation of dynamic cytoskeletal patterns on SLBs by a membrane-targeted FtsZ mutant in the presence of GTP. (A) FtsZ mutant assembles into circular vortices. (B) Snapshots from a time-lapse experiment displaying different stages of ring formation. (C) Schematic representation of the main events described in (B), occurring on the SLB surface. White spheres correspond to FtsZ mutant in the GDP state. Red spheres correspond to FtsZ mutant in the GTP state. Adapted from Ramírez *et al.* 2016.

· **Proto-ring elements in droplets.** Encapsulation of aqueous samples in droplets dispersed in an oil phase is becoming a powerful method to perform biochemical assays. They serve as model systems mimicking some essential features of the chemical environments in living cells, like confinement, where components can be incorporated to gradually increase levels of complexity. Water-in-oil droplets generated by manual emulsion can be easily made by mixing oil and water, so that one of them forms microscopic droplets dispersed in the other phase (Torre *et al.* 2014). This is a simple method that allows fast screening of conditions to check for biochemical parameters of interest, such as protein distribution within the droplets. Produced in large numbers, droplets generated by bulk emulsion are not uniform in size or composition, but provide valuable qualitative information.

Microfluidic technology has been recently developed, through which hundreds of monodisperse droplets are generated in a continuous oil phase. The composition of each droplet can be controlled at will and, because they are identical in composition and size, each droplet constitutes an individual replicate. These features make them suitable for quantitative analysis. To prevent droplet coalescence, surfactants need to be used and, depending on the composition, they can provide a functional surface for molecules. Droplets generated by microfluidics can be analysed by a wide range of techniques such as fluorescence microscopy, cytometry, Surface Enhanced Raman Scattering or mass spectroscopy.

This technology was applied to probe the polymerization of FtsZ into fibrous networks as a function of the concentration of crowding agent, FtsZ and GTP using for the first time an *E.coli* lipid mixture as surfactant to stabilize the droplets (Mellouli *et al.* 2013). The distribution of FtsZ bundles confined in the droplets depended on specific properties inherent to the system and the geometry of the droplet, conferring specific boundary conditions. The polymerization showed to be fully reversible, since complete disassembly of FtsZ occurred upon GTP depletion. Finally, the rate of FtsZ subunits exchange was determined by Fluorescence Recovery After Photobleaching (FRAP) and rendered a turnover similar to *in vivo* values (Figure I.10) (Stricker *et al.* 2002). In this work, it was shown that microfluidic platforms constitute a very powerful tool amenable to be used to test the properties of FtsZ in the presence of other elements present in the cell potentially influencing its behaviour, which will help to complete the understanding of the functional role of FtsZ in cell division.

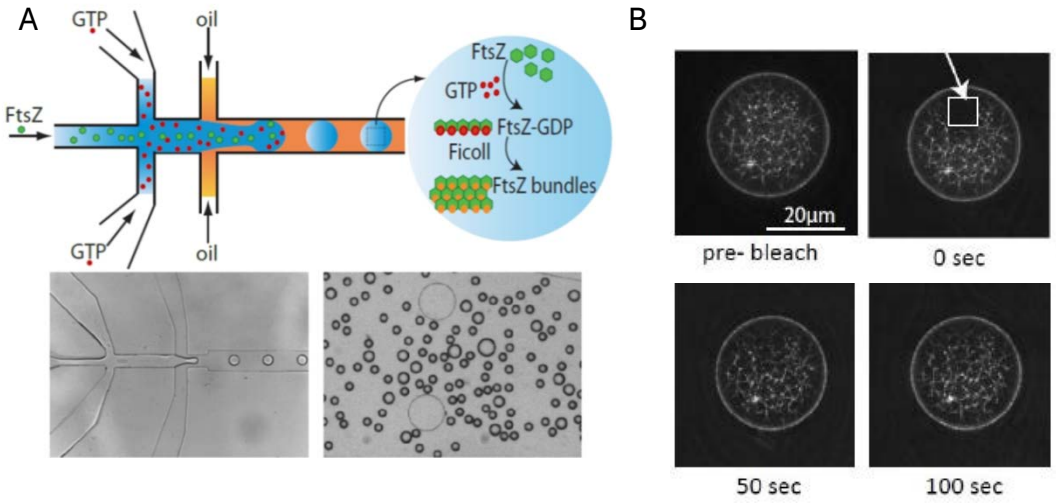

Figure I.10. Encapsulation of dynamic FtsZ bundles in droplets generated by microfluidics. (A) Scheme of the microfluidics chip micropattern and generation of uniform droplets accumulated in the reservoir of the microchip (see Materials and Methods). (B) FRAP on FtsZ bundles inside a microfluidic droplet. Time lapse series of fluorescence images showing the time course of fluorescence recovery. The white arrow shows the bleached region. Adapted from Mellouli *et al.* 2013.

· **Proto-ring elements in giant unilamellar vesicles (GUVs).** One of the most commonly used membrane systems for encapsulation of biomolecules are giant unilamellar vesicles, which are closed lipid bilayers with diameters above the optical resolution limits (~200 nm), from several to hundreds of micrometers. Like the microdroplets, due to their large size, giant vesicles are very suitable for investigating, by imaging and microspectroscopy techniques, the spatial/dynamic organization of proteins trapped in their interior, their interacting properties and the changes in the distribution of membrane components linked to binding events, among others (Sezgin and Schwille 2012, Walde *et al.* 2010). Moreover, permeable vesicles can be formed by the addition of pore-forming molecules, such as α-hemolysin and DMPC, allowing the intake of outer ligands (Cisse *et al.* 2007). Ideally, these applications require simultaneous control of vesicle size, unilamellarity, encapsulation yield, biocompatibility, and lipid composition. Production of GUVs that range in size from 1 to 20 µm was initially accomplished by rehydration or swelling thin lipid films with water or by electroformation; the resultant suspension contains a broad distribution of sizes, and only a few of the vesicles produced are unilamellar. To help overcome some of these limitations, the “droplet-transfer” method was developed (Pautot *et al.* 2003). This method comprises the assembly of two independently formed monolayers of lipids into unilamellar vesicles by forcing water-in-oil droplets to cross a lipid interface and

sediment towards the oil-buffer interface. Upon crossing the interface, the droplets acquire a second layer of lipid, forming a bilayer (Figure I.11).

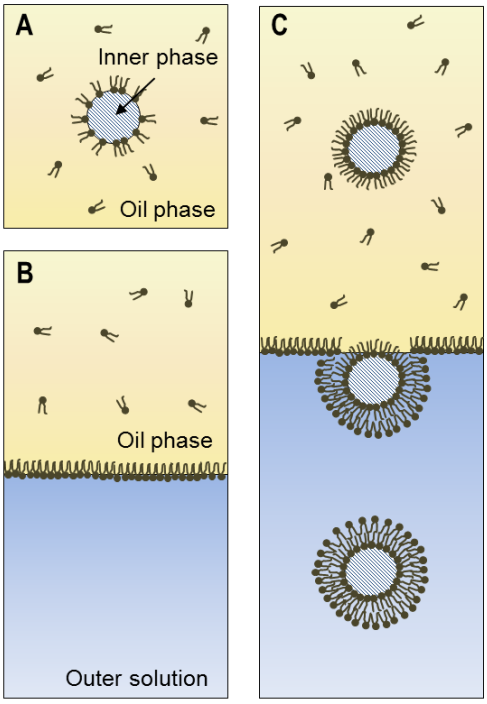

Figure I.11. Schematic illustration of vesicle preparation by droplet-transfer method. (A) Aqueous solution is emulsified in oil with lipid as surfactant, forming a stable inverted emulsion. (B) A lipid monolayer forms at the oil-water interface. (C) Solution A is poured on top of the preparation in panel B. The droplets sediment on top of the second water phase. As they pass through the interface, the bilayer is completed and the vesicles are formed. Adapted from Pautot *et al.* 2003.

Microfluidic techniques for the formation GUVs (fully produced on chips) have emerged in recent years because of the high reproducibility and encapsulation control of this method. For this purpose, new microfluidic patterns have been produced to prepare vesicles containing, so far, one aqueous phase in such a way that water-in-oil droplets formed in a lipid-containing oil flow are transferred across and oil-water interface, facilitating the self-assembly of a phospholipid bilayer (Arriaga *et al.* 2014, Karamdad *et al.* 2015, Matosevic and Paegel 2011).

Several studies to analyze the interactions between proto-ring elements, by using traditional vesicle formation methods, have been reported. The first evidence supporting the role of FtsZ as a contractile element in a lipid vesicle was provided by optical micrographs showing that polymers of an artificially membrane-attached variant of FtsZ (FtsZ-mts) were able to narrow the regions of elongated liposomes in which the FtsZ variant was located (Osawa *et al.* 2008). The incorporation of FtsZ polymers on the external face of the liposomes caused their deformation (Osawa and Erickson 2011), a result also observed in vesicles through the interaction of wild type FtsZ and ZipA in the outer membrane (Jiménez *et al.* 2013). The geometry of the distortion depends upon the FtsZ terminal region at which the membrane targeting sequence is attached, indicating that FtsZ polymer bending (associated to the natural curvature of FtsZ) is an important factor in membrane deformation. Membrane dilation of ZipA-containing vesicles was observed upon FtsZ polymerization mediated by caged-GTP inside the vesicle, suggesting a possible role for FtsZ in the modulation of membrane plasticity (López-Montero *et al.* 2013).

The question of how the surface concentration of ZipA in lipid membranes influences the binding properties of both the GDP and GTP form of FtsZ has also been studied in GUVs. The shrinkage of permeable giant vesicles caused by FtsZ-ZipA binding was found to be critically dependent upon surface receptor density at the membrane (Cabré *et al.* 2013) (Figure I.12).

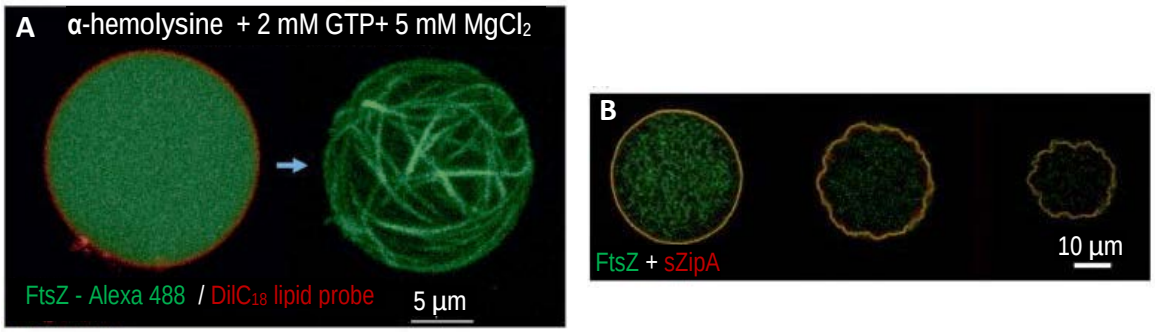

Figure I.12. Encapsulation and polymerization of FtsZ inside permeable vesicles, and vesicle shrinkage and collapse induced by interaction of membrane bound ZipA with FtsZ polymers. (A) Permeable vesicles containing FtsZ labelled with Alexa 488 in the presence of GDP (left) and GTP (right); the membrane layer is stained with the lipid dye $DiIC_{18}$. (B) Permeable vesicle containing a soluble mutant of ZipA (s1ZipA) labelled with Alexa 647 attached to the membrane through DGS-NTA lipids and FtsZ labelled with Alexa 488 in the presence of GMPCPP. Progressive shrinking of permeable vesicles occurs as a result of the interaction of FtsZ polymers with membrane-associated ZipA at elapsed times 0, 5 and 10 minutes. Adapted from Cabré *et al.* 2013.

FtsZ has also been incorporated, together with FtsA, inside electroformed giant vesicles obtained from inner bacterial membrane, which naturally contains ZipA (Jiménez *et al.* 2011). The assembly of FtsZ modified the spatial distribution of the soluble proto-ring elements, resulting in the displacement of FtsA from the membrane, which was to be found associated with FtsZ polymers at the vesicle lumen, as observed by confocal microscopy.

4. The crowded cytoplasm and FtsZ

The assembly and reconstitution of functional bacterial division complexes *in vitro* needs environments in which the natural crowding conditions are carefully reproduced. There are major differences between the intact bacterial cytoplasm and conventional solutions studied in the laboratory: the large difference in total protein concentration and the large difference in the fraction of total volume that lies adjacent to the surface of either a membrane or a fibrous structural element. It is estimated that around 25-

30% of the bacterial cytoplasm volume is occupied by macromolecules (among them *ca.* 200-300 mg/mL protein, *ca.* 100 mg/mL RNA and *ca.* 15 mg/mL DNA, (Vendeville *et al.* 2011)) (Figure I.13), while no single macromolecule needs to be highly concentrated; for example, the estimated average concentration of FtsZ, one of the most abundant cell division proteins, is 0.1-0.4 mg/mL (Lu and Erickson 1998, Rueda *et al.* 2003).

Although much of the chemistry related with bacterial division reactions takes place in environments containing a substantial volume fraction of macromolecules, local composition may vary widely within the bacteria, and macromolecules inside the cell seem to be transiently clustered in functional and structural networks rather than homogeneously distributed. It is expected that the relative contributions of crowding, confinement and adsorption to protein reactivity will be different within each of these microenvironments; however, despite such complexity, it is true that background interactions arising from steric repulsion in volume-occupied cell-like environments will have to be taken into account, independently of the presence or absence of other types of interactions.

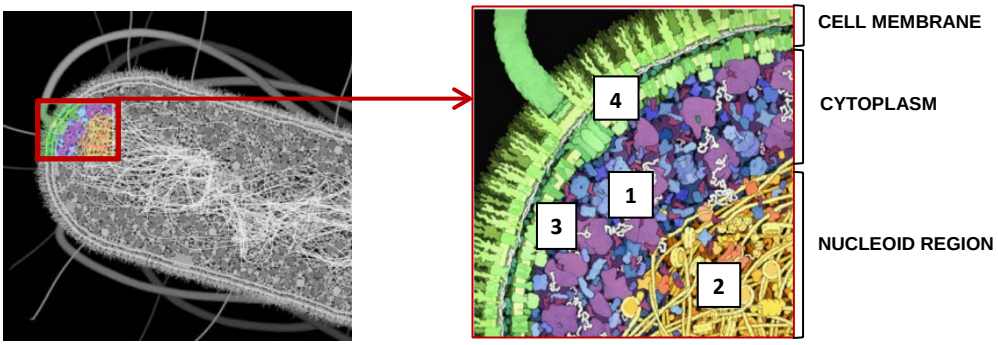

Figure I.13. Cartoons of the crowded cytoplasm of the *E. coli* cell. (1) Cytoplasm consisting of soluble proteins, ribonucleic acids and macromolecular assemblies such as ribosomes. (2) Interior of the nucleoid, with an extremely high local concentration of DNA and DNA-binding and DNA-condensing proteins. (3) Region adjacent to the inner plasma membrane, containing a high concentration of membrane lipids and intrinsic membrane proteins. (4) Periplasm, containing high local concentrations of membrane proteins and interstitial proteoglycans. Cartoons adapted from David S. Goodsell.

4.1 Macromolecular crowding and biochemical reactions

Excluded volume effects due to crowding arise from the mutual impenetrability of macromolecules and are related with the cumulative influence of high concentrations of macromolecules upon the behaviour of one or more diluted molecular species with which the space-filling macromolecules only interact in a nonspecific way (steric repulsion, weak electrostatic or hydrophobic interactions). Individual macromolecular

species in crowded media exhibit both dynamic and equilibrium properties, including chemical reactivity, that may be substantially different from those of the same molecular species in a dilute or un-crowded medium. This has been demonstrated both experimentally and theoretically (Minton 2001, Rivas and Minton 2016). Fractional volume occupancies of the order of those found in the bacterial cytoplasm are expected to increase the chemical potential activity of all macromolecular species in the solution in a size and shape-dependent manner. A fundamental chemical consequence of macromolecular crowding is that provides a generalized nonspecific force to facilitate processes leading to a reduction in excluded volume, namely macromolecular compaction and association (Ellis 2001, Minton 2000, Minton 2001). Additionally, crowding should result in the increase of the rate of slow, transition-state-limited association reactions and the decrease of the rate of fast, diffusion-limited association reactions. Many of these effects have been observed experimentally (Zhou 2008).

It has been shown that larger and less compact macromolecules, such as division protein polymers, are more sensitive to crowding effects than smaller and more compact species. Under certain circumstances, crowding will provide a non-specific force towards various forms of spatial ordering of highly anisotropic macro-solutes and crowding-induced spontaneous alignment and bundling of self-assembled filaments, a phenomenon with particular significance for cytoskeletal organization (Herzfeld 2004). Crowding may facilitate the formation of functional micro-compartments through phase separation phenomena, which may influence the spatial reorganization of functional assemblies and the self-organization of intracellular processes (Hyman and Simons 2012, Walter and Brooks 1995) (see section 5).

4.2 Impact of crowding on FtsZ activities, association and assembly

The addition of unrelated background proteins (bovine serum albumin and hemoglobin) at concentrations as high as 150 g/L was found to enhance the tendency of the GDP-containing form of FtsZ to self-associate forming oligomers, as measured by nonideal tracer sedimentation equilibrium (NITSE) (Rivas *et al.* 2001). The composition-dependence of the buoyant molar mass of FtsZ was quantitatively described by a model in which it is assumed that FtsZ interacts with each protein crowder via steric repulsion. This description of the data is in excellent agreement with the predictions of excluded volume theory, providing evidence that crowding can modulate, in a non-specific manner, FtsZ self-association.

In the case of polymeric FtsZ, the enhancement of the formation of fibrous protein assemblies has been found (and it is expected) to be one of the major effects of crowding on macromolecular reactions. The addition of unrelated background macromolecules (Ficoll and dextran, both with average molar mass around 70000 Da) at concentrations as high as 150 g/L was found to promote the GTP-dependent assembly of FtsZ into dynamic multi-stranded fiber networks, as measured by turbidity and sedimentation assays and observed by electron microscopy (Figure I.14). These polymers seem to adopt a ribbon-like structure as revealed by atomic force microscopy (González *et al.* 2003, González *et al.* 2005). The self-organization of FtsZ polymers induced by crowding was found to retard the GTPase activity of the protein and the dynamics of FtsZ polymers when compared with the measurements obtained using FtsZ single-stranded filaments in the absence of crowding agents. In a separate study, toroidal FtsZ structures were observed in electron micrographs of FtsZ polymerized in the presence of methylcellulose or polyvinyl alcohol (Popp *et al.* 2009). When mixed, crowders also enhance the tendency of the protein to assemble, but the extent of the effect is dependent on the composition of the mixture and, in general, a nonadditive behaviour is observed (Monterroso *et al.* 2016). Nonadditive effects of mixed crowders, reflected as an enhanced or reduced effect regarding the sum of those from the individual crowding agents, may have profound implications for macromolecular function inside cells.

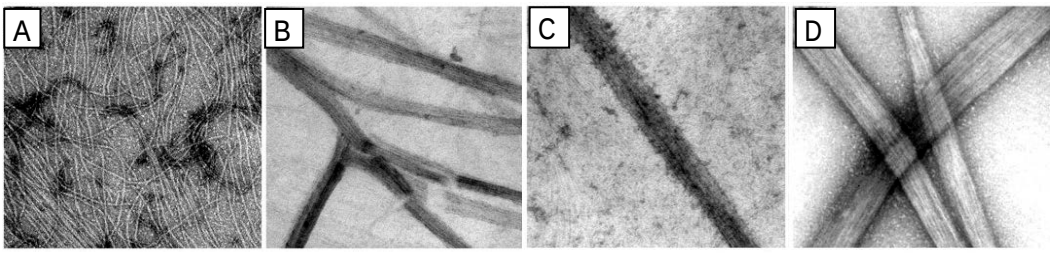

Figure I.14. Electron microscopy analysis of FtsZ assembly in the presence and absence of macromolecular crowders. (A) FtsZ in the presence of GTP (no crowders). (B) FtsZ in the presence of GTP and Ficoll 70. (C) FtsZ in the presence of GTP and dextran T70, (D) FtsZ in the presence of GMPCPP and Ficoll 70. Images taken from González *et al.* 2003.

5. Compartmentalization induced by phase separation of macromolecules

Although compartmentalization is more obvious in eukaryotic cells, which contain membrane surrounded organelles and nucleus, it is now widely recognized that both eukaryotic and prokaryotic cells are divided in subcompartments (Amster-Choder 2011, Brangwynne 2013, Holthuis and Ungermann 2013) thought to be important for many

cellular processes. However, *in vitro* studies of their role in, and impact on, these processes remain scarce, particularly for bacterial microenvironments. The bacterial nucleoid is hypothesized to be a liquid phase condensed by a combination of multivalent cations, such as spermine and spermidine, DNA-binding proteins and other crowding agents (Cunha *et al.* 2001, de Vries 2010, Pelletier *et al.* 2012). It is very similar to a complex coacervate, liquid droplets formed by phase separation of mixtures of macromolecules with opposite charges that retain a large amount of solvent (Koets 1944). Additionally, highly dynamic membraneless organelles formed by assemblies in direct contact with the surroundings have been described (Amster-Choder 2011, Brangwynne 2013, Cheng *et al.* 2008, Holthuis and Ungermann 2013, Lefèvre 2011, Parsons *et al.* 2010, Wirth and Gruebele 2013, Yeates *et al.* 2008). These cellular bodies may be considered liquid droplet phases, suggested to be formed via intracellular phase separation (Brangwynne 2013). The differential partition of molecules in these "liquid organelles" might provide additional levels of control for essential biological processes such as bacterial division, tightly regulated in space and time. In the cytoplasm and nucleoplasm of cells, liquid-liquid phase separation (LLPS) can provide distinct environments with particular physicochemical properties (Amster-Choder 2011, Brangwynne 2013, Holthuis and Ungermann 2013). They originate from the different effects of macromolecules in the two phases on the structure and solvent properties of water (Albertsson 1986), creating distinct environments commonly leading to unequal partition of solutes (small organic molecules, proteins, nucleic acids, RNPs, etc.) which can be enhanced by, but does not generally require, their interactions with phase forming macromolecules (Ferreira *et al.* 2016, Madeira *et al.* 2011, Madeira *et al.* 2008, Zaslavsky, B 1994).

LLPS can be reproduced by the mixture of two crowders with predominantly repulsive interactions which at high concentrations results in LLPS systems with one phase enriched in each of the crowders. Figure I.15A illustrates the phase diagram for a solution of two crowders in water. At low concentrations of crowder, the solution exists as a single phase, and at high concentrations phase separation occurs (Keating 2012). A coexistence curve separates these two regions of the diagram (Albertsson 1986, Keating 2012). The presence of distinct liquid phases means that molecular solutes may partition between the two phases or between one of the phases and the aqueous/aqueous interface (Walter and Brooks 1995, Zaslavsky, B 1994) (Figures I.15B and I.15C). Partitioning is quantified in terms of the partition coefficient, *K*, which equals the concentration of solute in the top phase divided by its concentration in the bottom phase. Whether a given solute partitions strongly into one of the aqueous

phases or is more uniformly distributed depends on the properties of the LLPS system (*e.g.*, crowder structure, crowder molecular weight, and concentration) as well as the chemistry of the solute itself (Walter and Brooks 1995, Zaslavsky, BY *et al.* 1978).

LLPS systems have been less studied in bacterial cells, which due to their smaller size are difficult to image at high resolution. Recent work by Huck and coworkers demonstrated an advantage to LLPS in bacterial cell lysate, where transcription rates increased upon phase separation in lysate droplets (Sokolova *et al.* 2013). Experimental assays using LLPS systems to mimic cellular microenvironments have shown that the selective accumulation of molecules in one of the phases may deeply influence the location and rates of enzymatic reactions (Cacace *et al.* 2015, Dominak *et al.* 2010, Koga *et al.* 2011, Strulson *et al.* 2012). Larger structures such as lipid vesicles and protein aggregates can collect at the aqueous/aqueous interface, and this interfacial assembly can stabilize droplets against coalescence (Balakrishnan *et al.* 2012, Dewey *et al.* 2014, Nguyen *et al.* 2013). The interface can further serve as a reservoir for excess lipid membrane: Dimova and coworkers demonstrated that lipid nanotubes pulled from giant liposome membranes were stored at the interface and incorporated back into the bilayer under liposome expansion (Li *et al.* 2011). Phase separation and membrane accumulation at the aqueous/aqueous phase boundary can also facilitate the separation of LLPS-containing liposomes into distinct daughter vesicles (Andes-Koback and Keating 2011). Bacterial division interactions have never been, so far, analysed in LLPS systems.

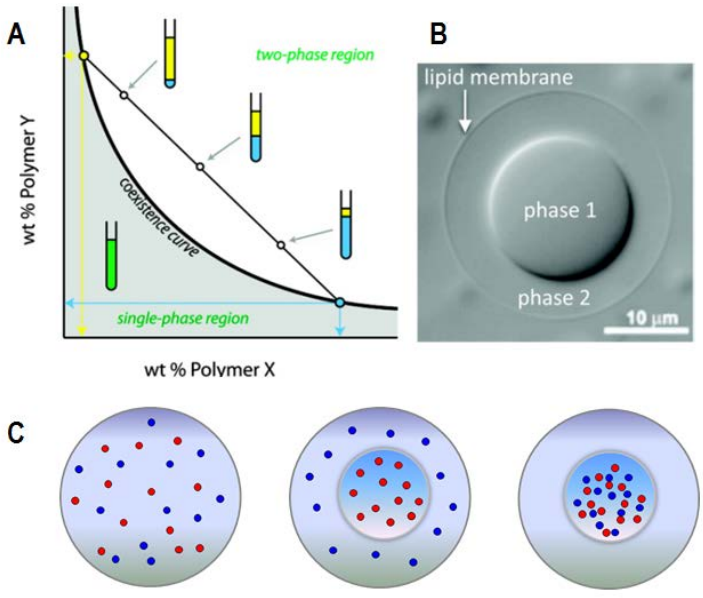

Figure I.15. Phase separation diagram and impact on protein-protein interactions. (A) Generic phase diagram for an aqueous solution of two polymers. (B) Compartmentalization induced by phase separation inside a lipid vesicle. (C) The interaction of molecules is dependent on the preferential distribution of each element, increasing the probability of interaction when both are confined to the same phase and decreasing when each molecule distributes in a different phase. Red and blue dots represent two different interacting proteins. Images (A) and (B) were taken from Keating 2012.

5.1. Encapsulation of systems exhibiting phase separation

LLPS systems have been recently encapsulated within lipids to form compartmentalized primitive artificial cells that mimic some aspects of intracellular organization, such as microcompartments which perform specialized functions (Holthuis and Ungermann 2013). Apart from limiting the encapsulated volume, the lipid membrane provides a semipermeable, flexible boundary around the crowder solution. This type of work has focused on PEG/dextran systems since it is a well-known biphasic system (Li *et al.* 2011, Long *et al.* 2005).

One of the strategies for the encapsulation of LLPS systems involves passive encapsulation of the two composing crowders during vesicle formation by gentle hydration in conditions under which they do not phase separate and subsequent induction of their segregation by shifting experimental conditions (Long *et al.* 2008). Water can pass the membrane but the crowders cannot, hence the inner volume and crowder concentrations can be controlled by changes in osmolarity. This procedure leads to a distribution of different crowder concentrations and, hence, different compositions and relative volumes of phases within a population (Dominak *et al.* 2010, Long *et al.* 2005) generating substantial vesicle-to-vesicle variability in protein localization (Dominak *et al.* 2010, Long *et al.* 2008). Encapsulation of LLPS systems in water-in-oil droplets stabilized by non-lipidic surfactants has been described (Torre *et al.* 2014), which presents advantages such as the high yield of droplets containing the LLPS system without the need to alter the conditions after encapsulation to induce phase separation. Microfluidics methods have been recently used for the generation of compartmentalized structures as droplets, including two-droplet multisomes (Elani *et al.* 2016), nested liposomes (Deng *et al.* 2017) and for surfactant stabilized single-phase droplets where separation was subsequently induced (Yuan 2017). Despite these advances, the controlled encapsulation of LLPS systems within model membranes remains challenging and there is a need for new procedures to improve the yield and uniformity of the containers in terms of size and composition under mild conditions compatible with biomolecules.

AIMS

This thesis aims to contribute to the understanding of the biochemical reactivity and organization of the essential bacterial division FtsZ protein, and how these properties are modulated by specific molecular interactions in membranes and by the crowded intracellular environment.

In chapters 1 and 2, we first analyze the association and assembly properties of FtsZ in the presence of ZipA contained in supported lipid bilayers. This is a minimal reconstruction of the proto-ring, the first molecular assembly of the divisome. Previous work from our laboratory has shown that dynamic interactions between FtsZ and ZipA when assembled in permeable giant vesicles caused vesicle shrinkage. This observation, that partially reproduces functional constriction forces, was found to be critically dependent upon ZipA concentration at the membrane, suggesting that ZipA surface density is a modulator of the biochemical properties of FtsZ.

1. **Quantitative characterization of FtsZ binding to ZipA-containing lipid coated microbeads**. Microbeads are used to immobilize a His-tagged soluble variant of ZipA at controlled surface densities. The impact of ZipA density on the interactions with the GDP and GTP forms of FtsZ are analysed and discussed. Differencial centrifugation and fluorescence spectroscopy are employed to quantify the amount of FtsZ bound to its receptor.

2. **Biophysical study of the structural organization and dynamics of proto-ring elements at the membrane using surface-sensitive techniques**, such as Quartz Crystal Microbalance with Dissipation monitoring (QCM-D) and Spectroscopic Ellipsometry (SE). These techniques provide *in situ* experimental data on FtsZ binding to controlled amounts of a soluble variant of ZipA immobilized on the lipid bilayer.

In chapters 3 and 4 we study the behaviour of FtsZ in crowded cell-like environments. Crowding is likely to affect the organisation of FtsZ-ring components into active divisomes as the high abundance of macromolecules inside the bacteria causes volume exclusion effects, both in solution and in membranes, altering the effective concentration and reactivity of proteins and thus modulating the extent and rate of protein-protein and protein-membrane interactions. Crowding can lead to phase separation phenomena and it may also modify the spatial organization and distribution of macromolecular networks, thus acting as a natural modulator of the functional organization of the intracellular space.

3. Analysis of the distribution of FtsZ in the presence of coexisting liquid phases to mimic intracellular compartmentalization, for a better understanding of how microenvironments might influence the location of FtsZ as a function of its polymerization state. Analysis of the potential functional implications of the preferential distribution of FtsZ polymers in microcompartments formed by phase transitions in cell-like containers.

4. Development of a microfluidics-based method for the direct encapsulation of LLPS systems. Inclusion of FtsZ inside droplets stabilized by a lipid monolayer and conversion into permeable GUVs. Induction of FtsZ polymerization by the diffusion of GTP into the vesicles.

MATERIALS AND METHODS

MATERIALS

E. coli polar lipid extract (EcL; containing 67% phosphatidylethanolamine, 23% phosphatidylglycerol, 10% cardiolipin), 1,2-dioleoyl-sn-glycero-3-phosphocholine (DOPC), 1,2-dioleoyl-sn-glycero-3-[(N-(5-amino-1-carboxypentyl) iminodiacetic acid) succinyl] nickel salt (DGS-NTA), lissamine-rhodamine B labelled PE (1,2-dioleoyl-sn-glycero-3-phosphoethanolamine-N-(lissamine rhodamine B sulfonyl)) and 2,2-dimyristoyl-sn-glycero-3-phosphocholine (DMPC) were from Avanti Polar Lipids, Inc. (USA), and they were kept as 10-20 g/l stocks in chloroform at -20ºC. Tris-nitriloacetic acid (tris-NTA), a lipid analogue of DGS-NTA, with chelator headgroups comprising three nitriloacetic acid moieties, was synthetized and kindly provided by Changjiang You and Jacob Piehler (Osnabrück University, Germany) and stored in chloroform at -20ºC. Alexa Fluor 488 and 647 succinimidyl ester dyes, FITC labelled dextran 500 (dextran 500-FITC) and silicone isolators for microscopy were from Molecular Probes/Invitrogen (USA). Analytical grade chemicals, acetate kinase, acetyl phosphate, GTP, Dextran 500, Dextran T40, PEG 8 and BSA were from Sigma (USA). Ficoll 70 was from GE Healthcare. The GTP analogue GMPCPP was purchased from Jena Bioscience (Germany). Ionic exchange, affinity and size exclusion chromatography columns for protein purification were from GE Healthcare (USA). DNA from salmon sperm was from Wako Pure Chemical Industries (Japan). Polydimethyl siloxane (PDMS) was from Corning GmbH (Germany). Aquapel was from Pittsburgh Glass Works (USA). Mineral oil was from Sigma and fine bore polythene tubing was from Portex (USA). Silica microbeads (nominal diameter ~5 μm) were from Bangs Laboratories, Inc. (USA). Silica QCM-D sensors (QSX303) were from Q-Sense (Biolin Scientific, Sweden) and silicon wafers for ellipsometry measurements were purchased from University Wafers (USA). Silicon masters with microfluidics chip designs were kindly provided by Dr. A. Piruska and Prof. Wilhelm T. S. Huck (Radboud University Nijmegen, The Netherlands).

METHODS

1. Expression and purification of FtsZ

FtsZ was purified following the method described in Rivas *et al.* (Rivas *et al.* 2000), based on the ability of the protein to form polymers in the presence of GTP and calcium.

Expression was induced using BL21 cells transformed with plasmid pMFV56, by adding 1 mM IPTG and incubating at 37 ºC for 3 hours. Cells were harvested by 10 minutes centrifugation at 10000 × *g* and 4 ºC and stored at -80 ºC for subsequent purification. The pellet was resuspended in 50 mM PIPES, 5 mM $MgCl_2$, 1 mM EDTA, pH 6.5 and, after lysis by sonication, the soluble fraction containing FtsZ was separated by centrifugation (100000 × *g*, 2 hours at 4 ºC). The supernate was subjected to two successive calcium-induced precipitation cycles by adding 1 mM GTP and 20 mM $CaCl_2$ and incubating for 15 minutes at 30 ºC. FtsZ polymers were pelleted (9000 × *g*, 15 minutes at 4 ºC) and disassembled by resuspension in buffer without calcium for its later purification by ionic exchange chromatography using a Hi-TRAP Q-Sepharose column. This column was equilibrated in 50 mM Tris-HCl, 5 mM $MgCl_2$, 0.1 mM EDTA, 10% glycerol, pH 8. FtsZ was eluted with a KCl gradient (0-1 M). Purity was checked by SDS-PAGE and concentration was determined by absorbance (ε_{280nm}=14000 M^{-1} cm^{-1} (Rivas *et al.* 2000)). Protein was stored at -80 ºC.

2. Expression and purification of ZipA soluble mutants

Overexpression of His-tagged soluble mutants of ZipA (Figure M.1), $ZipA_{25-328}$ (s1ZipA, without the transmembrane region of ZipA) and $ZipA_{188-328}$ (s2ZipA, C-terminal domain of ZipA), was performed following the protocol described in Martos *et al* (Martos *et al.* 2010). Cells were grown in LB media (Luria-Bertani) supplemented with ampicillin and expression was induced with 1 mM IPTG incubating at 37 ºC for 3 hours. The pellet was resuspended in 20 mM Tris-HCl, 500 mM NaCl, 5 mM Imidazole, pH 8, cells were lysed by sonication and the soluble fraction containing the protein mutants was separated by centrifugation (10000 × *g*, at 4 ºC for 15 minutes). This supernate was purified by affinity chromatography in a Ni-NTA affinity column. Purity was checked by SDS-PAGE and concentration was determined by absorbance (s1ZipA, ε_{280nm}=10430 M^{-1} cm^{-1}; s2ZipA, ε_{280nm}=4470 M^{-1} cm^{-1}). Proteins were stored at -80 ºC.

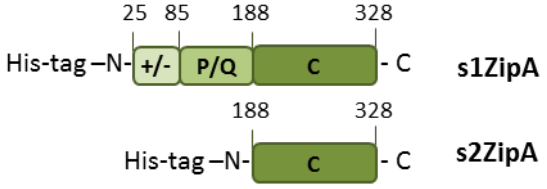

Figure M.1. Scheme of the structure of the soluble mutants of ZipA; +/−, charged domain signifying a basic region that precedes the acidic motif; P/Q, proline/glutamine rich domain; C, C-terminal domain.

3. Fluorescent labelling of FtsZ and PEG 8

Covalent labelling of FtsZ in the amino groups with Alexa 488 or Alexa 647 Fluor carboxylic acid succinimidyl ester dyes was performed as described in (González *et al.* 2003, Reija *et al.* 2011). The protein, previously dialyzed in 20 mM HEPES, 1 mM EDTA, 50 mM KCl, 5 mM $MgCl_2$, pH 8, was incubated together with the dye dissolved in dimethyl sulfoxide (DMSO) for 15 minutes at 30 ºC after polymerization induction, by adding 2 mM GTP and 20 mM $CaCl_2$, to minimize any possible interference of the dye with FtsZ assembly. Labelled polymers were harvested by centrifugation (19000 × *g*, 15 minutes at 4 ºC) and resuspended in 50 mM Tris-HCl, 500 mM KCl, 5 mM $MgCl_2$, pH 7.5. After elimination of irreversible aggregates by centrifugation (19000 × *g*, 15 minutes at 4 ºC), the sample was loaded onto a Hi-TRAP column to remove the remaining free dye by size exclusion chromatography. The labelling ratio was determined by absorbance using absorption coefficients of the dye (ε_{280nm} Alexa 488 = 71000 M^{-1} cm^{-1}; ε_{280nm} Alexa 647 = 239000 M^{-1} cm^{-1}) and the FtsZ protein (ε_{280nm}=14000 M^{-1} cm^{-1} (Rivas *et al.* 2000)), being generally 0.5-0.7 moles of dye per mole of protein. Labelled FtsZ was stored at -80 ºC.

Labelling of PEG 8 with Alexa 488 or Alexa 647 was conducted by covalently linking them to an amino derivative of the polymer (NH_2-PEG-NH_2). The labelling buffer was 50 mM sodium borate at pH 8.5. PEG was incubated with the dye for 4 hours at room temperature and the excess of dye was removed by loading the solution onto a Hi-TRAP column. The concentration of dye after labelling was estimated from its molar absorption coefficient.

4. ZipA-FtsZ binding assays in lipid-coated microbeads

4.1 Microbead washing and coating

Before coating, a homogeneous solution of microbeads was washed by centrifugation (9700 × *g* at 4 ºC) and successive resuspensions in a water:ethanol solution (7:3 v/v) and, in the last step, with a 1% ethanol solution (spectroscopic grade). After supernate separation, residual aqueous solution was evaporated by vacuum centrifugation and dried microbeads were resuspended in 50 mM Tris-HCl, 100 mM KCl, 5 mM $MgCl_2$, pH 7.5. A polar extract of *E. coli* lipids (EcL) and DGS-NTA were employed for microbead coating. Both lipid solutions, dissolved in chloroform, were mixed at different DGS-NTA molar percentages: 10%, 5%, 2%, and 0.5%, dried under nitrogen stream and kept under vacuum for at least one hour. Multilamellar vesicles

(MLVs) were formed by rehydration of the dried lipid film in 50 mM Tris-HCl, 100 mM KCl, pH 7.5 and incubating the solution for 1 hour at 37 ºC. Microbeads were incubated together with the lipid mixture at 4 ºC and gentle shaking (Figure M.2). The amount of lipid was an excess of 5 times with respect to that required to coat the beads (see below). Tubes were then centrifuged at 4 °C, supernatant removed and excess of lipids eliminated by three repeated cycles of washing and pelleting, with a buffer volume at least two times the initial volume of sample and centrifugation at 10000 × *g*. After sonication in a cold water bath for 30 seconds to get even coating of the microbeads, three extra washing cycles were conducted. Resuspension of the microbeads was done in 50 mM Tris-HCl, 100 mM KCl, 5 mM $MgCl_2$, pH 7.5.

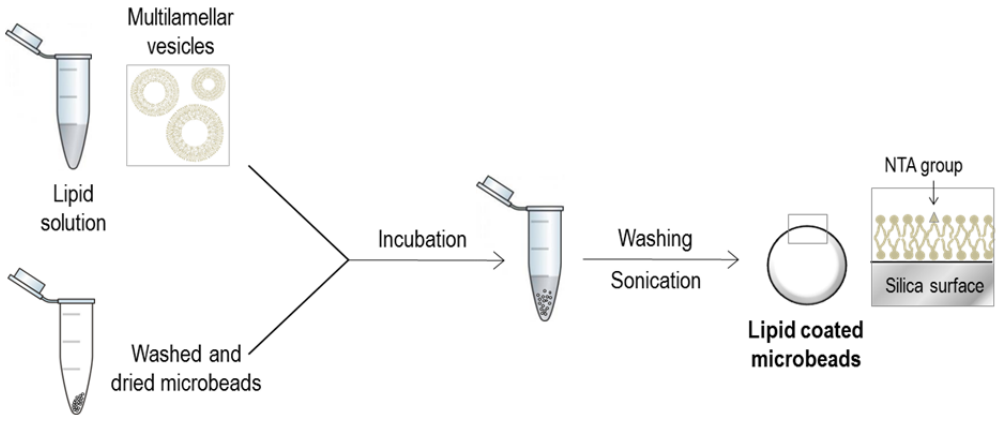

Figure M.2. Scheme of the procedure followed for lipid coating of microbeads.

4.2 Calculation of lipid content per bead

The amount of lipid coating the microbeads was estimated, assuming a single bilayer, from the surface area of a gram of beads and the surface of the polar head of a lipid molecule (taking the value reported for phosphatidylcholine in a bilayer (Hauser 2000), 0.65 nm^2). DGS-NTA amount was then calculated assuming it mixed homogeneously with the EcL ternary mixture and that the percentage, hence, was maintained in the lipid bilayer.

4.3 Assay of protein binding to coated beads

Binding experiments were conducted using microbeads coated with the mixture of DGS-NTA:EcL, at the specified ratios. The coated beads were incubated for 10 minutes at room temperature with a concentration of s2ZipA between 20-80 μM

depending on the beads concentration, ensuring saturation of all NTA groups. Supernatant with s2ZipA excess was then removed by 5 minutes centrifugation at 13000 × *g* (Figure M.3). The affinity of the interaction of s2ZipA with DGS-NTA was submicromolar under our experimental conditions as verified by independent titrations of the labelled protein with variable bead concentration. The lipid coated microbeads with bound s2ZipA were then incubated for 10 minutes with 0.5 µM FtsZ labelled with Alexa 488 dye (FtsZ-Alexa 488) supplemented with unlabelled FtsZ to reach the final concentrations. The samples were then centrifuged during 5 minutes at 13000 × *g* to separate the FtsZ bound to the lipid coated microbeads with s2ZipA from the unbound protein (Figure M.3), which was quantified using a fluorescence plate reader (Varioskan Flash, Thermo) with 495 and 520 nm as excitation and emission wavelengths, respectively. When required, GTP was added to FtsZ before incubation with the beads to a final 1 mM concentration and polymers were kept in solution using a GTP regeneration system (RS; 15 mM acetyl phosphate, 2 u/mL acetate kinase). Assays were performed by triplicate. Independent measurements of samples collected at different incubation times revealed the system was equilibrated within 10 minutes, time after which binding isotherms were equal within error. The linearity of the signal of the labelled protein with its concentration was verified.

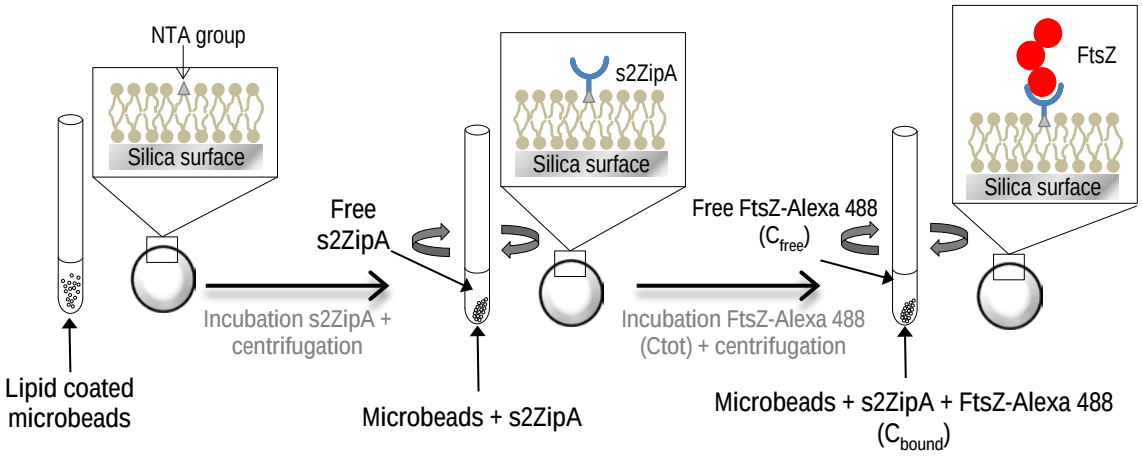

Figure M.3. Scheme of the procedure followed for FtsZ binding assays to s2ZipA immobilized in microbeads. C_{tot}, C_{free} and C_{bound} respectively denote the total concentration of FtsZ, the free concentration of FtsZ in the supernatant and the concentration of FtsZ that is specifically bound to immobilized s2ZipA.

4.4 Estimation of the fraction of bead surface available for nonspecific adsorption in the presence of a given concentration of immobilized ZipA

We take $6.5 \cdot 10^{-15}$ cm^2 as the surface area of bead occupied by a molecule of lipid (Hauser 2000). Since the surface area of a bead is $7.8 \cdot 10^{-7}$ cm^2, there are $7.8 \cdot 10^{-7}$ /$6.5 \cdot 10^{-15}$ = $1.2 \cdot 10^{8}$ lipids/bead. Beads have been prepared containing NTA-derivatized lipids amounting to 0.5%, 2%, 5%, and 10% of total lipid (molar ratio), or $6 \cdot 10^{5}$, $2.4 \cdot 10^{6}$, $6 \cdot 10^{6}$, and $1.2 \cdot 10^{7}$ NTA lipids/bead respectively. We assume that every NTA-derivatized lipid anchors a His-tagged s2ZipA molecule. The radius of a sphere with the same mass and density as s2ZipA is approximately $1.5 \cdot 10^{-7}$ cm, and the circular footprint of that sphere is $7.3 \cdot 10^{-14}$ cm^2. The fraction of surface area occupied by immobilized s2ZipA is thus approximated by (#NTA/bead × surface area per ZipA)/surface area per bead. Thus, the fraction of surface area occupied by immobilized s2ZipA corresponding to each of the NTA densities employed, denoted by ϕ, is estimated to be 0.06, 0.22, 0.56, and ~ 1 respectively. The amount of unoccupied bead surface area that is available for placement of a nonspecifically adsorbed molecule of FtsZ is less than the actual unoccupied area due to the mutual impenetrability of the adsorbed molecules. Assuming that nonspecifically adsorbed FtsZ does not interact with surface-immobilized s2ZipA except via steric repulsion, the area available for placement of a molecule of FtsZ on a surface occupied by volume fraction ϕ of ZipA may be estimated using the two-dimensional scaled particle theory of hard convex particle fluids, as presented in the appendix to Chatelier & Minton (Chatelier and Minton 1996). The natural logarithm of the activity coefficient of nonspecifically adsorbed FtsZ was calculated using the special case of equation (A9) of Chatelier & Minton for a tracer circle in a fluid of circles occupying area fraction ϕ, with $\varepsilon = f_c = f_a = 1$ and $f_R = 1.45$, the ratio of radii of the circular representations of FtsZ and ZipA. The fraction of available area is then calculated according to (Minton 2001) as $f_A = 1/\exp(ln\, \gamma_{FtsZ})$, where γ_{FtsZ} corresponds to the activity coefficient.

5. Reconstitution of ZipA-FtsZ interaction in supported lipid bilayers

5.1 Liposome preparation

Lyophilized dioleoylphosphatidylcholine (DOPC) and a DGS-NTA analogue with chelator headgroups comprising three nitrilotriacetic acid moieties (tris-NTA) were dissolved in chloroform and mixed at the desired molar ratios (0, 0.1, 0.5, 1, 2 and 5%

tris-NTA) and prepared as described earlier (Beutel *et al.* 2014). Mixtures were dried, first under a stream of nitrogen gas and then in vacuum, and then resuspended in 10 mM HEPES, 150 mM NaCl, pH 7.4. Small unilamellar vesicles (SUVs) were prepared by sonication, as described previously (Eisele *et al.* 2010). SUVs at a stock concentration of 2 mg/mL were stored at 4 ºC and used for up to one month. Before use, vesicle suspensions were diluted to 50 µg/mL in 50 mM Tris-HCl, 300 mM KCl, 5 mM $MgCl_2$, pH 7.5 supplemented with 2 mM $NiCl_2$.

5.2 Quartz crystal microbalance with dissipation monitoring (QCM-D)

QCM-D measures changes in resonance frequency, Δf, and dissipation, ΔD, of a sensor crystal upon interaction of soft matter with its surface. The QCM-D response is sensitive to the mass (including hydrodynamically coupled water) and the mechanical properties of the surface-bound film (Reviakine *et al.* 2011). The sensor crystal is typically coated with metal films on the top and bottom faces to act as electrodes (Figure M.4). The top face, bare or coated with additional layers (in our case, silica), is used as the experimental substrate. Silica-coated QCM-D sensors were cleaned by immersion in 2% sodium dodecyl sulfate (SDS) for at least 30 min, abundant rinsing with ultrapure water and blow-drying in nitrogen gas.

Prior to use, sensors were activated in a UV/ozone environment (Bioforce Nanoscience, USA) for at least 30 min. QCM-D measurements were performed with a Q-Sense E4 system equipped with Flow Modules with flow rates of typically 10 µL/min controlled by a syringe pump, at a working temperature of 23 °C. Although Δf and ΔD were collected at six overtones (i = 3, 5, 7, 9, 11, 13), only the changes in dissipation, ΔD, and normalized frequencies, $\Delta f = \Delta f_i/i$, for i = 5 are presented in this thesis for clarity. All other overtones provided similar information. For dense monolayers of globular proteins such as s1ZipA, the film thickness can be estimated from $d = -C / \rho \times \Delta f$, where the density ρ = 1.2 g/cm^3 represents the protein film density to within an error of less than 20% and C = 18 ng/cm^2/Hz is the sensor's mass sensitivity constant (Reviakine *et al.* 2011).

Commonly used QCM-D sensors have a diameter of 14 mm, a thickness of ~300 µm, and a fundamental resonance frequency of ~5 MHz. The active sensing area is confined to a central, circular spot of ~5 mm diameter. Application of oscillatory voltage results in a cyclical shear deformation of the sensor. In the ring-down method, which is

used by QCM-D, the driving voltage is intermittently switched off and the decay in time of the oscillation is monitored. From the decay curve, the resonance frequency (*f)* and the energy dissipation (*D)* are extracted for soft or rigid films (Figure M.4).

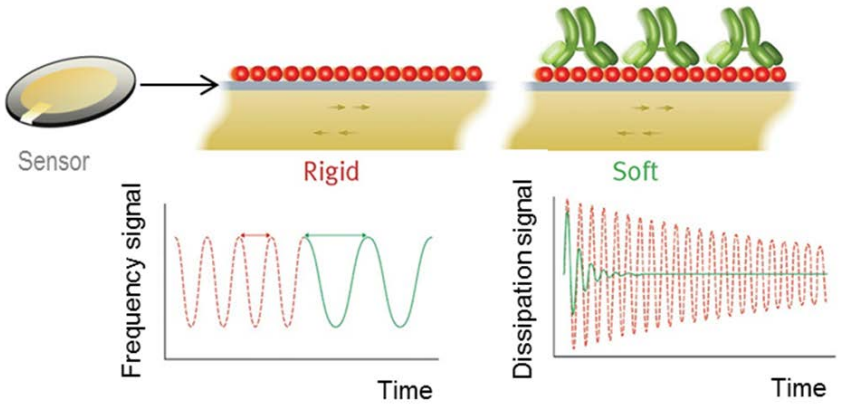

Figure M.4. QCM-D sensor and sensing principle. Examples of the frequency and dissipation signals generated by the incorporation of receptors (red circles) or receptor-ligand complexes (red and green molecules). The incorporation of receptors like the red ones showed in the scheme is expected to form a rigid thin film, fully coupled to the surface. However, the incorporation of bigger molecules on top of the receptor makes the film softer. Dashed red line and continuous green line show, respectively, the expected signals for a rigid and a soft film. Adapted from Biolin Scientific (www.biolinscientific.com/qsense).

The resonance frequency depends on the total oscillating mass of the sensor and sensor surface adhering layers, including coupled water. The frequency decreases when a lipid or protein film is attached to the sensor. If the film is thin and rigid the decrease in frequency is proportional to the mass of the film (Richter *et al.* 2014). The dissipation, however, depends on the viscoelastic properties of the film. It increases for soft films but also with the amount of material attached to the sensor.

5.3 Spectroscopic ellipsometry (SE)

SE measures changes in the polarization of light upon reflection from a surface. The SE response is sensitive to the thickness and refractive index of surface-bound layers. The measured parameters are the ellipsometric angles Ψ and Δ. They describe the change in polarization that occurs when the incident beam interacts with a sample surface. The incident light beam contains electric field components parallel (*p*-) and perpendicular (*s*-) to the plane of incidence (Figure M.5), and the ellipsometric angles relate to their differences in phase and amplitude. With well-established optical models,

the measured values (Ψ and Δ) can be related to the optical properties of the interface, including the thickness and refractive index of biomolecular films.

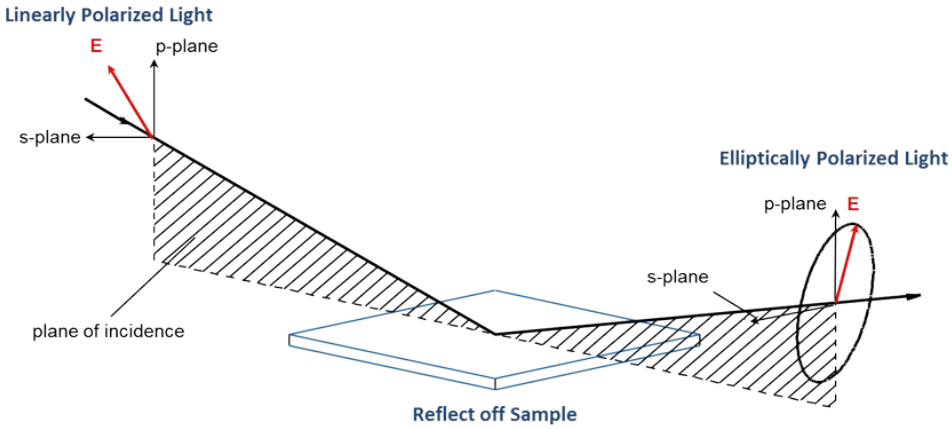

Figure M.5. Ellipsometry principle. The incident light beam contains electric fields both parallel (*p*-) and perpendicular (*s*-) to the plane of incidence. The surface differentiates between the *p*– and *s*–light, causing a change in the outgoing polarization. Taken from J.A. Woollam (www.jawoollam.com).

In this work, silicon wafers were used as surfaces to attach lipids and proteins of interest. The sensor was cleaned by sequential rinsing with acetone, ethanol and ultrapure water, and subsequently activated with UV/ozone for 30 minutes. SE measurements were carried out at room temperature (~23 ºC) with a M2000V ellipsometry system (J.A.Woollam, USA) using a cuvette made of polyetheretherketone polymer (PEEK), containing glass windows for the entry and exit of light and inlet/outlet tubing for the exchange of sample solution. Inside the cuvette, the sample solution with continuous stirring using the magnetic stirrer at the cuvette bottom (Figure M.6). Prior to the measurement, the cuvette was passivated with 10 mg/mL bovine serum albumin (BSA) diluted in water, rinsed with ultrapure water and blow-dried with nitrogen gas. Samples were pipetted and diluted to desired concentrations directly in the cuvette, and rinsing with buffer was performed with a peristaltic pump at a flow rate of 350 µL/min.

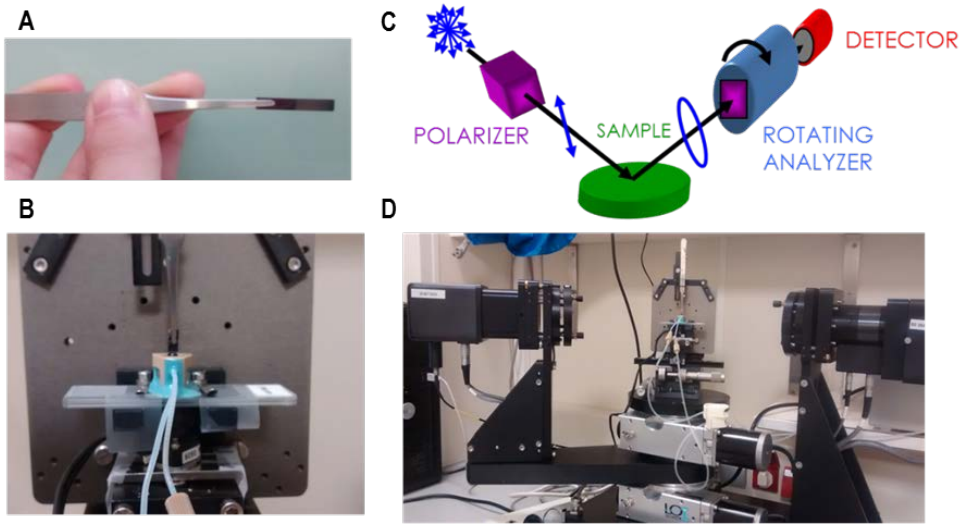

Figure M.6. Ellipsometry setup. (A) A piece of silicon wafer used as a substrate for adsorption of lipids and proteins. (B) Wafer inside the PEEK cuvette with glass windows. (C) Scheme of the ellipsometer configuration. The linearly polarized light reflects from the sample surface, becomes elliptically polarized and the detector converts light into electronic signal to determine the reflected polarization. This information is compared to the known input polarization to determine the polarization change caused by the sample reflection. This is expressed by the ellipsometric angles Ψ and Δ. (D) Setup for an ellipsometry measurement.

Data were analysed with the software CompleteEASE (J. A. Woollam) using a model of multiple optically homogeneous layers, as previously described in other studies (Carton *et al.* 2010, Eisele *et al.* 2010). The protein film (index F) was treated as a transparent Cauchy medium with optical thickness d_F and a wavelength-dependent refractive index $n_F(\lambda) = A_F + B_F / \lambda^2$, being A_F and B_F coefficients that describe the dispersion (*i.e.* the wavelength dependence of the refractive index). The bulk solution (index S) was treated as a transparent Cauchy medium with $n_S(\lambda) = A_S + B_S / \lambda^2$. We set $A_S = 1.328$, *and* $B_S = B_F = 0.00322$ μm^2, as described in the literature (Carton *et al.* 2010). d_F and A_F were the adjustable fit parameters. Protein surface densities were determined through de Feijter's equation (De Feijter *et al.* 1978),

$$\Gamma = d_F \, \Delta n \, / \, (M_w \times dn/dc)$$

where M_w is the molecular mass, and Δn is the difference in refractive index between the protein film and the buffer solution ($\Delta n = n_F(\lambda) - n_S(\lambda) = A_F - A_S$). We used a refractive index increment of $dn/dc = 0.180$ cm^3/g for all proteins (Richter *et al.* 2014). All the experiments were performed in 50 mM Tris-HCl, 300 mM KCl, 5 mM $MgCl_2$, pH 7.5.

6. Analysis of FtsZ properties in liquid-liquid phase transition (LLPS) systems

6.1 DNA fragmentation and purification

DNA (from salmon sperm) was subjected to 15 minutes sonication in a bath and purified by the phenol:chloroform:isoamyl alcohol extraction method followed by ethanol precipitation, basically as described (Biswas, N *et al.* 2012). Briefly, a DNA solution in water was mixed with equal volume of a phenol:chloroform solution. The mixture was then centrifuged and two distinct phases were separated, the aqueous phase being on top. This phase, which contained the DNA, was carefully separated from the organic phase and the material at the interface. DNA was finally precipitated with ethanol, centrifuged and dried under vacuum. The dried pellet was resuspended in 50 mM Tris-HCl, 300 mM KCl, pH 7.5, and stored at −20 °C until used. Obtained DNA consisted on fragments of up to 300 base pairs as characterized in agarose gels. DNA concentration was estimated from its dry weight after purification.

6.2 Preparation of LLPS systems

Among the different combinations of the crowders tested, PEG 8, dextrans T40 and 500, Ficoll 70 and DNA, under our experimental conditions (nearly neutral pH, 300 mM KCl and room temperature) and at concentrations compatible with those of our stock solutions, phase separation was only achieved when one of the phases in the mixture was PEG (*i.e.* with PEG/dextran 500, PEG/dextran T40, PEG/Ficoll 70 and PEG/DNA). This was verified by visual inspection of the tubes and from confocal microscopy images of the fluorescently labelled enriched components after emulsification. The crowders, without further purification except for DNA (see above) were equilibrated by extensive dialysis in 50 mM Tris-HCl, 300 mM KCl, pH 7.5. Before use, individual enriched phases were purified as follows. For each particular binary mixture, defined volumes of each crowder were thoroughly mixed to yield a final nominal concentration rendering phase separation as visually determined. These concentrations were 53 and 82 g/L for PEG 8 and dextran 500, respectively; 53 and 82–92 g/L for PEG 8 and dextran T40, respectively; 113 and 165 g/L for PEG 8 and Ficoll 70, respectively; and 92 and 183 g/L for PEG 8 and DNA, respectively. The mixture was centrifuged at 3000 rpm for 5 minutes in a bench centrifuge to favour phase separation. The stability with time of the system thus separated was checked and no change was found for at least 4

hours. Enriched phases were then isolated by pipetting, discarding the material nearby the interface, and their final concentrations were determined from the refractive index increment (dextran 500 and PEG 8, 0.142 and 0.136 mL/g respectively (Liu *et al.* 2012); dextran T40, 0.147 mL/g (APS Corp); Ficoll 70, 0.141 mL/g (Fodeke and Minton 2010)). We found that, after equilibration, all the crowders reached a concentration almost twofold their initial concentrations in the mixture, the phase enriched in PEG always lying on top of that with the other crowder in the tubes.

6.3 Preparation of emulsions of LLPS systems

The simplest emulsions were formed by thoroughly mixing the corresponding enriched phases at the desired volume ratio. The mixture PEG/dextran 500 was used to check the distribution of several volume ratios of the crowders, usually rendering droplets of the minor phase surrounded by the major phase (Figure M.7). In general, the 3:1 ratio resulted suitable in all the LLPS systems for visualisation in bulk. FtsZ, containing a tracer amount of FtsZ-Alexa 488 or FtsZ-Alexa 647 (1 µM), was directly added to this mixture and, when required, polymerization was triggered by diffusion of GTP directly added over the mixture of the two phases containing FtsZ. Emulsions were prepared in 50 mM Tris-HCl, 300 mM KCl, 1 mM $MgCl_2$, pH 7.5. To assess colocalisation of FtsZ with either phase, one of them was labelled with a dye (1 µM final concentration) spectrally different from that of the protein. Images were acquired with different combinations of dyes (FtsZ-Alexa 488 with PEG-Alexa 647, FtsZ-Alexa 647 with PEG-Alexa 488 or dextran-FITC) with equivalent results.

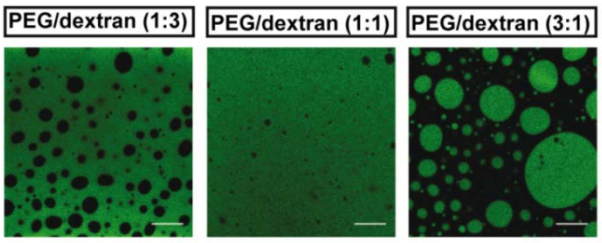

Figure M.7. Distribution of the PEG/dextran 500 LLPS emulsions at varying v/v ratios. Fluorescence signal corresponds to dextran 500-FITC, used as a tracer for the dextran 500 phase. Bars are 40 µm.

6.4 Calculation of partition coefficients

Partition coefficients, *K*, within a binary mixture of LLPS systems in bulk were calculated as the ratio of the concentration of FtsZ in the PEG-rich phase to that in the other phase from evaluation of the fluorescence emission arising from labelled FtsZ using PolarStar Galaxy (BMG Labtech, GmbH, Germany) or Varioskan (Thermo) Plate

Readers. FtsZ-Alexa 488 (0.5 μM) and unlabelled FtsZ up to the concentration required in each sample were gently mixed with the phases obtained by mixing the two crowders in 50 mM Tris-HCl, 300 mM KCl, 1 mM $MgCl_2$, pH 7.5, unless otherwise specified, in a 1:1 volume ratio and allowed to equilibrate until reaching phase separation for 30 minutes. When required, 1 mM GTP was added to the samples. After centrifugation, phases were isolated (top phase being always PEG) and the fluorescence intensity of an aliquot of each of the phases was measured. The concentration of protein was calculated by comparison with samples containing known amounts of FtsZ-Alexa 488 diluted in the corresponding phase, the signal of which is linear with FtsZ concentration as verified through control measurements. The fraction of FtsZ at the interface was calculated as the difference between the total amount and the sum of those in each phase, except in the case of FtsZ-GTP in the PEG/DNA LLPS system, as explained in Chapter 3. Reported values correspond to the average of, at least, 3 independent measurements ± SD.

6.5 Preparation of LLPS systems encircled by a lipid membrane

Emulsions were obtained following a procedure based on that described (Mellouli *et al.* 2013) that we specifically optimized for the encapsulation of binary mixtures. The protocol involves the use of an aqueous and an oil solution. The latter was prepared drying under nitrogen flow, shortly before use, a determined amount of *E. coli* lipids (1.5 mg per sample), subsequently kept under vacuum for at least one hour and dispersing them in mineral oil (final concentration 25 g/L) by two cycles of 10 minutes in a sonication bath. This concentration of lipids in mineral oil was found suitable for the encapsulation of the mixtures. For the aqueous solution, the enriched phases were thoroughly mixed by vortexing to enhance the formation of very small droplets of one in the other. 3:1 or 1:1 volume ratios of PEG to the other phase were employed with similar results. Protein was added on the phases thus mixed and, when required, GTP was also included to a final concentration of 1–2 mM. This mixture was subsequently added on the oil solution containing the dispersed lipids and all components gently mixed by pipetting up and down. This rendered water in oil emulsion droplets of the LLPS systems with protein in 50 mM Tris-HCl, 300 mM KCl, 1 mM $MgCl_2$, pH 7.5, stabilized by lipids (Figure M.8).

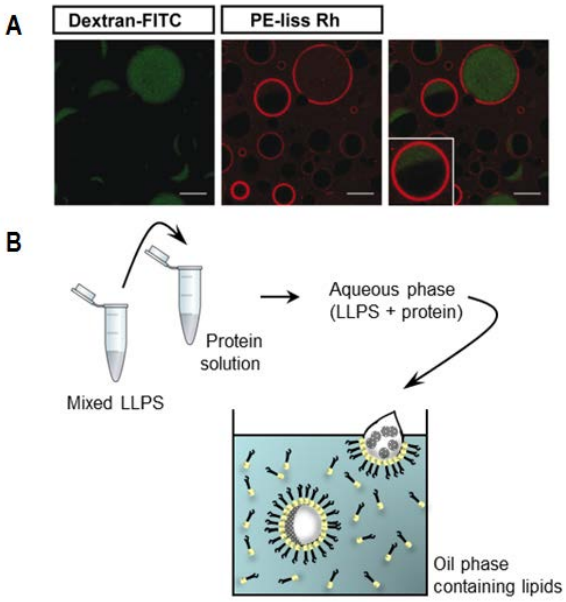

Figure M.8. Encapsulation method of LLPS systems into lipid stabilized droplets. (A) Representative images of the LLPS system encapsulated into lipid containers. *E. coli* lipids were doped with rhodamine labelled phosphatidylethanolamine (PE-liss Rh) and used to encapsulate the PEG/dextran 500 (3:1) LLPS system. Inset displays a magnification evidencing the presence of both phases inside the lipid container. Bars are 40 µm. (B) Scheme of the procedure followed to encapsulate LLPS systems into containers stabilized by a lipid layer

6.6 Confocal microscopy measurements and data analysis

Emulsions (~70 µL) were placed in silicone chambers glued to coverslips and visualized by confocal microscopy. Images were collected with a Leica TCS-SP2-AOBS inverted confocal microscope with a HCX PL APO 63x oil immersion objective (N.A. = 1.4–1.6; Leica, Mannheim, Germany). Ar (488–514 nm) and He-Ne (633 nm) ion lasers were used to excite Alexa 488 or FITC and Alexa 647, respectively. DiodeP (561 nm) ion laser was used to excite lissamine-rhodamine. To follow depolymerization of FtsZ inside lipid droplets, a time series was taken every three minutes. Intensity profiles were generated with Image J (National Institutes of Health, USA) within the line defined in the images using the straight line tool.

7. Encapsulation of LLPS systems by microfluidics

7.1 Microfluidic chip fabrication

The devices used were constructed by conventional soft lithographic techniques from a silicon master containing the chip design (Mellouli *et al.* 2013). PDMS base Sylgard^{TM} 184 and curing agent were mixed in a 10:1 (w/w) ratio, degassed, decanted onto the master and heated at 65°C for at least 4 hours. Inlet and outlet holes through which solutions will flow were punched in the PDMS peeled from the master, and the channels were sealed by a glass slide, activating the surfaces by oxygen plasma

(Plasma Cleaner Zepto, Diener Electronic, GmbH, Germany). Devices were coated with a hydrophobic layer flushing Aquapel in the channels and allowing it to dry overnight at 65 °C (Figure M.9).

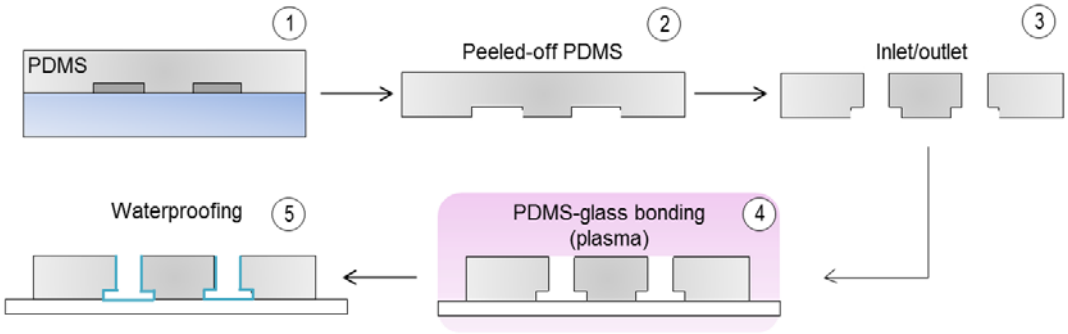

Figure M.9. Scheme of microfluidic chip fabrication procedure. (1) PDMS poured onto the master. (2) Peeled-off PDMS with the micropattern imprinted on its surface. (3) PDMS is punched to form the inlet/outlet holes. (4) Surfaces are activated by oxygen plasma and PDMS is bonded to a glass slide. (5) Aquapel is flushed through the inlet holes to make surfaces hydrophobic.

7.2 Microfluidics experimental setup

Aqueous and oil phases were loaded into Hamilton syringes, connected by tubings to the inlet holes of the fabricated chip (Figure M.10). Automated syringe pumps (Cetoni GmbH, Germany) were used to control the flows of the solutions. Our chips contain one inlet for the oil phase, and two inlets for two aqueous phases. These two mix closely before the production junction, point at which they meet the oil stream and are encapsulated. The generation of droplets was monitored by using an Axiovert 135 fluorescence microscope (Zeiss) with a digital camera of a smartphone (LG K10) coupled to its eyepieces (Figure M.11).

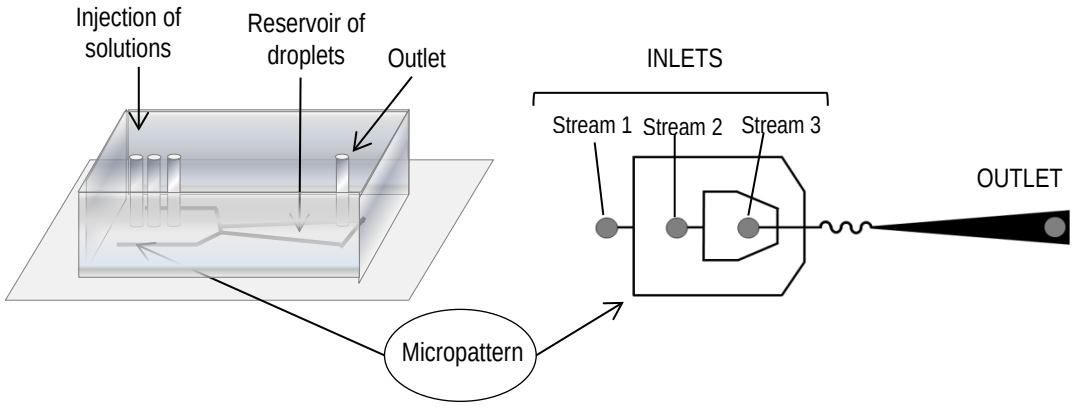

Figure M.10. Schematic overview of microfluidic chip design used for droplet production. The design, imprinted in the PDMS polymer, consists of three inlets for an oil phase and two aqueous solutions. Close to the production junction, droplets pass through a wavy region allowing the surfactant to stabilize at droplets interface. Droplets accumulate at the reservoir for on-chip visualization.

The droplets were imaged directly on-chip, keeping them in the device reservoir by simultaneously cutting the inlets tubing before stopping the flow, or off-chip collecting them through the outlet tubing. The vesicles were visualized by placing ~70 µL in chambers fabricated by gluing a silicone isolator to coverslips.

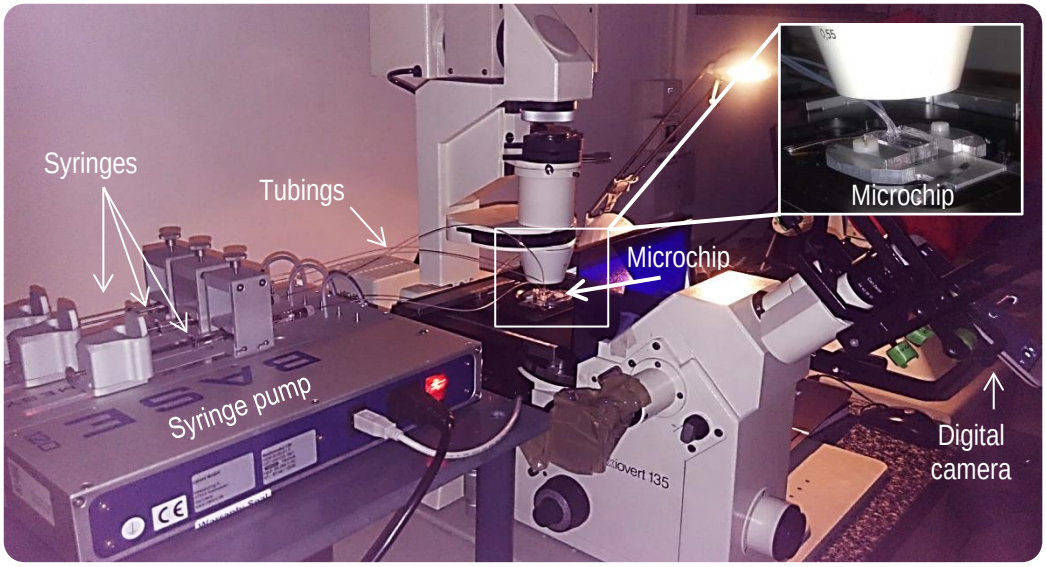

Figure M.11. Image of the microfluidic experimental setup. The system includes three dosing units flushing the solutions through the inlet holes of the microchip at defined flow rates. A digital camera was coupled to the microscope to monitor the generation of droplets.

7.3 Encapsulation of PEG/dextran solutions by microfluidics

Encapsulation was conducted by mixing two streams of dispersed aqueous phases, one with dextran 500 and the other with PEG 8, in an approximately 1:1 ratio prior to the droplet formation junction (Figure M.12). Alexa-647 labelled PEG (2 µM) was included in the PEG solution. FtsZ (25 µM) with a tracer amount labelled with Alexa 488 (1 µM FtsZ-Alexa 488) was added to the two aqueous phases. When induction of protein polymerization before encapsulation was required, one of the solutions contained FtsZ (25 µM) with FtsZ-Alexa 488 (2 µM) and the other the nucleotide GTP (4-6 mM). The buffer for the aqueous solutions was 50 mM Tris-HCl, 300 mM KCl, 1 mM $MgCl_2$, pH 7.5. The third stream supplied the *E. coli* lipid mixture at 20 g/L in mineral oil. We found no differences in the microdroplet formation step derived from the presence of DMPC, included for the subsequent generation of permeable vesicles. All experiments were conducted at room temperature. Data presented in Chapter 4 correspond to experiments delivering solutions at 120 µL/h (oil phase) and 5 and 7 µL/h (dextran and PEG aqueous phases, respectively) by automated syringe pumps yielding uniform droplets with average diameter of 16 µm (~2

pL). In some instances the final flows of the two aqueous phases were slightly different but no significant effect was observed in the encapsulation. Decreasing of the oil phase flow resulted in average diameters somewhat increased.

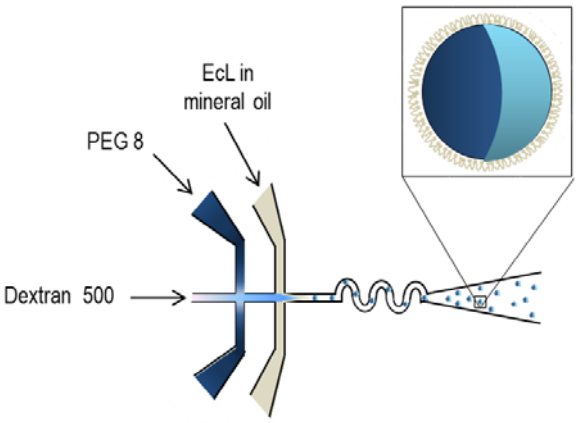

Figure M.12. Microfluidics encapsulation of a LLPS system inside microdroplets. Scheme of the junction in the microfluidic chip.

7.4 Formation of Giant Unilamellar Vesicles and triggering of FtsZ polymerization

For their subsequent conversion into GUVs, droplets were collected, once stable production was achieved, introducing the outlet tubing from the microfluidic chip into 700 µL of oil phase stabilized for at least 1 hour over 400 µL of outer solution (see below). Collection was initially tested positioning the outlet tubing either slightly above or slightly below the oil/air interface, in both cases close to the centre of the tube section avoiding contact with the walls. In the first case, the encapsulated material accumulated mostly within the oil surface and subsequent steps rendered very low amounts of GUVs. Positioning of the tubing slightly below the oil surface proved to be more suitable for successful generation of GUVs. Upon delivery of the microdroplets from the outlet tubing, they migrated throughout the whole oil volume until reaching the oil/outer solution interface, where they accumulated. Probably this migration through the oil phase helped to further stabilize the lipid monolayer before subsequent centrifugation into the aqueous solution, plus avoids impact of microdroplets against the oil/air interface and their accumulation into a less friendly environment. Composition of the outer solution was that of the solution inside the vesicles (50 mM Tris-HCl, 300 mM KCl, 1 mM $MgCl_2$, pH 7.5), supplemented with 117 mM sucrose that rendered an osmolarity ~25 mOsmol/Kg above the highest osmolarity of the encapsulated solutions. The osmolarities, measured in a Osmomat 3000 (Gonotec GmbH, Germany), of the PEG and dextran solutions were close to each other (PEG *ca* 740 mOsmol/Kg, dextran *ca* 710 mOsmol/Kg). Similar results were obtained when glucose was used instead of sucrose to adjust the osmolarity of the outer solution.

Droplet collection times were varied from 10 to 30 minutes, being 30 minutes the one selected to improve the yield of the method. The solutions were then centrifuged (15 min, 1500 rpm in a bench centrifuge), the oil phase removed and the droplets washed with outer solution and centrifuged again (15 min, 2000 rpm). For triggering of FtsZ polymerization, 20 mM GTP was added in this last step. Pelleted vesicles were visualized as described below. All experiments were conducted at room temperature.

7.5 Fluorescence microscopy and measurement of droplets diameter

The droplets and giant vesicles were visualized by confocal microscopy with a Leica TCS-SP2-AOBS or a Leica TCS-SP5-AOBS inverted confocal microscope with a HCX PL APO 63x oil immersion objective (N.A. = 1.4–1.6; Leica, Mannheim, Germany). Ar (488–514 nm) and He-Ne (633 nm) ion lasers were used to excite Alexa 488 and Alexa 647 dyes, respectively.

ImageJ (National Institutes of Health, USA) was used to measure the distribution of diameters applying the line tool of the software through the equatorial section of the droplets/vesicles and to obtain the intensity profiles in the red and green channels. Size distributions shown correspond to 3 representative experiments for the droplets and 2 different experiments for the GUVs, independent from the ones corresponding to the droplets.

CHAPTER 1

Nucleotide and receptor density modulate binding of bacterial division FtsZ protein to ZipA- containing lipid coated microbeads

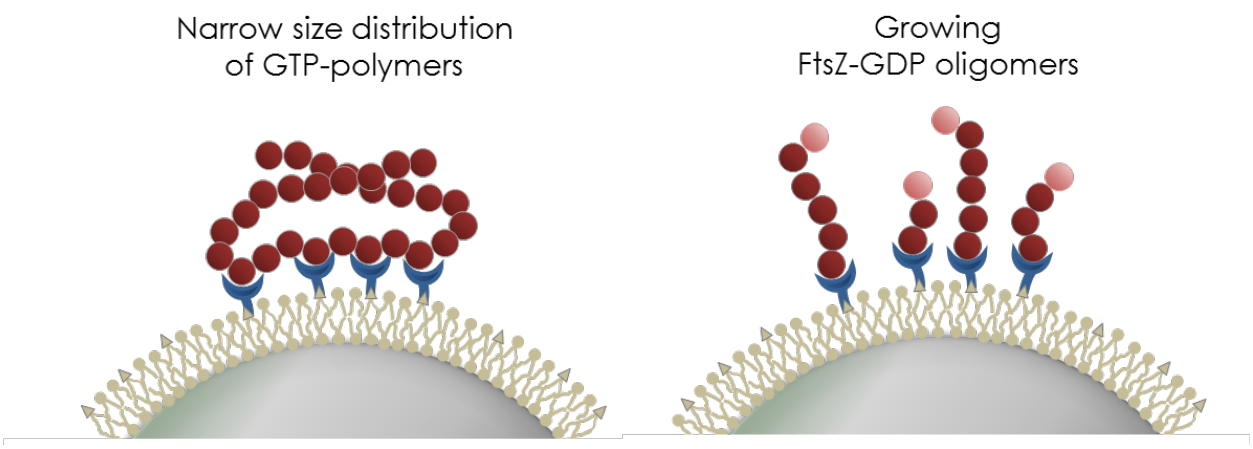

ZipA protein from *Escherichia coli* is one of the essential components of the division proto-ring that provides membrane tethering to the septation FtsZ protein. A sedimentation assay was used to measure the equilibrium binding of FtsZ-GDP and FtsZ-GTP to ZipA immobilized at controlled densities on the surface of microbeads coated with a phospholipid mixture resembling the composition of *E. coli* membrane. We found that for both nucleotide-bound species, the amount of bound FtsZ exceeds the monolayer capacity of the ZipA immobilized beads at high concentrations of free FtsZ. In the case of FtsZ-GDP, equilibrium binding does not appear to be saturable, whereas in the case of FtsZ-GTP equilibrium binding appears to be saturable. The difference between the two modes of binding is attributed to the difference between the composition of oligomers of free FtsZ-GDP and free FtsZ-GTP formed in solution.

RESULTS

In order to quantitatively characterize the role of ZipA surface density on the interactions with the GDP and GTP forms of FtsZ, we used lipid coated microbeads to immobilize a His-tagged soluble variant of ZipA at controlled surface densities (s2ZipA, residues 188-328, Figure M.1). Various concentrations of FtsZ-GDP and FtsZ-GTP were equilibrated with a known amount of beads containing immobilized ZipA at various surface densities. The beads were then sedimented and the concentration of unbound FtsZ in the supernate was quantified by fluorescence spectroscopy. The difference between total and unbound FtsZ is then the amount of bound FtsZ. Our results showed a markedly different mode of binding to immobilized ZipA depending on the nucleotide present that may be interpreted in light of the different features of the FtsZ self-association in each case.

1.1 FtsZ binding to s2ZipA immobilized in microbeads

The raw data consist of arrays of the concentrations of free FtsZ in the supernate as a function of the total concentration of FtsZ in a suspension containing 60 g/L of beads. The concentration of bound FtsZ is then the difference between the two quantities, which are plotted as functions of the concentration of free FtsZ-GDP (Figure 1.1A) and FtsZ-GTP (Figure 1.1B) for different densities of immobilized s2ZipA. It is recognized that a certain amount of FtsZ adsorbs nonspecifically on the beads and precipitates with them in the absence of surface-immobilized s2ZipA. Correction for nonspecific adsorption is described below.

In order to ascertain the mode of binding, attention must be paid to accessible surface area of beads. The beads utilized have a radius of $2.5 \cdot 10^{-4}$ cm. Thus, the volume of a bead is $6.5 \cdot 10^{-11}$ cm^3 and the surface area is $7.8 \cdot 10^{-7}$ cm^2. The specific volume of beads is 0.5 cm^3/g (manufacturer's specifications), so in one liter of a 60 g/L suspension of beads the volume of beads is 30 cm^3. Thus, the number of beads per liter is $30/6.5 \cdot 10^{-11} = 4.6 \cdot 10^{11}$. The surface area of beads per liter of suspension is thus $7.8 \cdot 10^{-7} \times 4.6 \cdot 10^{11} = 3.6 \cdot 10^5$ cm^2.

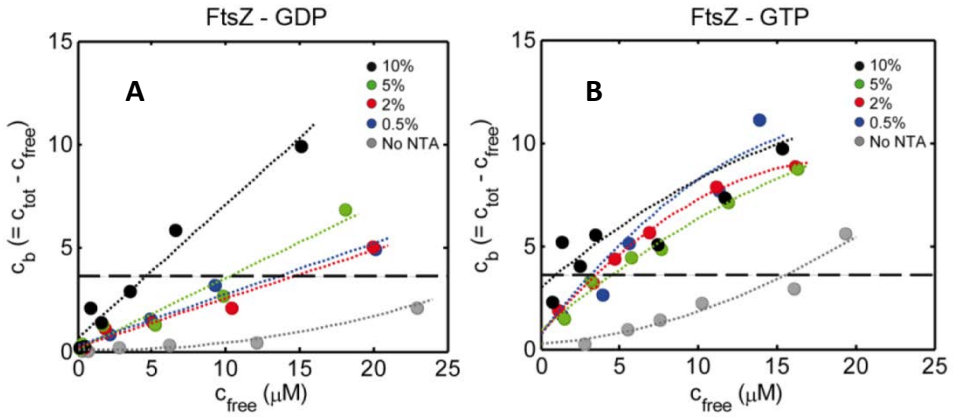

Figure 1.1. FtsZ binding to s2ZipA immobilized in microbeads. Concentration of bead-associated FtsZ-GDP (A) and FtsZ-GTP (B) plotted as a function of the concentration of free FtsZ-GDP and FtsZ-GTP, respectively, for different densities of immobilized ZipA, proportional to the percentage of total lipid bearing NTA (in the legend) coating a 60 g/L suspension of 5 micron diameter beads. Symbols are the data. Dotted lines are only meant to guide the eye. The horizontal dashed line represents the amount of FtsZ that would completely cover the bead as a monolayer, calculated as described in the text.

For purposes of estimating the concentration of FtsZ that would completely fill the surface area of the beads with a single monolayer, a molecule of FtsZ is approximated by a sphere with volume equal to that calculated from the mass and density of the monomeric protein, which has a radius equal to $2.2 \cdot 10^{-7}$ cm. Its circular "footprint" (projection onto a surface) is thus $1.5 \cdot 10^{-13}$ cm^2. Let us assume that the maximum amount of FtsZ that can be packed into a surface monolayer would correspond to hexagonal close packing, according to which each circle occupies 0.91 of the planar area per circle. Thus, the area/FtsZ molecule of a hexagonal close packed array = $1.5 \cdot 10^{-13} / 0.91 = 1.65 \cdot 10^{-13}$ cm^2. The number of FtsZ molecules in a hypothetical hexagonal close packed monolayer on 60 g/L of beads would then be $3.6 \cdot 10^5 / 1.65 \cdot 10^{-13} = 2.2 \cdot 10^{18}$, corresponding to a micromolar concentration of $2.2 \cdot 10^{18} / 6.02 \cdot 10^{17} = 3.6$ μM. This value is indicated as a horizontal line in Figures 1.1-1.3. It is evident upon inspection that the binding exceeds the monolayer capacity of the bead at high free protein concentrations at the highest receptor density in the case of FtsZ-GDP and at all receptor densities in the case of FtsZ-GTP.

This demonstrates that binding of FtsZ to the beads is not limited to a single surface layer. This apparent anomaly may be accounted for by the fact that both FtsZ-GDP and FtsZ-GTP reversibly form oligomers, the average size of which depends upon total free FtsZ concentration (Ahijado-Guzmán *et al.* 2013, Rivas *et al.* 2000).

According to the light scattering data of Ahijado-Guzmán *et al* (Ahijado-Guzmán *et al.* 2013), the weight-average size of oligomeric FtsZ-GTP is on the order of ten times as large as the average size of oligomeric FtsZ-GDP under the conditions of the experiments reported here. Thus, the binding of a single monomeric subunit or a substoichiometric number of subunits of an FtsZ oligomer to an immobilized s2ZipA could increase the total amount of FtsZ bound per bead manifold.

1.2 Phenomenological model of s2ZipA-FtsZ binding

In view of the paucidisperse distribution of sizes of GDP- and GTP-bound FtsZ oligomers (Ahijado-Guzmán *et al.* 2013, Rivas *et al.* 2000) and the many possible ways in which each species of oligomer could bind to one or more immobilized s2ZipA acceptors, it is not feasible to construct a complete scheme to account for the total binding. Instead we propose a phenomenological model that attempts to take into account the combination of both nonspecific adsorption and specific binding of FtsZ to beads containing various densities of immobilized s2ZipA. The model is based upon the following assumptions.

Total binding to beads is taken as the sum of non-site-specific adsorption and specific binding of FtsZ to either immobilized s2ZipA or to s2ZipA-bound FtsZ:

$$c_b(c_{free}, c_{ZipA}) = c_{ads}(c_{free}, c_{ZipA}) + c_{spec}(c_{free}, c_{ZipA}) \quad (1.1)$$

, where c_{ads} and c_{spec} respectively denote the amount per unit volume of nonspecifically adsorbed and specifically bound FtsZ, written as functions of the concentrations of free FtsZ (c_{free}) and immobilized s2ZipA (c_{ZipA}). Nonspecific adsorption is modeled as an empirical dependence of nonspecifically bound upon free FtsZ:

$$c_{ads}(c_{free}, c_{ZipA}) = f_a(c_{ZipA}) c^0_{ads}(c_{free}) \quad (1.2a)$$

$$c^0_{ads}(c_{free}) = A_1 c_{free} + A_2 c^2_{free} \quad (1.2b)$$

, where c^0_{ads} denotes the concentration of FtsZ bound to the bead in the absence of immobilized s2ZipA, and f_a denotes the fraction of bead surface area available for

adsorption when a certain concentration of s2ZipA is immobilized on the bead surface. The value of f_a, estimated as described in the Materials and Methods section, is 0.70 for 0.5% NTA, 0.15 for 2% NTA, and ~ 0 for 5 and 10% NTA.

Specific (saturable) binding is empirically modeled as a Langmuir adsorption isotherm:

$$c_{spec} = c_{spec}^{(max)} \frac{(c_{free}/c_{50})}{1+(c_{free}/c_{50})} \tag{1.3}$$

where $c_{spec}^{(max)}$ denotes the hypothetical upper limit of saturable binding and c_{50} the concentration of free FtsZ at which specific binding is one half the value of $c_{spec}^{(max)}$. Equations (1.1) – (1.3) were fit by the method of nonlinear least squares to the measured dependence of total bound FtsZ as a function of free FtsZ for all densities of immobilized s2ZipA, subject to the condition that the values of A_1, A_2 and c_{50} are independent of s2ZipA density, *i.e.* common to all data sets obtained under a single set of experimental conditions. The binding data obtained for FtsZ-GDP at each s2ZipA density and the corresponding best fit of equations (1.1) - (1.3) to all data sets, calculated using the best-fit parameters given in the figure caption, are plotted in Figure 1.2, and the comparable data and best-fit parameters obtained for FtsZ-GTP are plotted in Figure 1.3.

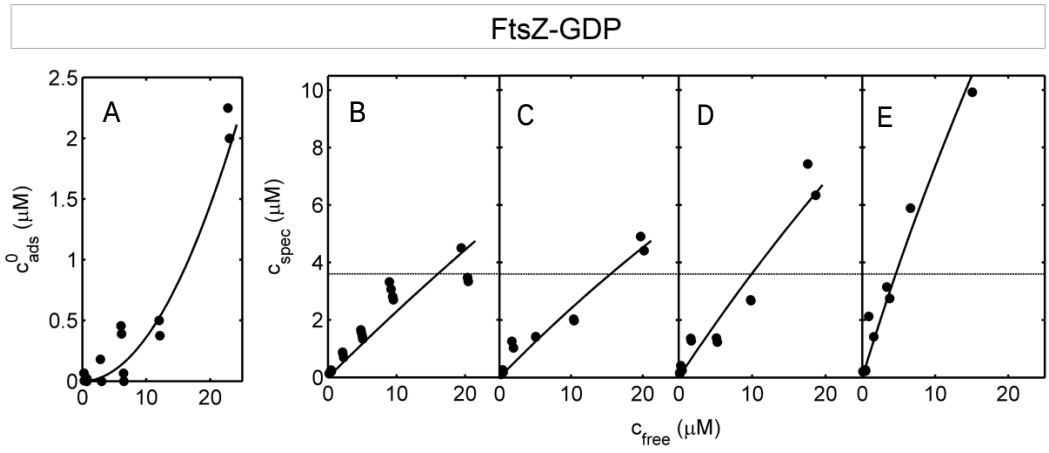

Figure 1.2. FtsZ-GDP binding as a function of receptor density. Nonspecific adsorption (A) and specific binding (B-E) of FtsZ-GDP plotted as a function of the concentration of free FtsZ-GDP for various densities of s2ZipA, proportional to the percentage of NTA-bearing lipid coating the beads: (A) 0% NTA, (B) 0.5% NTA, (C) 2% NTA, (D) 5% NTA, (E) 10% NTA. Symbols are the data. Horizontal dotted lines are the amount of FtsZ that would completely cover the bead as a monolayer, calculated as described in the text. Curves were calculated using equations (1.1) – (1.3) with the following parameter values: A_1 = 0; A_2 = 0.00363; c_{50} = 150; $c_{spec}^{(max)}$ = 37 (B), 38 (C), 58 (D), and 116 (E).

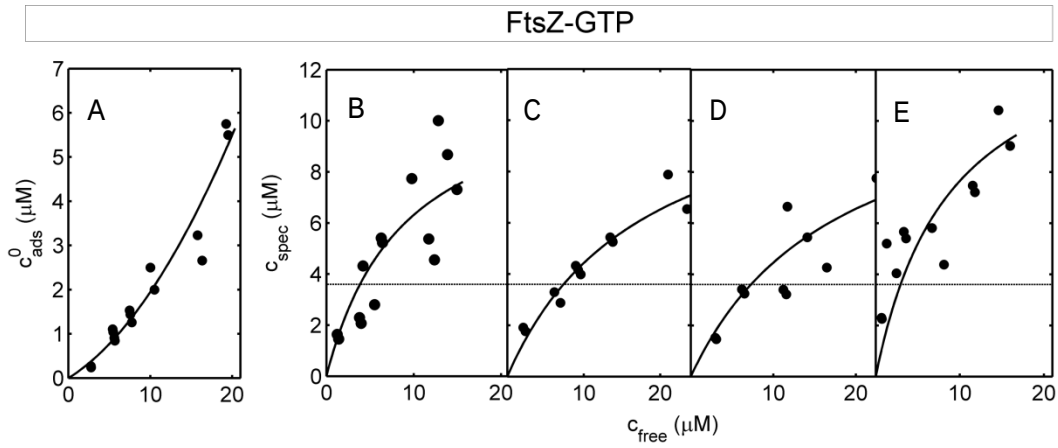

Figure 1.3. FtsZ-GTP binding as a function of receptor density. Nonspecific adsorption (A) and specific binding (B-E) of FtsZ-GTP plotted as a function of the concentration of free FtsZ-GTP for various densities of s2ZipA, proportional to the percentage of NTA-bearing lipid coating the beads: (A) 0% NTA, (B) 0.5% NTA, (C) 2% NTA, (D) 5% NTA, (E) 10% NTA. Symbols are the data. Horizontal dotted lines are the amount of FtsZ that would completely cover the bead as a monolayer, calculated as described in the text. Curves were calculated using equations (1.1) – (1.3) with the following parameter values: A_1 = 0.115; A_2 = 0.0080; c_{50} = 8.9; $c_{spec}^{(max)}$ = 12.0 (B), 12.3 (C), 12.4 (D), and 14.5 (E).

In order to explore the extent to which the value of a best-fit parameter is determined by the data, the method of parameter scanning was employed (Saroff 1989). In brief, the parameter selected is constrained to a series of values within a range of values encompassing the best fit value and a constrained best fit is obtained via minimization of the sum of squared residuals through variation of the remaining parameters. The variance of the sum of squared residuals obtained from each of the constrained fits is compared to that obtained from the unconstrained fit via the Fisher F-test to determine the probability that the best least-squares fit obtained for a given value of the constrained parameter is statistically indistinguishable from that obtained from the unconstrained fit. The dependence of this probability is plotted as a function of c_{50} for the combined fits of all binding data for FtsZ-GDP and FtsZ-GTP in Figure 1.4.

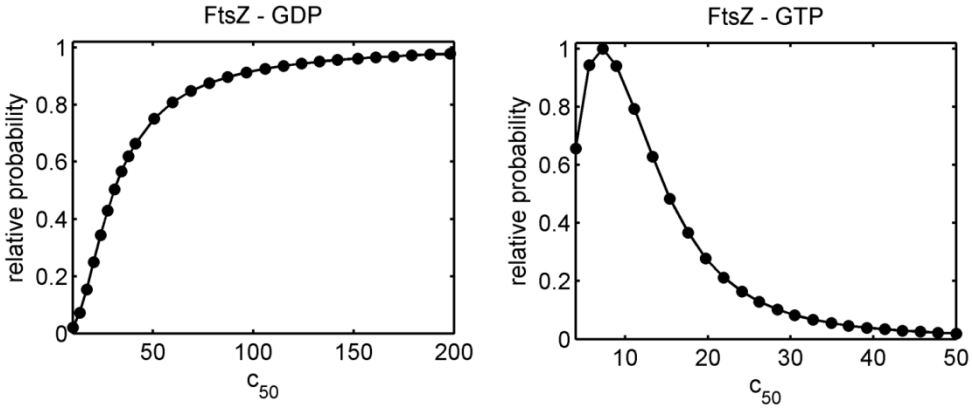

Figure 1.4. Probability distribution of c_{50}. Relative probability of a given value of c_{50} calculated from an F-test for equality of variances. Left – FtsZ-GDP, right – FtsZ-GTP.

These results may be summarized as follows. 1) The data for binding of FtsZ-GDP do not permit an upper limit to be established for c_{50}, *i.e*. the binding of FtsZ-GDP to bead-immobilized ZipA does not appear to be saturable. 2) The ratio of specifically bound to free FtsZ-GDP does appear to increase in rough proportion to the density of immobilized ZipA. 3) In contrast, the results obtained for binding of FtsZ-GTP indicate a well-defined upper limit to the possible value of c_{50}, *i.e*., the binding of FtsZ-GTP to bead-immobilized ZipA appears to be saturable and of substantially higher affinity than that of FtsZ-GDP. 4) The capacity of a bead for binding FtsZ-GTP does not appear to vary significantly with the density of immobilized s2ZipA. Any hypothesis as to the mechanism of binding FtsZ-GDP and FtsZ-GTP to bead-immobilized s2ZipA must account for these qualitative results as well as the observation, noted above, that binding of both FtsZ-GDP and FtsZ-GTP can substantially exceed the monolayer capacity of the beads.

DISCUSSION

In order to understand the binding of FtsZ to bead-immobilized s2ZipA and the differences between the binding of FtsZ-GDP and FtsZ-GTP, it is necessary to consider the states of association of free FtsZ-GDP and FtsZ-GTP in solution. Prior solution studies, as summarized in the introduction, have shown that under conditions very similar to those under which the present experiments were carried out, FtsZ-GDP from *E. coli* self-associates reversibly to form oligomers in accordance to a quasi-isodesmic association scheme, such that over the range of concentrations of free FtsZ

employed in the present study the weight-average molar mass can increase to around 4 times that of monomer. In contrast, under the conditions of our experiments, GTP elicits the concerted Mg-linked formation of a narrow size-distribution of higher-order oligomers, the mean size of which varies with pH and the amount of added electrolytes (Ahijado-Guzmán *et al.* 2013, González *et al.* 2005, Monterroso *et al.* 2012, Monterroso *et al.* 2012). Under the experimental conditions of the present study the oligomers so formed contain of the order of 50 monomers, and their relative homogeneity is compatible with the formation of closed cyclic (ring-like) structures, whose actual conformation in solution may be far from planar and not even close to circular in shape. The existence of the hypothesized cyclic oligomers was confirmed by electron microscopy and atomic force microscopic images (Mingorance *et al.* 2005). Interestingly, the formation of chiral ring-like vortices of FtsZ in lipid membranes under similar conditions to the ones used here has been recently described (Ramírez *et al.* 2016).

The consequences of the difference in states of association of free FtsZ-GDP and FtsZ-GTP are several. (1) Although the intrinsic affinity of an individual FtsZ for s2ZipA does not seem to depend upon whether it is complexed to GDP or GTP, as evidenced in nanodiscs (Hernández-Rocamora *et al.* 2012), the significantly larger-sized FtsZ-GTP oligomer has a correspondingly larger avidity when presented with multiple immobilized s2ZipA acceptors. (2) Because FtsZ-GDP oligomers are linear at the protein concentrations used in this study and self-association of FtsZ-GDP is not affected by the binding of ZipA (Hernández-Rocamora *et al.* 2012, Martos *et al.* 2010), the binding of FtsZ-GDP to immobilized s2ZipA does not diminish the number of sites available for growth of these oligomers, and a corresponding increase in the amount of bead-bound FtsZ is observed. In contrast, under the conditions of our experiments the FtsZ-GTP oligomers are large and fixed in size, and therefore do not provide additional binding sites to subsequently introduced FtsZ-GTP. Once a sufficient number of these oligomers are bound to the surface to render any un-complexed s2ZipA sterically inaccessible to additional free FtsZ-GTP oligomers, the beads appear to become saturated.

Prior studies of the binding of FtsZ to surface-immobilized ZipA at higher densities than the limiting lower case (namely, the nanodisc measurements described by Hernández-Rocamora *et al*. (Hernández-Rocamora *et al.* 2012)) were based upon observations made with total internal reflection fluorescence microscopy (Loose and Mitchison 2014), atomic force microscopy (Mateos-Gil *et al.* 2012), and by internal

reflection interferometry (Du *et al.* 2015). The former two studies correspond to complex formation of FtsZ-GTP while the latter one involves FtsZ-GDP. The present study differs from these three in two major respects. 1) The results presented here are obtained from direct measurements of binding under equilibrium conditions, whereas the prior studies report measurements of properties that are indirect measures of binding, where the relationship between the magnitude of reported signal and the actual amount bound was not quantified. 2) The present results were obtained over a much broader range of concentration of free FtsZ, up to 20 μM, as contrasted with concentrations less than 2 μM in the earlier studies. On the other hand, assays in these three studies were performed at fixed s2ZipA concentrations high enough to almost cover the entire membrane surface.

The second factor is of primary importance because a broader range of protein concentration provides a clearer and more comprehensive picture of the total binding phenomena. Under the conditions of our experiments, as the concentration of FtsZ in solution increases from 1 μM to 20 μM, the weight-average stoichiometry of FtsZ-GDP *in solution* increases from ~ 1 at 1 μM to ~5 at 20 μM (Rivas *et al.* 2000), while the weight-average stoichiometry of FtsZ-GTP *in solution* increases from ~ 1 at 1 μM to ~55 at 20 μM (Ahijado-Guzmán *et al.* 2013). Hence, as the concentrations of FtsZ-GDP and FtsZ-GTP increase, we are increasingly observing binding of small FtsZ oligomers of FtsZ-GDP and very large oligomers of FtsZ-GTP to the bead. These oligomers do not need to lie parallel to the plane of the surface, and as the fractional area occupancy of the surface becomes significant, steric repulsion between adjacent oligomers will increasingly favour “end-on” conformations of bound oligomers in order to minimize the high free energy cost of area exclusion (Minton 1999). It follows that FtsZ can bind in excess of the amount calculated to correspond to a monolayer of FtsZ per bead, as we have observed.

The mechanism of binding of FtsZ-GDP and FtsZ-GTP to surface-immobilized ZipA proposed here may be compared to that proposed by Du *et al* (Du *et al.* 2015). We both agree that higher-order FtsZ-GDP oligomers bind more strongly to immobilized ZipA. We extended these measurements to FtsZ-GTP, showing the significantly larger-sized FtsZ-GTP oligomer has a correspondingly larger avidity when presented with multiple immobilized ZipA acceptors, accounting for its smaller c_{50}. However, in Figure 9 of Du *et al*., a mechanism is proposed according to which FtsZ binds to surface-immobilized ZipA as linear oligomers in a single layer parallel to the surface,

independent of whether it is complexed to GDP or GTP. This mechanism is qualitatively incompatible with results of the direct measurement of equilibrium binding under well-defined conditions reported here.

In conclusion, the experiments reported here show that the amount of FtsZ bound to surface-immobilized s2ZipA can greatly exceed a stoichiometric ratio of unity due to the oligomerization of FtsZ. In the case of FtsZ-GDP, the ability of linear surface-associated FtsZ oligomers to continue to grow in the presence of increased concentrations of free FtsZ-GDP leads to bead unsaturability, as illustrated schematically in Figure 1.5A. Although oligomers of FtsZ-GTP are much larger than those of FtsZ-GDP, they form narrowly-sized compatible with cyclic structures that cannot further grow, and so when the bead has been "covered" by bound FtsZ-GTP oligomers, the bead is saturated, as illustrated schematically in Figure 1.5B.

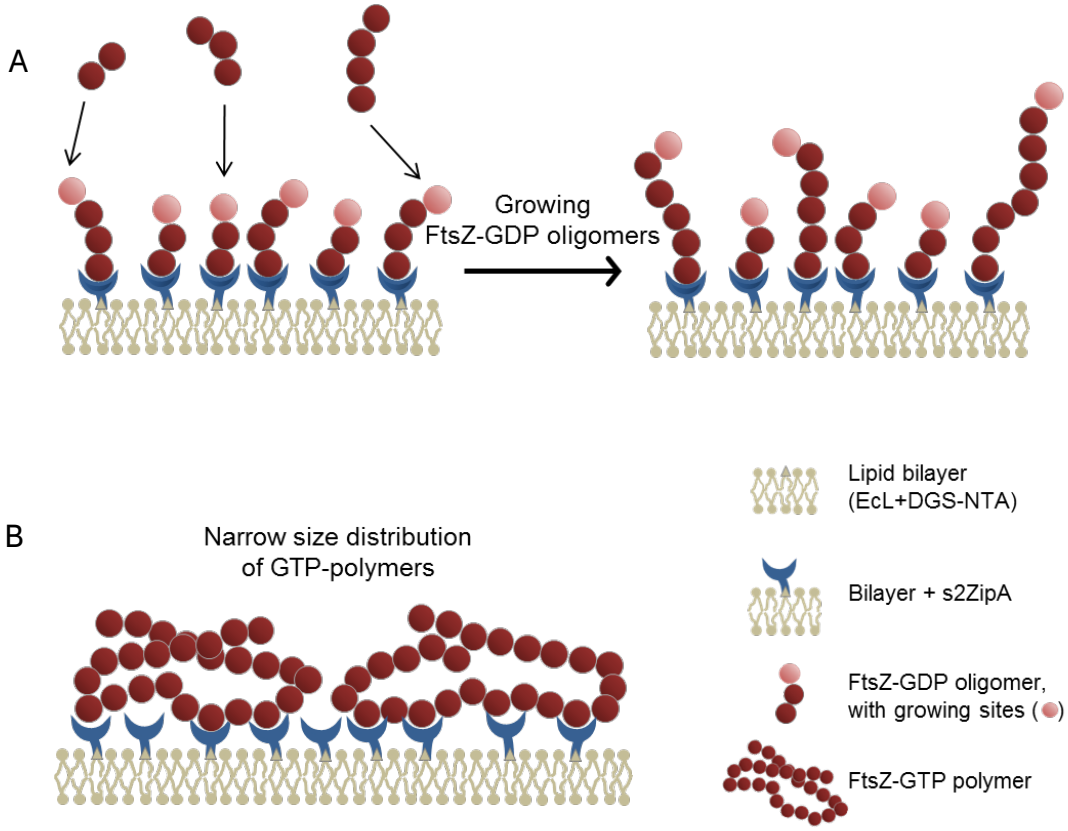

Figure 1.5. Schematic illustrations of FtsZ binding to bead-immobilized s2ZipA. (A) Surface-bound linear FtsZ-GDP oligomers have the ability to continuously incorporate more FtsZ through binding to free fibril ends (indicated in light pink) upon increase of FtsZ concentration. (B) In contrast, upon binding to the bead surface in sufficient quantity, the narrow size distribution of the FtsZ-GTP oligomers block access to growth sites, thus precluding additional FtsZ binding.

CHAPTER 2

Reversible membrane-tethering by ZipA determines FtsZ polymerization in two and three dimensions

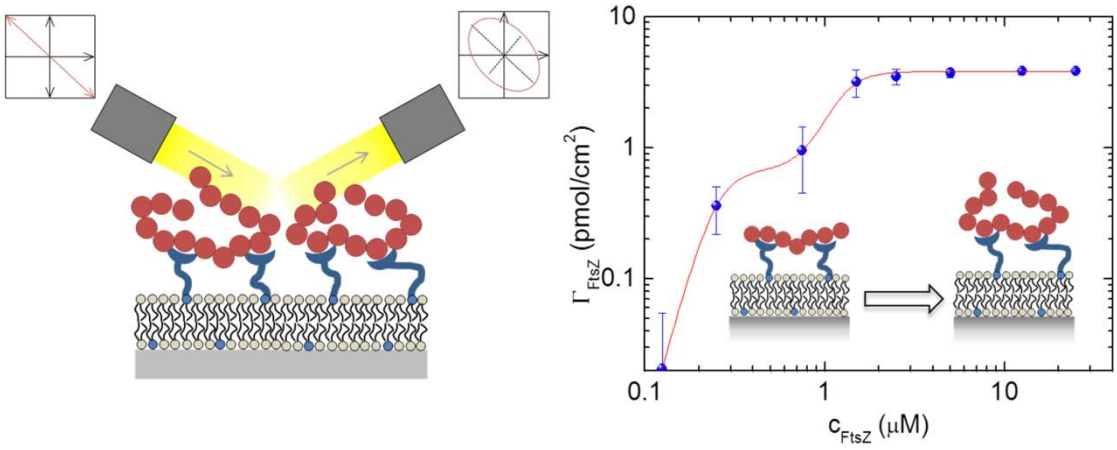

The initial steps of divisome assembly in most bacteria are linked to the attachment of the cytosolic FtsZ protein to the membrane through interactions with additional proteins, ZipA and FtsA in the case of *E. coli*, forming the scaffold structure (the proto-ring) into which the rest of the division proteins are subsequently incorporated. Here we measured the binding of FtsZ to ZipA incorporated in supported lipid bilayers at controlled surface receptor densities by using a combination of biophysical surface-sensitive techniques and analysed how ZipA density and the state of assembly of FtsZ (modulated by nucleotide) influence the binding and mechanical properties of the complexes formed. In this way, we have demonstrated that the receptor density modulates both the binding of FtsZ-GMPCPP to ZipA and the organization of the polymer film at the membrane, as revealed by biophysical approaches (QCM-D and SE). Our studies have also established that FtsZ-GMPCPP binding to ZipA-containing bilayers occurs in two phases, corresponding to the different modes of polymer extension on the surface and to the bulk solution. Both the equilibrium binding properties and the kinetics of dissociation from the membrane of FtsZ-GMPCPP polymers were different from the ones found for the GDP form of FtsZ. These results provide insights on the mode of interaction of proto-ring elements in minimal membrane systems and contribute to complete our understanding of the early events of bacterial division.

RESULTS

2.1 Preparation of model membranes displaying s1ZipA

Supported lipid bilayers made of DOPC provided a suitable platform to anchor s1ZipA to the lipid layer, as schematically illustrated in Figure 2.1A. The density of anchoring sites was tuned by controlling the amounts of tris-NTA-functionalized lipids in the SLB to which s1ZipA binds specifically. The s1ZipA grafting density (Γ_{ZipA}), quantified by spectroscopic ellipsometry (SE), was found to be linearly dependent on the fraction of tris-NTA lipids in the liposomes from which the SLBs were prepared (Figure 2.1B). From these data, the mean spacing s_{ZipA} between s1ZipA receptors could also be calculated (Figure 2.1B).

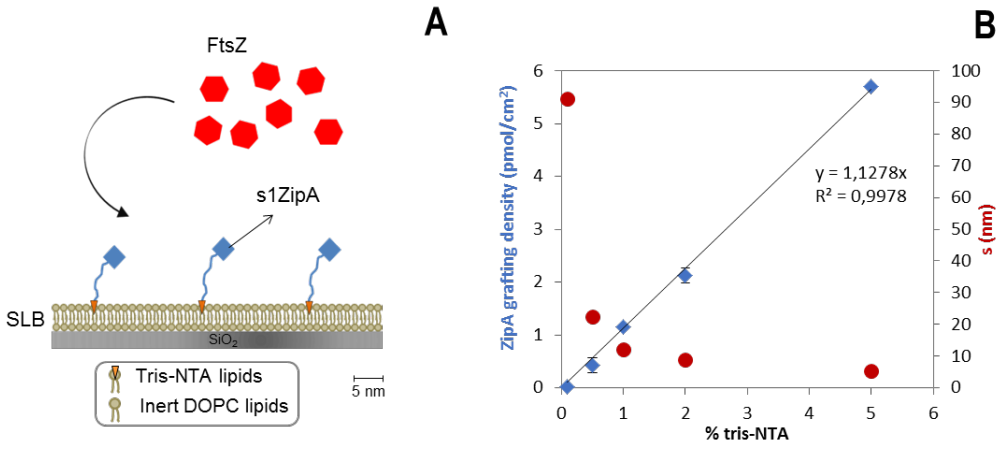

Figure 2.1. Design of s1ZipA dispaying model membranes. (A) Scheme of bacterial s1ZipA-FtsZ interaction reconstituted on a silica-supported lipid bilayer (SLB). Protein and lipid sizes are drawn approximately to scale. Scale bar is included for reference. (B) Variation of the s1ZipA grafting density (Γ_{ZipA}, blue symbols; measured by spectroscopic ellipsometry) and the average inter-s1ZipA spacing (s_{ZipA}, red symbols; calculated as root-mean-square distance) as a function of tris-NTA content in the SLB (expressed in % of tris-NTA lipids in the liposomes from which the SLBs were formed). Error bars represent standard deviations from at least two independent measurements. The black line is the result of a linear fit through the origin, giving a slope of 1.13 ± 0.02 pmol/cm² s1ZipA per % NTA.

The assembly of the model membranes with s1ZipA at selected surface densities was monitored by quartz crystal microbalance with dissipation monitoring (QCM-D). SLBs were formed by spreading vesicles with the appropriate proportion of tris-NTA lipids, on silica surfaces (Figure 2.2, step 1).

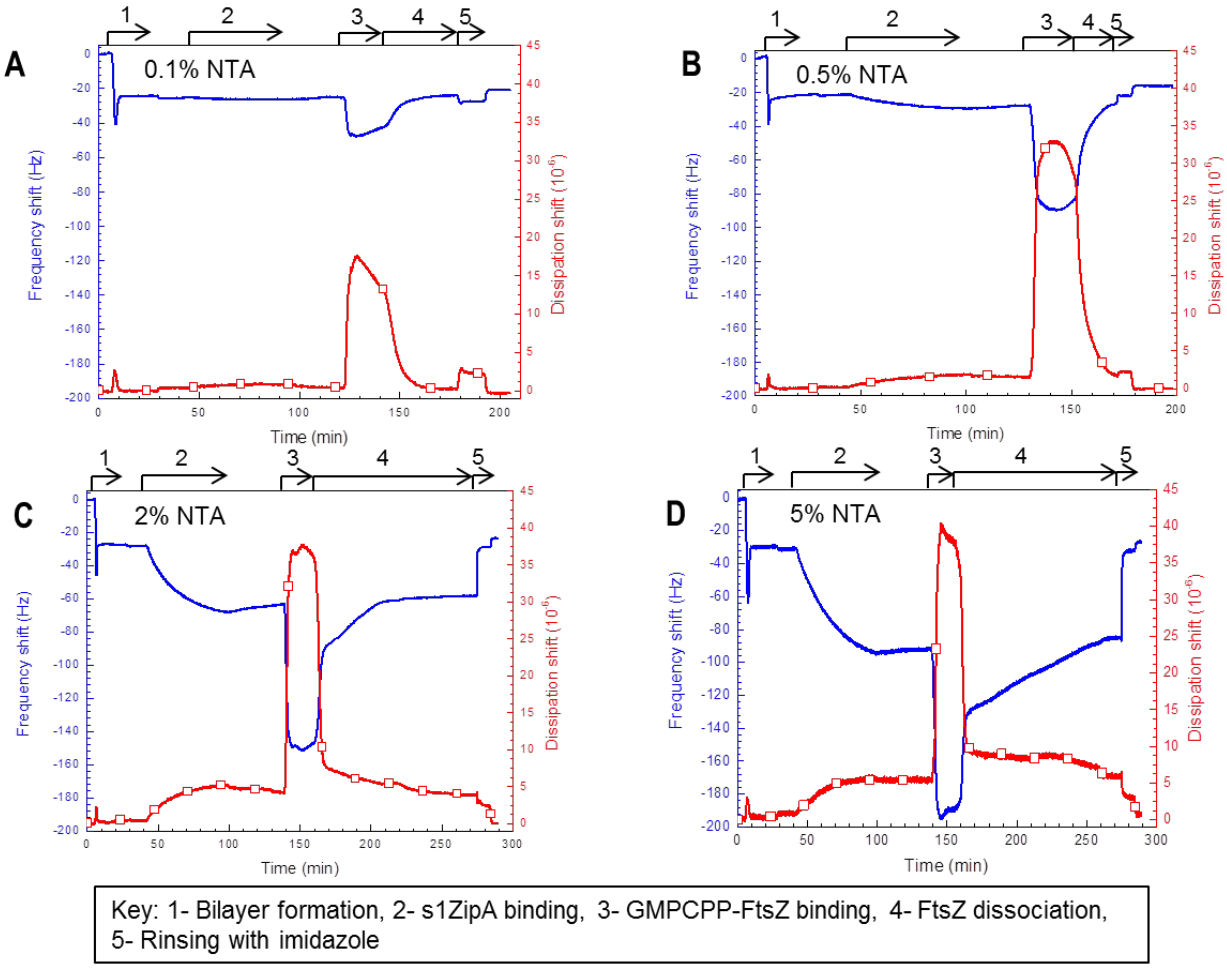

Figure 2.2. QCM-D analysis of model membrane assembly and FtsZ-GMPCPP (polymer) binding as a function of s1ZipA surface density. Data on four SLBs with distinct tris-NTA content are shown (A - 0.1%, B - 0.5%, C - 2%, D - 5%) corresponding to a range of s1ZipA surface densities (see **Figure 2.1B**). Shifts in frequency (Δf - blue lines) and dissipation (ΔD - red lines with open squares) were registered by QCM-D for the sequential incubation with NTA-containing vesicles (50 µg/mL; step 1, leading to the formation of SLBs), s1ZipA (10 µg/mL; step 2) and FtsZ-GMPCPP (10 µM; step 3). Step 4 corresponds to rinsing with GMPCPP-containing buffer, and step 5 to washing with 0.5M imidazole-containing ultrapure water. At all other times the surfaces were exposed to plain working buffer. QCM-D is mostly sensitive to process occurring close to the sensor surface; however, the changes in Δf and ΔD upon exchange from imidazole containing solution to plain working buffer do not reflect any changes on the surface but result from a change in the viscosity and/or density of the surrounding solution owing to the high imidazole concentrations.

The transient minima in the frequency shift and maxima in the dissipation shift reflect the binding of initially intact vesicles which subsequently rupture and coalesce into complete SLBs. The shifts of Δf = -25±2 Hz and $\Delta D \approx 0.2 \pm 0.1 \times 10^{-6}$ at the end of the vesicle incubation process were consistent with the formation of SLBs of good quality (Richter *et al.* 2006). The Δf and ΔD responses associated with the subsequent injection of s1ZipA (Figure 2.2, step 2) depended in their magnitude upon the Ni^{2+}-

loaded tris-NTA, as expected, and were consistent with the formation of s1ZipA monolayers of various surface densities. Whilst s1ZipA binding was hardly detectable at the lowest tris-NTA proportion (0.1% tris-NTA; Figure 2.2A), a frequency shift of $\Delta f \approx$ -63 Hz was reached at the highest proportion (5% tris-NTA; Figure 2.2D). This corresponds to a layer thickness of ~9 nm, consistent with the dimensions of the s1ZipA construct (globular domain of ~3 nm of diameter concatenated to a flexible region that can be found extended or folded, according to (Ohashi *et al.* 2002)). We can ascribe the relatively high associated dissipation shift ($\Delta D \approx 5 \times 10^{-6}$) to the presence of the flexible linker that connects the globular FtsZ binding domain to the SLB (Johannsmann *et al.* 2009) and provides some compliance to the protein film. A typically minor fraction of s1ZipA was released upon rinsing with buffer, whilst the rest remained largely bound upon rinsing (after step 2 in Figure 2.2) but was readily eluted with imidazole (Figure 2.2, step 5), indicating stable and specific anchorage through the His tags as desired. For quantitative analysis, Γ_{ZipA} was defined as the quasi-stable binding of s1ZipA after rinsing with buffer for at least 30 minutes.

2.2 Interaction of FtsZ-GMPCPP polymers with s1ZipA-displaying SLBs

Prior solution studies have shown that GMPCPP (0.5 mM) elicited the concerted and Mg^{2+}-dependent formation of polymers in solution, the mean size of which depends on pH and ionic strength (Ahijado-Guzmán *et al.* 2013). At the working conditions used here (300 mM KCl), they consist of 200-300 monomers. These higher-order FtsZ species formed hetero-complexes with s1ZipA contained at lipid bilayers, as revealed by QCM-D and SE assays.

· **Association.** QCM-D assays demonstrated binding of FtsZ-GMPCPP to all model membranes when incubated at 10 µM (Figure 2.2, step 3). Clear QCM-D responses were observed even on 0.1% tris-NTA (Figure 2.2A) where s1ZipA binding was at the detection limit. In contrast, no binding of FtsZ was detected on SLBs lacking s1ZipA (Figure 2.3A), confirming that FtsZ binds specifically to s1ZipA. It has previously been shown that peptides derived from the C-terminal region of FtsZ containing the central hub region (Ortiz *et al.* 2015) inhibited the binding of FtsZ polymers to ZipA contained in nanodiscs (Hernández-Rocamora *et al.* 2012). To check the specificity of FtsZ binding, similarly, we found here that such peptides also compete with FtsZ polymers for binding to s1ZipA anchored to SLBs (Figure 2.3B).

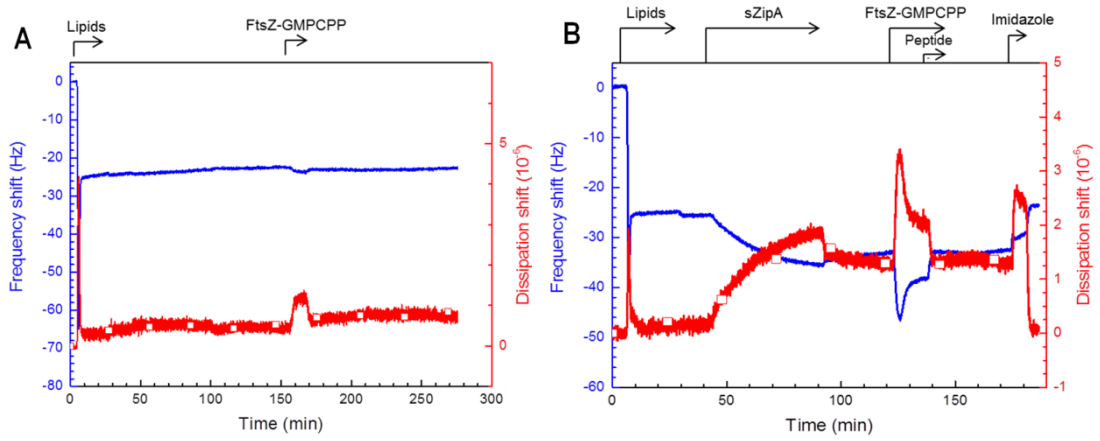

Figure 2.3. Controls for specificity of FtsZ binding. (A) Representative QCM-D data (frequency shift – blue line, dissipation shift – red line with open symbols) for the binding of FtsZ-GMPCPP to a s1ZipA-free bilayer. Arrows on top of the graph indicate the start and duration of incubation with liposomes (made of pure DOPC) and FtsZ-GMPCPP (10 μM); remaining times correspond to rinsing steps with working buffer. Only a very small response is observed upon FtsZ incubation, indicating that non-specific binding of FtsZ to SLBs is negligible. (B) Representative QCM-D data (displayed as in B) at 0.5% s1ZipA and 2.5 μM FtsZ-GMPCPP demonstrating effective displacement of FtsZ from s1ZipA-displaying SLBs by competition with a molar excess (110 μM) of peptide derived from the C-terminal ZipA binding domain of FtsZ. The concentration of imidazole was 0.5 M.

· **FtsZ film morphology and reorganization.** A prominent feature that can be observed for all s1ZipA surface densities is that FtsZ binding induced large dissipation shifts (Figure 2.2). Maximal dissipation shifts of typically several 10×10^{-6} are incompatible with the formation of a simple monolayer of globular proteins and thus indicate that FtsZ forms polymers at the SLB surface that emanate into the solution phase and generate a soft polymer film. These polymer films assemble fast, as witnessed by the rapid decrease in frequency during the first few minutes after FtsZ injection. Another salient feature of FtsZ binding is that the QCM-D responses do not appear to reach any equilibrium (Figure 2.2). Instead, frequency and dissipation show one (in the case of 2% and 5% tris-NTA even two) transient extrema and following this, the frequency slowly increases and the dissipation slowly decreases. This complex QCM-D response provides evidence that the FtsZ polymer film continues to reorganize over times of 20 minutes and more. Whilst QCM-D does not provide direct information about the ultrastructure of the polymer film, we can suggest based on the gross data that this reorganization reflects the formation of higher order polymer complexes such as polymer bundles.

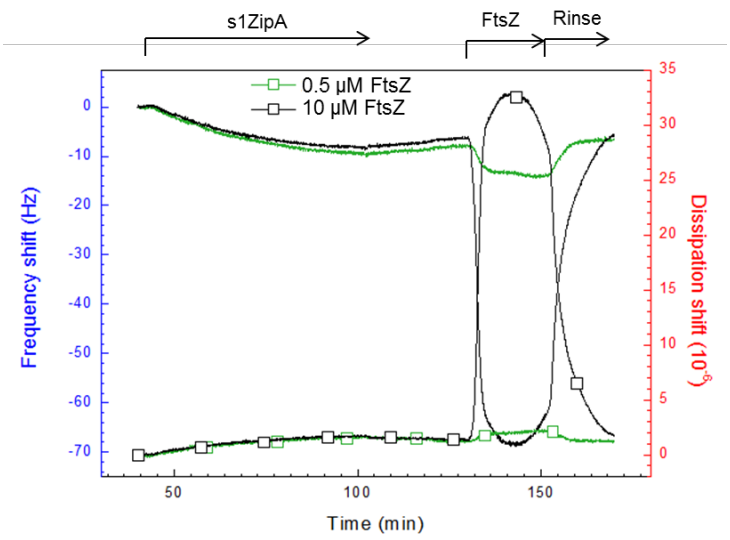

Figure 2.4. Dependence of FtsZ-GMPCPP film morphology on FtsZ concentration. QCM-D data (Δf - solid lines, ΔD – solid lines with open squares) on SLBs with a selected tris-NTA content (0.5%) and two distinct FtsZ-GMPCPP concentrations (0.5 μM – green, 10 μM – black). Start and duration of incubation steps with different samples are indicated with solid arrows on top of the plot; during remaining times the surfaces were exposed to plain working buffer.

It is notable that the complex QCM-D response was characteristic for high FtsZ concentrations (10 μM). When the FtsZ concentration was lowered to 0.5 μM, a much simpler response was obtained. As illustrated for 0.5% tris-NTA in Figure 2.4, FtsZ binding at 0.5 μM produced QCM-D responses of much smaller magnitude than at 10 μM but the binding readily attained equilibrium within 5 minutes of incubation. That the dissipation increased only marginally at 0.5 μM (by $\Delta D \approx 1 \times 10^{-6}$, compared to 32×10^{-6} at 10 μM) suggests that FtsZ polymers do no longer grow into the solution phase when the FtsZ concentration is lowered below the concentration required for polymerization in solution (1 μM at our working conditions) (Lutkenhaus 1998, Rivas *et al.* 2000).

· **Dissociation.** The dissociation of FtsZ-GMPCPP from the s1ZipA-displaying membrane, after rising with nucleotide-containing buffer, was fully reversible at all the receptor densities assayed (Figure 2.2, step 4). Interestingly, whilst FtsZ dissociated in a single continuous event on SLBs with the lower s1ZipA densities (0.1% and 0.5% tris-NTA, corresponding to average distances between s1ZipA molecules of about 90 and 20 nm respectively; Figure 2.2A-B), the detachment occurred in two clearly distinct phases at the higher s1ZipA densities (2% and 5% tris-NTA; Figure 2.2C-D). The frequency increased rapidly in the first phase (which lasted a few minutes) and much

more slowly (and markedly linear) in the second phase. These two phases may correspond either to the release of two different polymer species or to polymer conformational changes during the dissociation process. That the dissipation shifts reached a level of only a few times 10^{-6} at the end of the first phase (Figure 2.2C-D) suggests that polymers that emanate into the solution phase dissociate in the first phase whilst polymers that are closely associated to the membrane are retained for longer and dissociate in the second phase.

· **Quantification of FtsZ surface densities and identification polymer growth regimes.** To quantify FtsZ binding to s1ZipA-displaying SLBs, we performed titration assays with SE over a broad range of FtsZ concentrations (0.12 to 25 µM) and s1ZipA surface densities (0.5 to 5% tris-NTA, or 0.43 to 5.7 pmol/cm^2). These revealed binding in a FtsZ-concentration and s1ZipA-surface-density dependent manner (Figure 2.5). Even though the QCM-D assays indicated FtsZ films undergo prolonged reorganization processes at high concentrations, we found by SE that the FtsZ surface densities generally reached equilibrium within experimental time scales thus facilitating analysis with equilibrium thermodynamic models.

The binding isotherm of FtsZ-GMPCPP to s1ZipA contained on 0.5% tris-NTA SLBs revealed two discrete association processes (Figure 2.5A) occurring below and around the critical concentration for FtsZ polymerization in solution (1 µM), respectively. The steepest slopes defined by the experimental data (*i.e.*, between 0.12 and 0.25 µM for the first regime, and between 0.5 and 2 µM for the second regime are superior to one, indicating that both binding processes are cooperative. It is notable that the onset of the second binding phase coincides with the minimal concentration required for FstZ polymerization in solution (1 µM).

In addition to the protein surface density, SE also provides estimations of the protein film thickness. Interestingly, the film thickness ($d_{s1ZipA+FtsZ}$) also showed two distinct regimes (Figure 2.5B): up to 0.5 µM FtsZ-GMPCPP, the thickness was essentially constant (around 15 nm), and above 0.5 µM FtsZ-GMPCPP, the thickness increased sharply to reach a new and much higher plateau value (around 40 nm). The value of the increase in thickness was found to be dependent upon s1ZipA grafting density (Figure 2.6A) in a rather weak way, since only small differences were observed between s1ZipA densities.

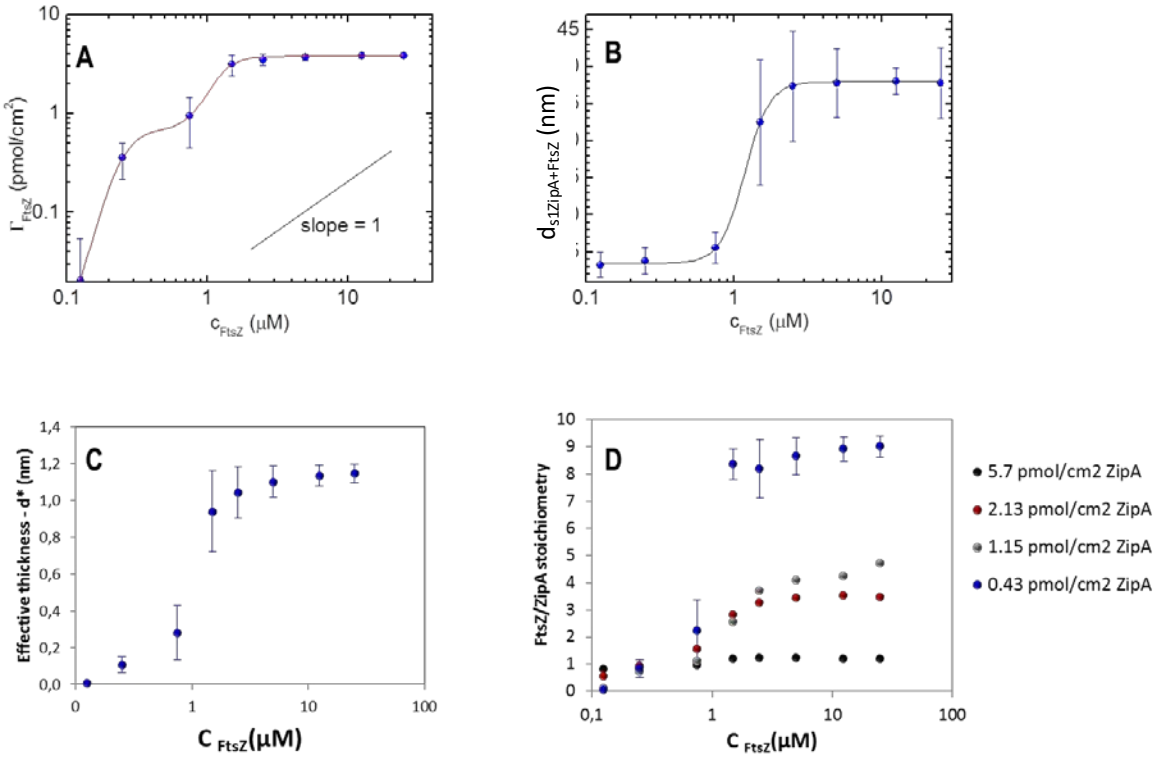

Figure 2.5. Quantification of FtsZ-GMPCPP binding to s1ZipA. (A-B) SE data for s1ZipA-displaying SLBs (0.5% tris-NTA, or 0.43 pmol/cm^2 s1ZipA), with mean and minima/maxima of at least two independent measurements: (A) Surface density of polymer-forming FtsZ as a function of FtsZ-GMPCPP concentration. In this double-logarithmic plot, a dashed line with a slope of 1 is shown for reference. The fitting of the data was modelled with a sum of two Hill terms. (B) Estimation of the s1ZipA+FtsZ-GMPCPP film thickness d_F as a function of FtsZ-GMPCPP concentration. These data were fitted with a conventional Hill equation. (C) Stoichiometry of FtsZ-GMPCPP binding to s1ZipA determined from SE titration assays for different s1ZipA surface densities (0.43 to 5.7 pmol/cm^2, as indicated). (D)SE data for FtsZ/ZipA binding stoichiometry, calculated from grafting density values of s1ZipA and FtsZ. All data are from individual measurements, except at 0.43 pmol/cm^2 s1ZipA where the mean and minima/maxima of two independent measurements are presented.

Consistent with the above-presented QCM-D data, we propose that the sharp increase in film thickness above 0.5 µM FtsZ-GMPCP (Figure 2.5B) can be ascribed to 3D polymerization whilst the constant thickness up to 0.5 µM represents a two dimensional FtsZ film. The 3D thickness growth was found to be well described by a conventional Hill equation. The resulting association constant was $K_{0.5}$ = 1.18 ± 0.04 µM and the Hill coefficient was 5.2 ± 0.4. These values should be considered effective since it is not known if thickness is proportional to FtsZ surface density; however, both the $K_{0.5}$ value and the high degree of cooperativity are fully consistent with previous reports on FtsZ polymerization in solution (Hernández-Rocamora *et al.* 2012, Martos *et al.* 2010).

The binding data (Figure 2.5A) was modelled with a sum of two Hill terms, in which the first term (index 2D) is attributed to 2D polymerization and the second term (index 3D) to 3D polymerization. Although all the parameters could not be determined simultaneously with good confidence, when K_{3D} and n_{3D} were fixed to the values obtained from the thickness analysis, all other parameters could be well determined within narrow confidence intervals. The results of this modelling exercise revealed that 1) the maximal binding for phase 1 (Γ_{2D} = 0.68 ± 0.20 pmol/cm^2) is of a magnitude comparable to the surface density of ZipA (0.43 pmol/cm^2) and 2) the Hill coefficient for 2D polymerization (n_{2D} = 5.2 ± 1.1) is comparable to the Hill coefficient for 3D polymerization estimated from thickness analysis. In this case, the best-fit value of the association constant (K_{2D}) was found to be 0.24 ± 0.04 µM.

These results strongly suggest a scenario in which FtsZ binding throughout the first regime is confined to the immediate vicinity of the s1ZipA-displaying membrane. A plausible explanation for the observed cooperativity of binding in this regime (≤ 0.5 µM) is that the high local concentration at the membrane promotes the polymerization of FtsZ in two dimensions. The second binding regime (>0.5 µM) would represent the three-dimensional growth of s1ZipA-tethered polymers into the bulk solution which may then also involve reorganization into higher-order polymer complexes (see Figures 2.2 and 2.4).

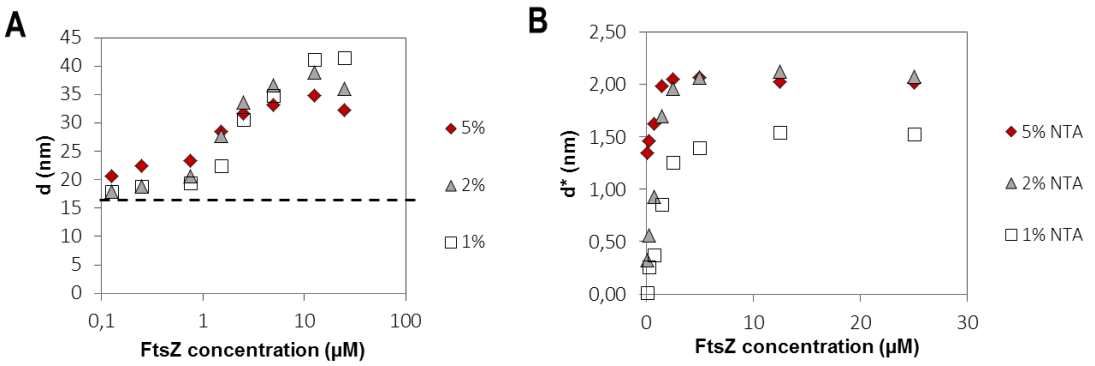

Figure 2.6. (A) Stimation of GMPCPP-FtsZ film thickness (*d*) in nanometers measured by ellipsometry at different s1ZipA densities. (B) Equivalent GMPCPP-FtsZ film thickness (*d**) in nanometers.

· **Density of the FtsZ polymer film.** The FtsZ surface density saturated at approximately 4 pmol/cm^2 (Figure 2.5A). The estimation of an equivalent film thickness (*d**) allowed us to discard the volume that FtsZ itself excludes and elucidate if the total amount of bound polymers could fit into a monolayer. This parameter is calculated as

(Γ_{FtsZ}*MW_{FtsZ})/ρ, where MW_{FtsZ} is the molecular weight of FtsZ and ρ = 1.35 g/cm^3 is the density of peptides in water. For densely packed films of globular proteins, we tend to find that water occupies around 50% of the volume in the film, so the geometric thickness is likely to be at least twice *d**. In our experiments, we find *d**≤ 2 nm (Figure 2.6B). If we assume FtsZ to be densely packed, then we can estimate a geometric thickness of 2*d**, which would be maximum 4 nm. The FtsZ monomer is ~4 nm long and ~5 nm wide (Lowe and Amos 1998), so the total amount of bound FtsZ would hence fit into a monolayer on the surface, even at the highest s1ZipA surface density. If instead, as the QCM-D and SE data show, the FtsZ polymers grow into the solution phase then this implies that the monomer crowding at the membrane is at most moderate.

· **Stoichiometry of ZipA-FtsZ binding.** The SE data also enabled a direct quantitative comparison of the surface densities of FtsZ and s1ZipA, and hence also allowed estimating the stoichiometry of binding of FtsZ-GMPCPP to s1ZipA. The results (Figure 2.5D) reveal that binding was saturable for all tested sZipA surface densities. The maximal number of FtsZ subunits bound per s1ZipA was found to decrease as the surface density of receptors increased, from a value close to 10 at 0.43 pmol/cm^2 s1ZipA (0.5% tris-NTA) to 1.0 at 5.7 pmol/cm^2 s1ZipA (5% tris-NTA). At high s1ZipA surface densities only a fraction of s1ZipA is occupied, meaning that steric hindrance between polymers rather than s1ZipA defines how dense the polymer film becomes. On the other hand, at low s1ZipA surface densities, almost all FtsZ molecules seem to be bound to s1ZipA in the first binding regime. In the second binding regime, the majority of FtsZ oligomers is not directly bound to s1ZipA (Figure 2.5D). These results show that the distance between s1ZipA molecules at low surface density allow the accommodation of a larger number of FtsZ assembled subunits at the vicinity of the membrane, whereas an excess of s1ZipA on the surface leads to steric hindrance among adjacent FtsZ polymers, thereby lowering the average occupancy of binding sites.

2.3 Interaction of FtsZ-GDP oligomers with s1ZipA-displaying SLBs

Next, to assay the effect of the nucleotide bound to FtsZ on the kinetics of association to s1ZipA at the membrane and its subsequent dissociation from it, QCM-D experiments were performed in the presence of GDP instead of GMPCPP. Under the conditions used in our assays (variable FtsZ concentrations in buffer with 300 mM KCl

and 5 mM $MgCl_2$), FtsZ-GDP has been shown to self-associate and form short oligomers from monomers in a non-cooperative fashion, with hexamers being the largest species detectable (Martos *et al.* 2010).

At 2.5 µM, FtsZ bound to s1ZipA-displaying SLBs (0.5% tris-NTA) in a single and rapid phase (Figure 2.7A) which presumably corresponds to the binding of pre-formed FtsZ-GDP oligomers to s1ZipA. Such a phase was also observed at 10 µM with slightly larger magnitude, but a second phase was additionally observed that was slow and did not saturate within the typical incubation time of 20 minutes in our experiments (Figure 2.7B). This behaviour was unlike FtsZ-GMPCPP polymers, for which binding was saturable (Figure 2.5) and involved prolonged reorganisation (Figure 2.2). The lack of saturation precluded a more detailed analysis of the binding process for FtsZ-GDP with thermodynamic models.

· **Dissociation of FtsZ-GDP from ZipA.** In contrast to FtsZ-GMPCPP polymers that was completely dissociated from s1ZipA during the washing step, at 0.5% s1ZipA and 10 µM FtsZ a significant fraction of FtsZ-GDP (corresponding to around 50% of the total bound protein) was found to remain stably bound to s1ZipA at the bilayer upon rinsing with buffer. Interestingly, this fraction could be dislodged from the membrane by a molar excess of a C-terminal FtsZ peptide (Figure 2.7B). This confirms that the bound FtsZ was specifically attached to s1ZipA via its genuine binding site. It highlights that the GDP-bound form of FtsZ dissociated more slowly from s1ZipA than the GTP/GMPCPP-bound form. The unsaturability of the interaction of s1ZipA with FtsZ-GDP precluded a more detailed analysis.

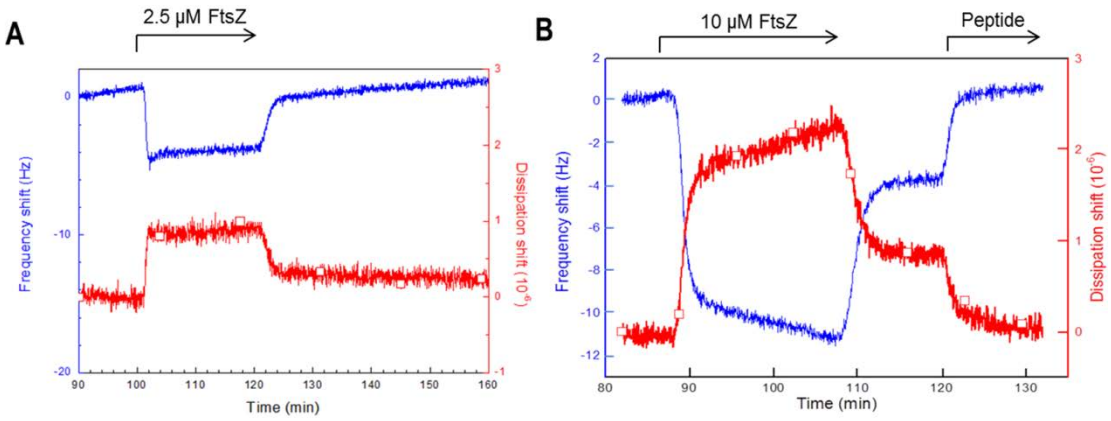

Figure 2.7. FtsZ-GDP binding to s1ZipA-displaying SLBs. QCM-D analysis (frequency shift – blue line; dissipation shift – red line with open symbols) of FtsZ-GDP binding to s1ZipA-displaying SLBs (0.5% tris-NTA, or 0.43 pmol/cm² s1ZipA): (A) 2.5 µM FtsZ-GDP, (B) 10 µM FtsZ-GDP and competition with FtsZ-derived peptide (110 µM). Arrows on top of the graphs indicate start and duration of injections with FtsZ-GDP or FtsZ-derived peptide, as indicated; during remaining times the surface was incubated with plain working buffer.

DISCUSSION

Despite their importance for bacterial cell division, multivalent interactions between proto-ring elements at membrane surfaces remain poorly characterized in quantitative terms. Here, using supported lipid bilayers as minimal membrane systems, we provide evidence that the surface density of s1ZipA modulates the binding of FtsZ-GMPCPP polymers to s1ZipA and the organization of the polymer at the membrane, as revealed by a combination of biophysical approaches (QCM-D and SE). Additionally, we show that binding association and dissociation of FtsZ-GMPCPP polymers were markedly different to the ones found for the GDP form of FtsZ.

Interestingly, our experiments were done using 0.1-5% tris-NTA lipids in order to control the density of ZipA on the bilayer to be closer to physiological levels than in previous reconstitution experiments (10% NTA: Mateos-Gil et al, 2013; Loose & Mitchison, 2014; Marquez et al. 2107). In fact, the lower surface density of s1ZipA used here corresponds to the expected for ZipA in *E. coli* cells, assuming that they were distributed uniformly.

The concentration dependence of FtsZ-GMPCPP binding to s1ZipA contained in the bilayer is compatible with two cooperative events. The first one, occurring at concentrations below the threshold value for FtsZ polymerization in solution, would correspond to binding of small oligomers of FtsZ to s1ZipA (Figure 2.8, reaction 1) followed by FtsZ polymerization in two dimensions at the surface (Figure 2.8, reaction 2). The second event would correspond to the three-dimensional growth of surface-bound FtsZ polymers towards the bulk solution, a behaviour that is compatible with the thickness estimated by SE (Figure 2.8, reaction 3).

Although the amount of FtsZ polymer bound to ZipA would fit in a monolayer at all densities, the polymers were found to grow in three dimensions rather than being confined to a monolayer at the vicinity of the membrane. This fact provides insights into the early stages of bacterial division, since the growth of FtsZ polymers into the bulk solution can have a biological implication for the division, probably related to the exposure of FtsZ central hub (C-terminal domain) to integrate signals from other proteins that are not located at the membrane. Our data suggests that the mode of polymerization that characterizes FtsZ in the solution phase persists for ZipA-tethered FtsZ, and is supplemented by the formation of higher-order polymer complexes (Figure 2.8, reaction 4).

QCM-D data showed that at all the ZipA surface densities assayed FtsZ-GMPCPP polymers behaved as a soft film, whose growth and softness was dependent upon FtsZ concentration. Interestingly, the equilibrium binding of FtsZ-GMPCPP polymers to ZipA-SLBs appears to be saturable at all the ZipA surface densities assayed. These observations are in very good agreement with results of Chapter 1 showing that the association of FtsZ-GTP polymers to ZipA-presenting lipid-coated beads also was saturable.

Contrary to the GMPCPP form of FtsZ, the binding of the FtsZ-GDP to ZipA was not saturable, in agreement with previous results on the association of FtsZ-GDP to ZipA contained in lipid-coated beads (Chapter 1). In this case, the binding unsaturability was related to the mode of association of the GDP form of FtsZ in solution, which is known to oligomerize according to a non-cooperative association scheme. In this way, the surface-associated FtsZ oligomers will continue growing as the free FtsZ concentration increases, leading to binding unsaturation. Interestingly, we have found that FtsZ-GMPCPP detaches from ZipA more easily than the FtsZ-GDP, despite the larger binding avidity of the FtsZ-GMPCPP polymers to membrane-associated ZipA when compared to the binding of the FtsZ-GDP oligomers. In this way, a significant fraction of the GDP form (around 50% of the total protein) remains stably attached to the surface and only can be dissociated by the addition of an FtsZ binding-sequence peptide.

These significant differences in the association/dissociation kinetics of both species may be due to different factors: (i) different modes of oligomers association to ZipA, (ii) different modes of FtsZ assembly or (iii) the presence of each nucleotide. This differential behaviour may have a biological implication on bacterial cell cycle, probably related to the requirements of FtsZ at the vicinity of the membrane at the moment of proto-ring formation. What looks clear from these differences is that GDP species seem to present a slowed-down binding/unbinding rate, while polymeric FtsZ shows a more dynamic behaviour, with quicker association/dissociation exchange rates, probably acting the nucleotide as a ‘switch’ activating the dynamism required for a proper bacterial division.

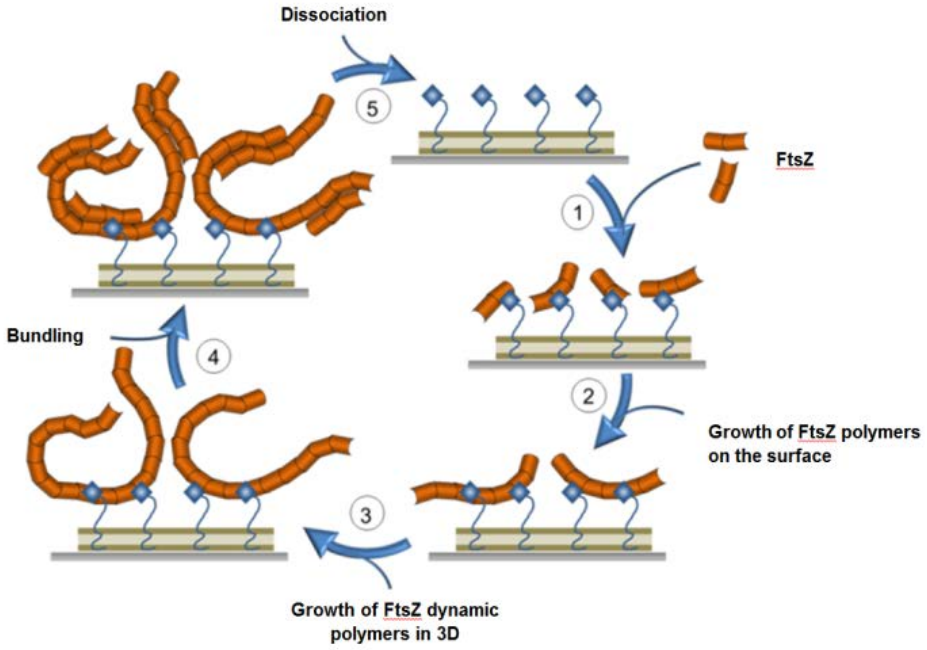

Figure 2.8. Model for dynamic association and dissociation of FtsZ from ZipA-containing membranes. ZipA recruits FtsZ oligomers to the membrane (1). Membrane-recruited FtsZ initiates the polymerization with the extension of FtsZ oligomers on the surface, in 2D (2). At this point, FtsZ polymers further polymerize in three dimensions, growing into the bulk solution (3). This favours the exposure of FtsZ C-terminal domain (central hub) for the potential recruitment of other modulators of FtsZ assembly. Lateral interactions allow FtsZ filaments to organize into higher-order structures, compatible with bundles (4). The detachment of FtsZ polymers from the membrane is complete upon rinsing (5).

To conclude, our experimental approach can easily be extended to other divisome elements or mixtures of them, and thus provides a robust tool for the screening of interactions with FtsZ in a well-controlled cell-like environment. Future studies will aim, in particular, at understanding the role of the C-terminus of FtsZ as a central hub integrating signals that modulate divisome assembly, and at elucidating the biochemical parameters that govern these multiple interactions at the proto-ring.

CHAPTER 3

Microenvironments created by liquid-liquid phase transition control the dynamic distribution of bacterial division FtsZ protein

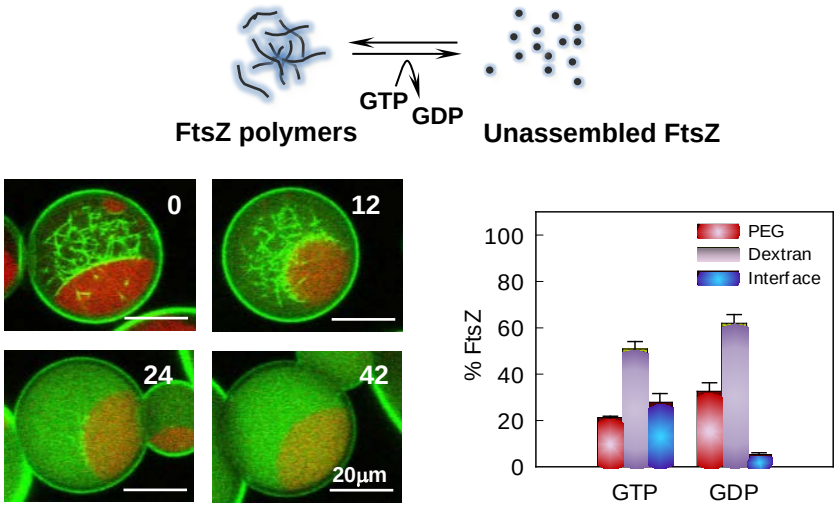

The influence of membrane-free microcompartments resulting from crowding-induced liquid/liquid phase separation (LLPS) on the dynamic spatial organization of FtsZ, the main component of the bacterial division machinery, has been studied using several LLPS systems. The GTP-dependent assembly cycle of FtsZ is thought to be crucial for the formation of the septal ring, which is highly regulated in time and space. We found that FtsZ accumulates in one of the phases and/or at the interface, depending on the system composition and on the oligomerization state of the protein. These results were observed both in bulk LLPS systems and in lipid-stabilized, phase-separated aqueous microdroplets. The visualization of the droplets revealed that both the location and structural arrangement of FtsZ filaments is determined by the nature of the LLPS system. Relocation upon depolymerization of the dynamic filaments suggests the protein may shift among microenvironments in response to changes in its association state. The existence of these dynamic compartments driven by phase transitions can alter the local composition and reactivity of FtsZ during its life cycle acting as a nonspecific modulating factor of cell function.

RESULTS

This chapter explores the assembly of FtsZ in the presence of coexisting liquid phases to mimic intracellular compartmentalization. Although macromolecular crowding is known to impact FtsZ polymerization, there are no studies of this protein in LLPS systems. We selected mixtures of crowders of different nature providing FtsZ with diverse environments and determined the distribution and partition of assembled and unassembled FtsZ in these systems. The potential functional implications of the preferential distribution of FtsZ polymers in microcompartments formed by phase transitions in cell-like crowded solutions are discussed. Prior work on functional consequences of intracellular microenvironments has focused on biomolecule partitioning and hypothesized that (co)localisation increases rates and regulation of enzymatic processes. This chapter adds a new dimension to thinking about potential intracellular roles for LLPS by showing how microenvironments might influence the distribution of key components of the bacterial cell division system as a function of their polymerization state.

To determine the effect of LLPS on the distribution of FtsZ species, we analysed the partition of the protein in biphasic systems of three different compositions. As polymerization is crucial for the function of FtsZ, we compared the behaviour of the polymers triggered by GTP with that of the small species the protein forms when bound to GDP. Three experimental approaches were conducted with all LLPS systems tested (Figure 3.1). Bulk emulsion and centrifuged bulk emulsion allowed the qualitative characterization of the distribution of the species and its quantification by fluorescence, respectively. Encapsulation of LLPS systems inside microscale lipid droplets was optimized for the characterization of the effect of relevant elements like boundaries and confinement in the distribution of the species and to evaluate the modulation of FtsZ location in response to changes in its association state.

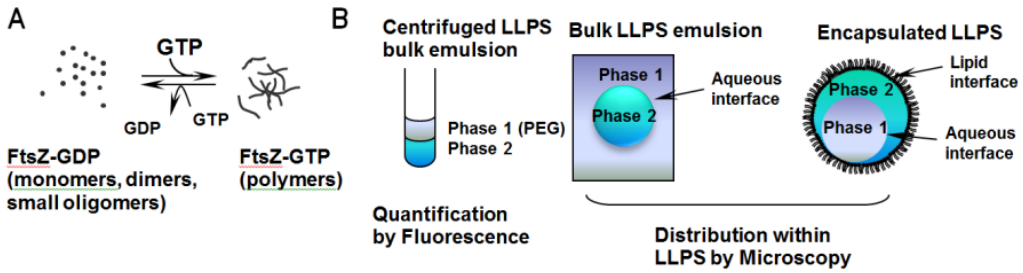

Figure 3.1. Overview of the biological system and experimental procedure. (A) Scheme of the association reactions of FtsZ. When bound to GDP, FtsZ is found as an ensemble of species of small size (Rivas *et al.* 2000). Upon GTP binding, and above the critical concentration of polymerization, FtsZ self assembles forming one subunit thick polymers of a defined size (Mateos-Gil *et al.* 2012, Monterroso *et al.* 2012), that in the presence of crowding agents interact laterally forming higher order structures (González *et al.* 2003, Monterroso *et al.* 2016, Popp *et al.* 2009). Depletion of the nucleotide by FtsZ GTPase activity increases the ratio of GDP, and the protein depolymerizes. (B) Experimental approaches followed. Left, LLPS systems with labelled FtsZ were centrifuged after thoroughly mixing. Both phases separate, the PEG-rich one being always located in the top part of the solution. The fluorescence in each phase is measured allowing quantification of FtsZ concentration. Qualitative distribution and organization of FtsZ was assessed by microscopy using bulk LLPS emulsions (middle) and LLPS emulsions encapsulated in lipid coated microdroplets (right). Each of these approaches was done with the three different LLPS compositions described in the main text.

3.1 The distribution of FtsZ in PEG/dextran LLPS systems is inhomogeneous and largely influenced by its association state

The first two-phase system selected to probe FtsZ behaviour was PEG/dextran 500, an LLPS system composed of two neutral polymers earlier used in phase separation studies (Dominak *et al.* 2010, Helfrich *et al.* 2005, Keating 2012). Confocal images of unassembled FtsZ-GDP showed colocalisation between FtsZ-Alexa 647 and fluorescein labelled dextran 500 droplets, indicating that most of the protein localises in this phase (Figure 3.2A). Significant FtsZ signal was also detected in the regions enriched in PEG, while no obvious accumulation of the protein was observed at the liquid/ liquid interface between the dextran droplets and the PEG rich phase. Fluorescence spectroscopy based determinations of the protein content in each of the phases indicated that ~60% FtsZ partitioned at the dextran-rich phase, ~30% into the PEG-rich phase and less than 10% was found at the interface (Figure 3.2B). The partition coefficient, *K*, was around 0.5, it did not substantially change within the 0.5–12 μM FtsZ concentration interval (Figure 3.3) and, under these conditions, was not sensitive to changes in the relative volumes of the two phases (Figure 3.4).

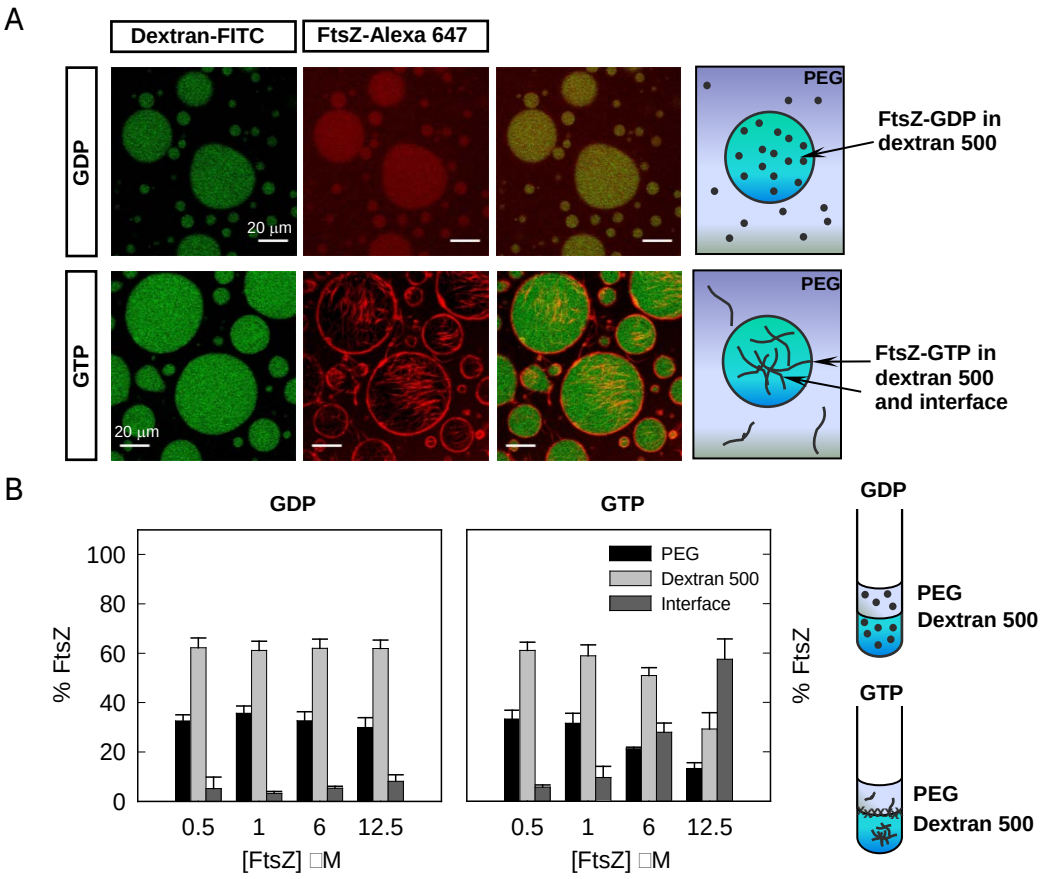

Figure 3.2. Distribution of FtsZ in the PEG/dextran 500 LLPS system. (A) Representative confocal images of FtsZ within the PEG/dextran 500 (3:1) emulsions in the absence and presence of 1 mM GTP. Total FtsZ concentration was 7 µM. A schematic illustration of the disposition of FtsZ within the phases is depicted on the right. (B) Concentration dependence of the distribution of FtsZ within the mixture as determined by fluorescence, together with an illustration on the right, in the absence and presence of 1 mM GTP. Data are the average of at least 3 independent measurements ± SD.

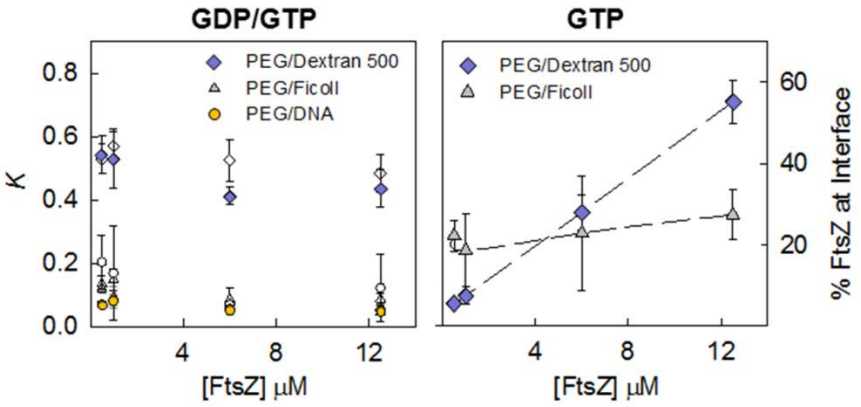

Figure 3.3. Partition coefficients and interfacial content of FtsZ in several binary mixtures. Left, evolution of the partition coefficient, *K*, with FtsZ concentration in the absence (open symbols) and presence of GTP (closed symbols). Right, variation of the percentage of FtsZ polymers at the interface of the specified LLPS systems with increasing protein concentration. Data are the average of at least 3 independent measurements ± SD

To assess the influence of FtsZ polymerization on its distribution in the PEG/dextran 500 system we studied the partition of the protein upon addition of GTP. Colocalisation of FtsZ-Alexa 647 polymers and dextran-FITC droplets was observed in the confocal images of the emulsion, with a remarkable accumulation of protein around the dextran droplets at the interface with the PEG phase (Figure 3.2A). Analysis of the distribution of FtsZ-GTP by fluorescence showed a strong dependence on protein concentration (Figure 3.2B). Below 1 µM FtsZ the behaviour of FtsZ-GTP was comparable to that observed for FtsZ-GDP, probably because at this low concentration most of the protein remains unassembled and the partition of FtsZ-GDP and FtsZ-GTP species may be similar. Above 1 µM FtsZ the amount of protein in the two phases decreased and an important fraction of the protein located at the interface between the two crowding polymers, in good agreement with the confocal images of the emulsion. The fraction of protein at the interface increased with protein concentration, likely due to an increase in the amount of assembled protein. The fraction of protein at the PEG and dextran 500 phases concomitantly decreased, rendering a nearly constant partition coefficient of 0.4–0.5 similar to that determined for FtsZ-GDP (Figure 3.3). The accumulation of the protein polymers at the liquid/liquid interface in the tubes was clear to the naked eye especially at the higher concentrations of FtsZ used (Figure 3.4C).

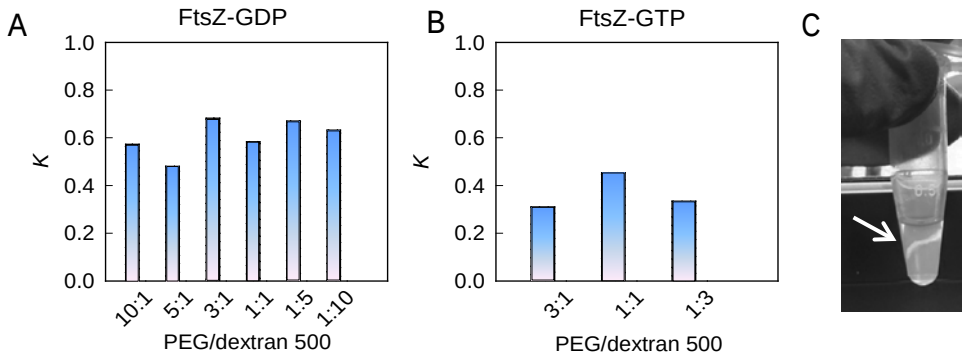

Figure 3.4. Evolution of the partition coefficient *K* of FtsZ species. Partition coefficients of FtsZ-GDP (A) and FtsZ-GTP (B) as a function of the volume ratios in PEG/dextran 500 LLPS system. FtsZ concentrations were 1 and 12.5 µM, respectively. (C) Distribution of FtsZ polymers within the PEG/dextran 500 LLPS system. Both phases were mixed in a 1:1 ratio. PEG locates at the top, dextran at the bottom. FtsZ concentration was 12.5 µM. The accumulation of protein at the interface is indicated with an arrow.

We conclude that the distribution of FtsZ species in the PEG/dextran 500 system was uneven and largely dictated by its association state. FtsZ species were mainly located in the dextran, rather than in the more hydrophobic PEG phase (Albertsson 1986) and the formation of thick bundles induced by GTP under crowding conditions favoured location of the protein at the interface between these two crowding polymers.

3.2 The LLPS system composition determines the final distribution of FtsZ species

We next analysed the partition of FtsZ-GDP and FtsZ-GTP in PEG/Ficoll 70. We found that the exclusion of unassembled FtsZ-GDP from the PEG-rich phase was even stronger in this mixture than in PEG/dextran 500, as shown by the low levels of colocalisation between the fluorescence signal of the FtsZ-Alexa 647 tracer and the emission of PEG 8 labelled with Alexa 488 (Figure 3.5A). The preference of the protein for the phase enriched in Ficoll was also evidenced by fluorescence measurements of the protein content, with most of the protein (>80%) located in this phase, and the remaining 10–15% shared between PEG and the interface (Figure 3.5B). The amount of protein in the interface was negligible at low protein concentration and increased slightly with the total FtsZ amount, reaching values comparable to those in PEG/dextran 500 at 12 μM FtsZ. The partition coefficient, around 0.1, was considerably lower than for the PEG/dextran mixtures (Figure 3.3), indicating a more uneven partition of FtsZ in the PEG/ Ficoll system.

As observed for the unassembled GDP form, FtsZ-GTP was almost completely excluded from the PEG phase, appearing the polymers in the confocal images randomly distributed within the Ficoll phase and, although far less obviously than in PEG/dextran, some of them could also be found at (or close to) the interface with PEG (Figures 3.2A and 3.5A). According to our partition coefficient determinations, among both phases FtsZ-GTP stays preferentially in the Ficoll-rich phase (Figure 3.5B). Similarly to that previously observed for PEG/dextran 500, where it is however notably higher, the partition coefficient remained basically unaltered with FtsZ concentration and comparable to that for the GDP-form (Figure 3.3).

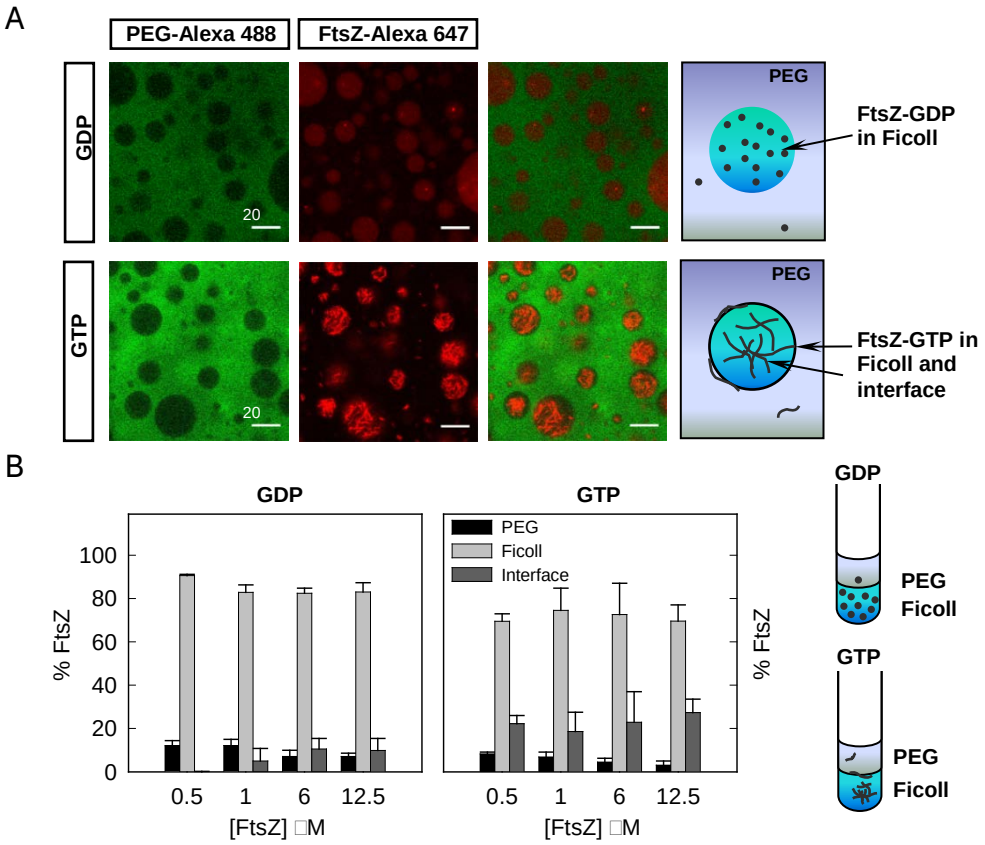

Figure 3.5. Distribution of FtsZ in the PEG/Ficoll 70 LLPS system. (A) Representative confocal images of FtsZ within the PEG/Ficoll (3:1) emulsions in the absence and presence of 1 mM GTP. Total FtsZ concentration was 7 μM. A schematic illustration of the disposition of FtsZ within the phases is depicted on the right. (B) Concentration dependence of the distribution of FtsZ within the mixture as determined by fluorescence, together with an illustration on the right, in the absence and presence of 1 mM GTP. Data are the average of at least 3 independent measurements ± SD.

Despite the higher dispersity of the measured values for FtsZ polymers, a certain fraction of the protein, only barely higher than with FtsZ-GDP, seemed to locate at the interface and did not significantly vary within the FtsZ concentration interval measured (0.5–12.5 μM; Figure 3.5B). At lower FtsZ-GTP concentrations the distribution was similar to that of FtsZ-GDP (Figure 3.6), probably because of the lack of polymers, suggesting that the minor fraction of protein detected at the interface, even at 0.5–1 μM, is likely assembled due to an enhancement in the association tendency at high concentration of Ficoll, as previously observed (Monterroso *et al.* 2016). The variability among samples in the content at the interface, particularly at high local concentrations, considering imaging and quantitative data, likely results from the random distribution of the polymers in Ficoll that enables their location anywhere within the phase, including the interface (Figure 3.6).

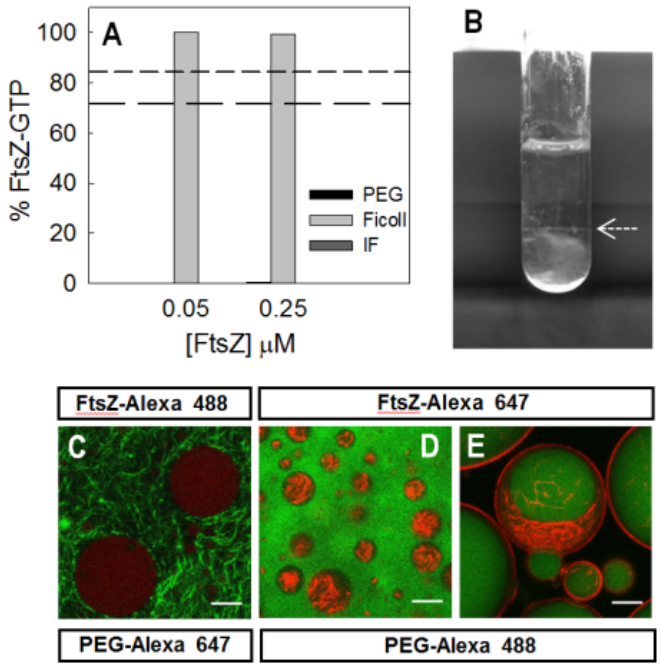

Figure 3.6. Distribution of FtsZ-GTP in the PEG/Ficoll 70 LLPS system. (A) Partition of FtsZ-GTP at low protein concentrations. IF, interface. For reference, the average content measured in the Ficoll phase of this LLPS for FtsZ-GDP (short dashed line) and FtsZ-GTP at higher FtsZ concentrations (at and above 0.5 µM; long dashed line) are depicted. (B) Distribution of 12.5 µM FtsZ-GTP. PEG locates at the top, Ficoll at the bottom. White arrow indicates the interface between both phases. (C) and (D) PEG/Ficoll (3:1) in bulk emulsion, total FtsZ concentration was 9 and 7 µM, respectively. (E) PEG/Ficoll (3:1) inside lipid droplets, total FtsZ concentration was 8 µM. Bars are 20 µm.

From our results it is clear that the distribution and behaviour of FtsZ was different in the PEG/dextran 500 and PEG/Ficoll mixtures. Despite that in both systems the protein was excluded from the PEG-rich phase, the effect was more marked for the Ficoll LLPS system and location of the protein polymers at the interface was more effective with dextran 500. To determine if the observed differences are related with the remarkably different size of the dextran and Ficoll used (500 *vs* 70 KDa) or from their different nature and shape (randomly coiled glucose polymers *vs* roughly globular sucrose polymers (Laurent and Granath 1967)), we studied the distribution of FtsZ species in an LLPS system consisting of PEG and dextran T40, more similar in molecular structure to dextran 500 but closer to Ficoll 70 in size. Confocal images of the emulsion showed preferential partition of unassembled FtsZ-GDP into the dextran T40 phase with some of the protein still remaining in PEG (Figure 3.7), the partition coefficient, 0.57 ± 0.09 at 12.5 µM FtsZ, being close to that for the dextran 500 system. The similarity with the PEG/dextran 500 mixture was further supported by the confocal images of the FtsZ-GTP species showing accumulation of the polymers at the interface around the dextran T40 droplets, and by fluorescence measurements indicating the presence of a significant fraction of protein at the interface that increased with FtsZ concentration (Figure 3.7). Noteworthy, the fraction of protein (at the highest concentration) at the interface was smaller in the mixture with dextran T40 than with dextran 500. The partition coefficient of FtsZ-GTP polymers was close to that found in

the mixture with dextran 500 and, as in this system, remained relatively insensitive to variations in FtsZ concentration (Figure 3.7).

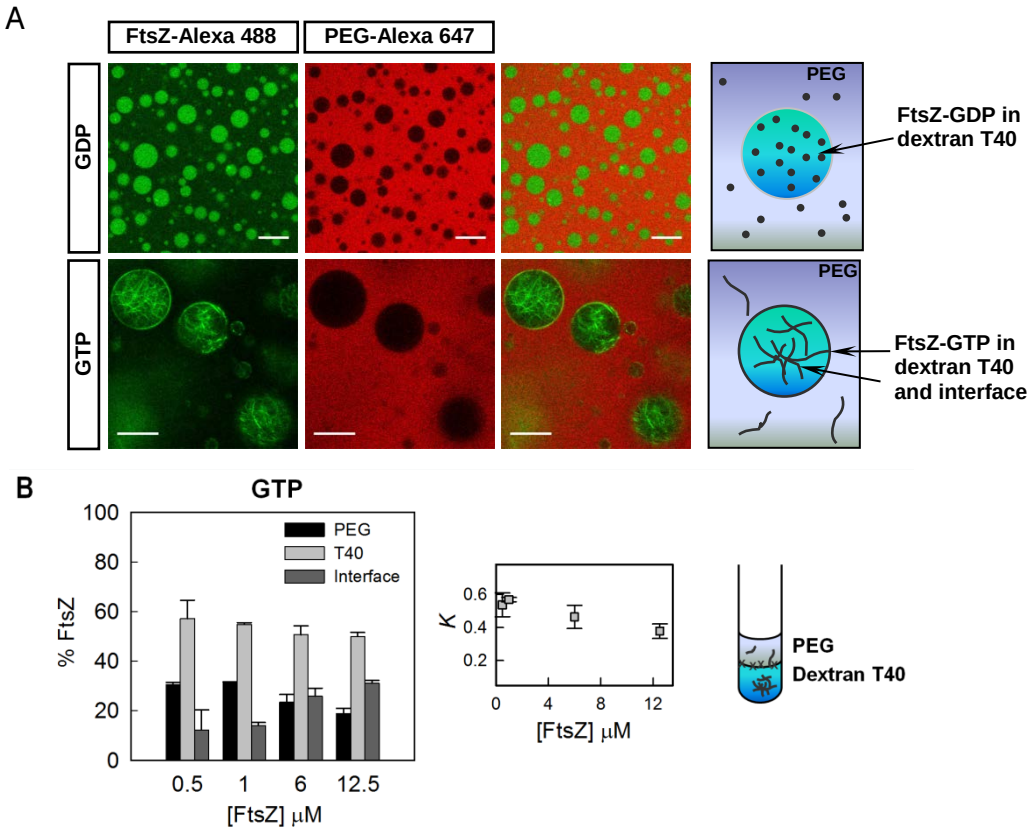

Figure 3.7. Distribution of FtsZ in the PEG/dextran T40 LLPS system. (A) Representative confocal images of FtsZ within the PEG/dextran T40 (3:1) LLPS in the absence and presence of 1 mM GTP. Total FtsZ concentration was 8 μM. Bars are 20 μm. A schematic illustration of the disposition of FtsZ within the phases is depicted on the right. (B) Concentration dependence of the percentage of FtsZ-GTP within the LLPS system as determined by fluorescence. Evolution of the partition coefficient *K* with FtsZ concentration is shown on the right, together with a schematic illustration of the disposition of FtsZ polymers within the phases.

Therefore, in all the LLPS systems composed of neutral polymers studied, FtsZ strongly partitioned into the non-PEG phase and the distribution was sensitive to its association state. Besides, the LLPS composition determines the level of exclusion from the PEG phase and the fractional amount of protein at the interface as well as its trend with protein concentration.

3.3 Condensation of FtsZ polymers induced by DNA in PEG/DNA mixtures

Nucleic acids, either DNA or RNA, are polymers particularly abundant in the bacterial interior. To address the possible influence of these charged polymers on the partition of FtsZ species, we generated an LLPS system including DNA as one of the components, the other one being PEG. For this purpose we used short DNA fragments prepared according to a previously published protocol (Biswas, Nea 2012), reaching DNA concentrations high enough to achieve phase separation when mixed with PEG. Although this DNA lacks proteins and is consequently less compact than in the bacterial nucleoid, it nonetheless allows us to introduce some of the electrostatic properties of nucleic acid-rich compartments that were absent in the PEG/dextran and PEG/Ficoll systems. Unassembled FtsZ was excluded from the PEG-rich phase to a similar extent than in the PEG/Ficoll mixture as evidenced by the lack of colocalization between FtsZ-Alexa 647 and PEG-Alexa 488 (Figure 3.8A). Measurements of the protein content in each phase showed FtsZ-GDP excluded from PEG partitioning mostly within the phase enriched in DNA with negligible amount at the interface (Figure 3.8B). The partition coefficient for this mixture was similar to that in PEG/Ficoll (Figure 3.3) and lower compared with PEG/dextran.

As for the unassembled FtsZ-GDP species, FtsZ-GTP polymers partitioned preferentially to the DNA phase, but instead of being homogeneously distributed they appeared highly condensed, leaving a noticeable part of the DNA phase free of protein as observed in the confocal images (Figure 3.8A). Interestingly, the protein polymers seemed to be expelled from the interface between the DNA droplets and PEG. The behaviour of FtsZ in this mixture was then remarkably different from the other mixtures, in which the polymers were distributed in the Ficoll (randomly) or dextran (evenly) phase and accumulated at the interface to a higher or lesser extent depending on the particular mixture. Fluorescence measurements of the protein content confirmed the large exclusion of the FtsZ polymers from PEG (Figure 3.8B). The anisotropic distribution of the polymers within the DNA made unreliable the measurement of the fraction of protein in this phase. Based on the confocal images, we may assume that no protein locates at the interface and, hence, the amount of protein in the DNA may be, for this particular case, calculated by difference with that determined in PEG. The partition coefficient obtained in this way was close to that for FtsZ-GDP species and that determined in PEG/Ficoll, and remained basically unaltered within the FtsZ concentration interval tested (Figure 3.3).

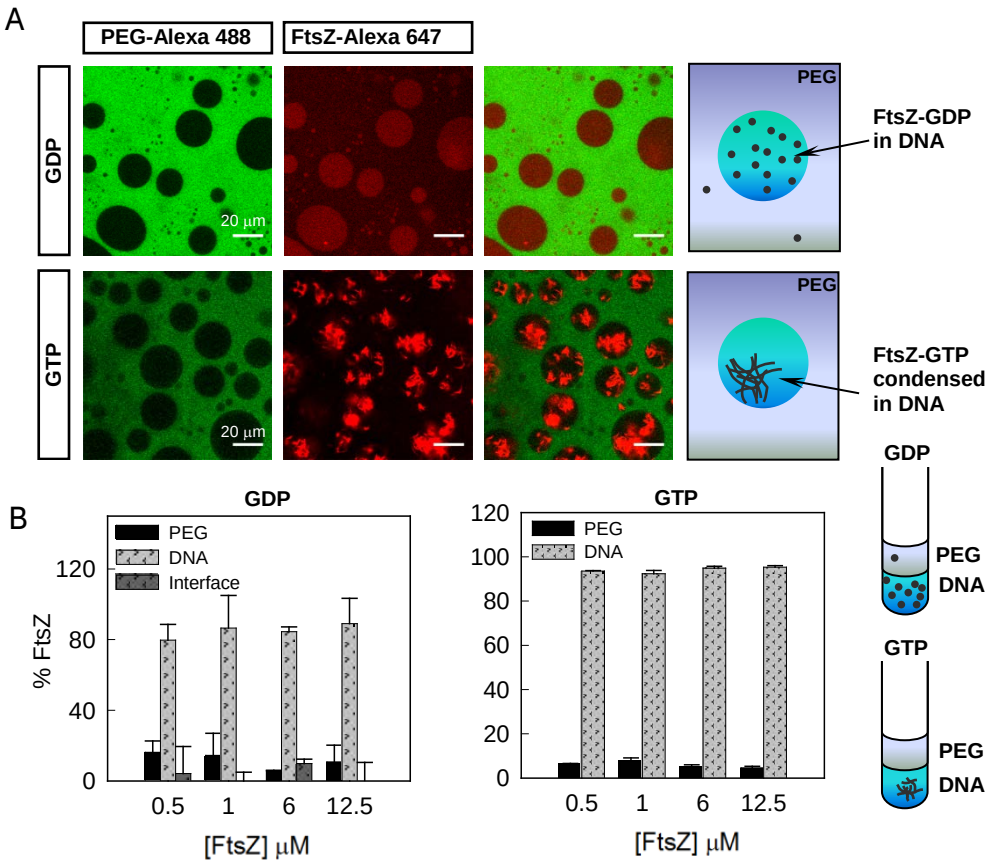

Figure 3.8. Distribution of FtsZ in the PEG/DNA LLPS system. (A) Representative confocal images of FtsZ within the PEG/DNA (3:1) emulsions in the absence and presence of 1 mM GTP. Total FtsZ concentration was 12 (GDP) and 8 µM (GTP). A schematic illustration of the disposition of FtsZ within the phases is depicted on the right. (B) Concentration dependence of the distribution of FtsZ-GDP and FtsZ-GTP within the mixture as determined by fluorescence together with illustrations on the right. In the case of the polymers, the concentration of FtsZ in the PEG phase was measured by fluorescence, and that in DNA was assumed to be the difference with the total amount of protein. Data are the average of at least 3 independent measurements ± SD.

Hence, in the PEG/DNA LLPS system FtsZ was preferentially located in the DNA phase, being homogeneously distributed when unassembled and forming condensed polymers completely excluded from the liquid/ liquid interface when polymerization was triggered with GTP.

3.4 Distribution of FtsZ in LLPS systems encapsulated in droplets stabilized by a lipid layer as cell-like containers

To better mimic the conditions found in a cell and also study the possible influence of the presence of a lipid boundary in the partition of FtsZ, we developed a procedure to encapsulate LLPS mixtures within a cell-like container surrounded by the ternary

mixture of *E. coli* lipids. In this procedure, lipids are dissolved in mineral oil at high concentration and, when in contact with the emulsion of the two phases previously mixed with the protein, they spontaneously encapsulate the mixtures inside water in oil droplets, thus generating droplets containing both phases and surrounded by a lipid layer (see Materials and Methods). With the protocol optimized here we have achieved a high yield of encapsulation of all the LLPS systems studied, PEG/dextran 500, PEG/Ficoll and PEG/DNA using 1:1 to 3:1 volume ratios of the phases, inside multiple droplets of different sizes. Indeed, we found that most of the droplets contained two phases, and sometimes even three phases (two of them equal) with this newly developed procedure.

The distribution of FtsZ species inside lipid stabilized droplets containing the different mixtures was analysed by confocal microscopy (Figures 3.9 and 3.10). According to the images, in the PEG/dextran 500 system FtsZ appeared preferentially in the dextran and to a lesser extent in PEG and, when polymerized with GTP, also at the liquid/ liquid interface, as observed with the non-encapsulated LLPS system. The colocalisation of FtsZ polymers with dextran-FITC and the accumulation of protein at the interface were clearly observed in the intensity profiles obtained from the corresponding images. A significant amount of FtsZ appeared also at the *E. coli* lipid interface, in good agreement with that previously observed in droplets containing Ficoll (Mellouli *et al.* 2013) and with unspecific binding measurements using *E. coli* lipid coated microbeads (see Chapter 1).

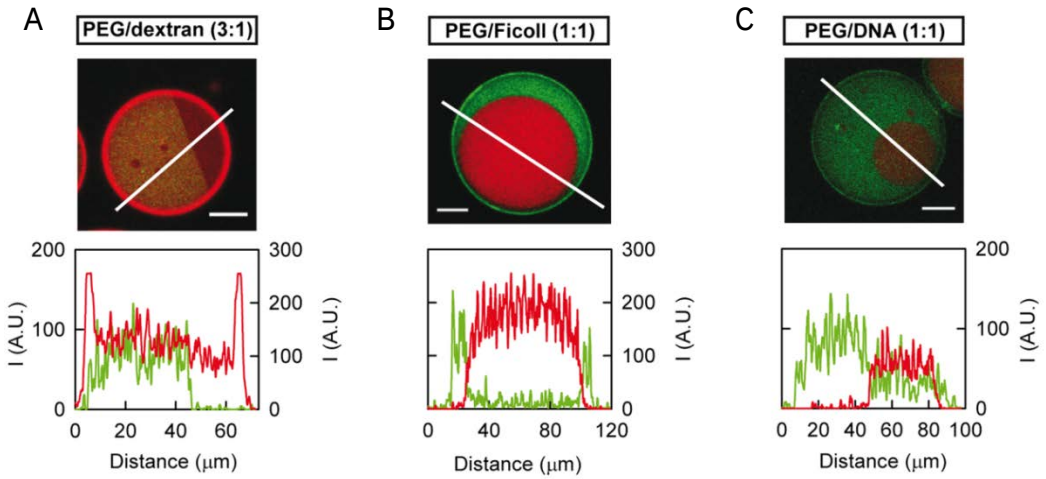

Figure 3.9. Distribution of FtsZ-GDP in LLPS encircled by a lipid layer. (A) Fluorescence signals correspond to dextran 500-FITC (green) and FtsZ-Alexa 647 (red). Total FtsZ concentration was 7 μM. (B) and (C) Fluorescence signals correspond to PEG-Alexa 647 (red) and FtsZ-Alexa 488 (green). Total FtsZ concentration was 6 and 12 μM, respectively. In all the images, lines depict the region through which the intensity profiles for each individual channel (red curve for Alexa 647, green curve for FITC or Alexa 488) were obtained. Bars are 20 μm.

Binding to lipids was maintained also with encapsulated PEG/Ficoll 70 mixtures (Figures 3.9B and 3.10B). As in the emulsions without lipids, the presence of the FtsZ polymers at the liquid/liquid interface was reduced regarding that with PEG/dextran and varied from sample to sample with the conditions. When in 1:1 mixtures, FtsZ-GTP located within the Ficoll 70 phase similarly to what was observed in bulk emulsions, and it also randomly appeared at the liquid/liquid interface confirming that there is no particular preference for this region. The decrease in the volume of the Ficoll phase in 3:1 mixtures fairly reduced the volume available for FtsZ (as PEG largely excluded FtsZ in this LLPS system). Because of the huge increase of the local concentration of FtsZ, bundles arranged to adopt conformations allowing their accommodation within the Ficoll, including alignment with the interface (Figure 3.6E). This behaviour goes in the line of that previously described in Ficoll containing droplets, where a depletion zone devoid of FtsZ is observed in the vicinity of the lipid layer. This zone, likely formed by the exclusion of stiff polymers from interfacial areas, practically disappeared as got populated with polymers upon increasing protein concentration (Mellouli *et al.* 2013). In the droplets with PEG and DNA the distribution of FtsZ polymers was, again, significantly different than in the other two systems, with the polymers clustered in the DNA phase leaving most of the volume of this phase and the liquid/liquid interface completely free of protein (Figures 3.9C and 3.10C).

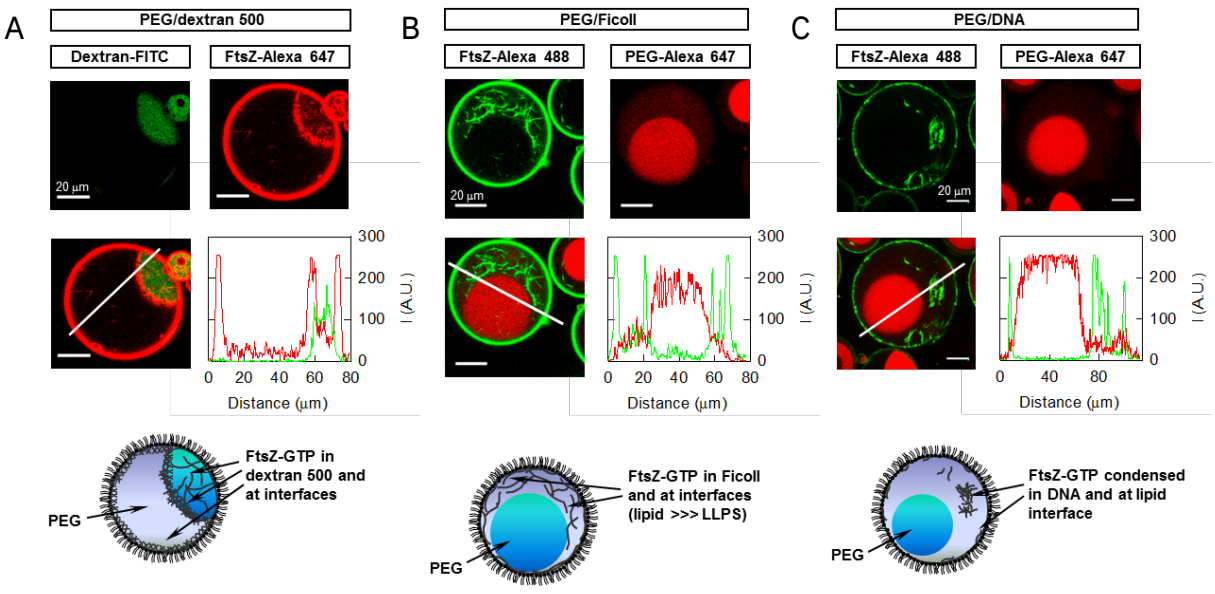

Figure 3.10. Distribution of FtsZ polymers in several binary mixtures encircled by a lipid layer. (A) PEG/dextran 500 (3:1), total FtsZ concentration 7 µM. (B) PEG/Ficoll (1:1), total FtsZ concentration 6 µM. (C) PEG/DNA (1:1), total FtsZ concentration 12 µM. In all the images of the superimposed channels, lines depict the region through which the intensity profiles for each individual channel (red curve for Alexa 647, green curve for FITC or Alexa 488) were obtained. The concentration of GTP was 1 mM. Cartoons represent the distribution of FtsZ within the encircled phases. Bars are 20 µm.

The assembly dependent location of FtsZ observed in the LLPS mixtures, particularly evident in the PEG/dextran 500 system with or without lipids, suggests that the protein may dynamically relocate from one compartment to another in response to changes in its association state. To prove this hypothesis, we sequentially imaged FtsZ polymers inside droplets stabilized by lipids containing the PEG/dextran 500 mixture (Figure 3.11A). Image acquisition started around 15 minutes after GTP addition, time point at which the protein polymers were apparent in the sample, with the expected distribution principally in the dextran-rich phase and at the liquid/liquid interface. In the sequence of images acquired, we observed that the bundles progressively disappeared due to GTP depletion as a result of its hydrolysis by FtsZ, with the concomitant increase of diffuse green fluorescence corresponding to the disassembled protein in the droplet lumen. Interestingly, upon disassembly the protein moved away from the liquid/liquid interface to the phases and preferentially to the dextran 500 (Figure 3.11A). The lack of polymers in the whole vesicle and not just in the observation plane was demonstrated through a z-scan, and depolymerization was consistently found within all vesicles of the sample after 1 hour. We concluded, therefore, that the protein moved from one location to another in response to changes in its association state.

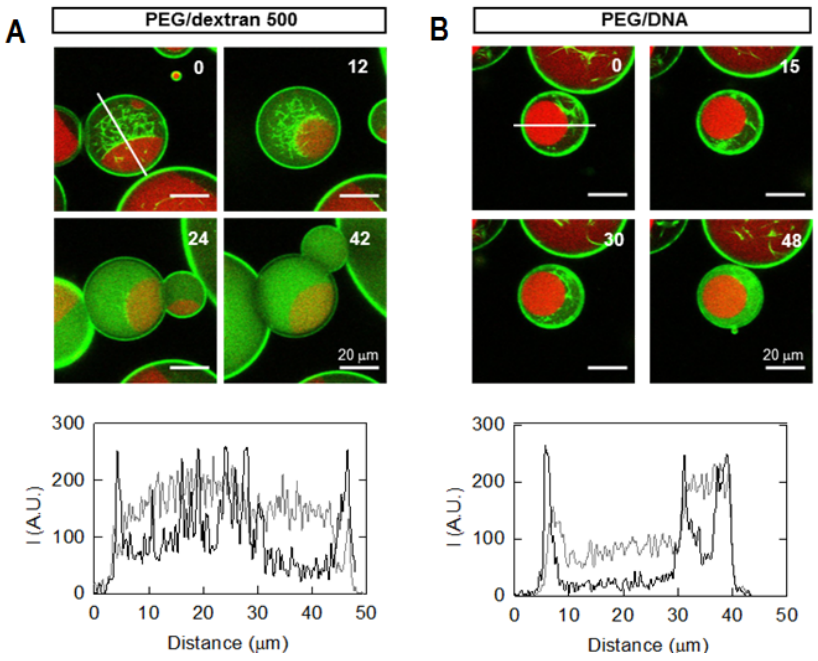

Figure 3.11. Dynamic behaviour of FtsZ polymers within LLPS systems inside lipid containers. (A) PEG/dextran 500 (3:1), total FtsZ concentration 6 µM. Monitoring of depolymerization started 14 minutes after GTP addition. (B) PEG/DNA (1:1), total FtsZ concentration 12 µM. Monitoring of depolymerization started ~2h 20 minutes after GTP addition. In all panels, distribution of FtsZ at the specified time in minutes, time zero being the beginning of visualization. GTP concentration was 0.75 mM. Fluorescence signals correspond to PEG-Alexa 647 (red) and FtsZ-Alexa 488 (green). Lines indicate the region, adapted in each image depending on the orientation of the droplet, through which the intensity profiles below depicting the distribution of FtsZ were obtained (black and grey, zero and end times, respectively). Random variations of the profiles due to subtle movements on the droplet during visualisation were corrected by matching maxima corresponding to the lipid boundary along the x axis.

We then took advantage of the stability in time of the LLPS encapsulated in lipid droplets to determine if the condensed FtsZ polymers observed in the PEG/DNA mixture were still dynamic. Image acquisition of these polymers was started around 2 hours and 15 minutes after GTP addition, with polymer content similar to that in a sample visualised around 15 minutes after nucleotide addition and the expected distribution within the phases (Figure 3.12). An increase in the diffuse fluorescence in the green channel indicative of depolymerization was clearly observed with time, mainly within the DNA phase (Figure 3.11B). In this case, however, depolymerization took place over a remarkably longer time than in the PEG/ dextran mixture, the time to achieve full depolymerization was very variable and, apparently, determined by droplet size. These results revealed that FtsZ polymers, although condensed in the DNA phase, remain dynamic and retain the ability to hydrolyse GTP.

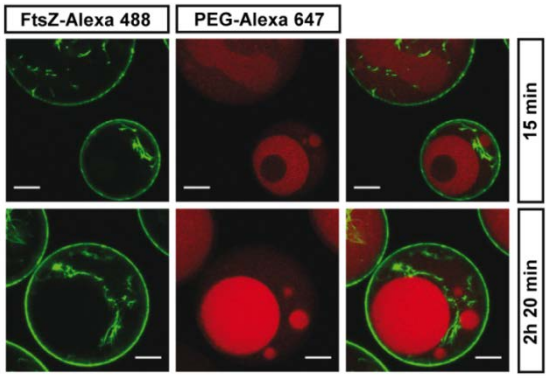

Figure 3.12. Distribution with time of FtsZ-GTP within PEG/DNA (1:1) LLPS system encapsulated by a lipid layer. Total FtsZ concentration was 12 µM. Images were taken at the specified times after GTP addition (0.7 mM). Superimposition of both channels is depicted on the right. Bars are 20 µm.

DISCUSSION

We have designed here simple LLPS systems to explore the consequences of coexisting membraneless microcompartments on the spatial organization of the essential bacterial division FtsZ protein. We show that FtsZ distributes distinctly in the LLPS systems used to mimic the intracellular heterogeneity and that this distribution is dynamic, largely dictated by the composition of the system, and reversibly modulated by the association state of the protein (Figure 3.13). This uneven partition of FtsZ suggests that phase transitions may contribute to the spatial regulation of FtsZ assembly, crucial for its role in division, as local accumulation of the protein would facilitate overcoming the concentration threshold for assembly, while exclusion from other regions would result in disassembly at those regions if the concentration falls

below the critical value. In this sense, the accumulation of polymers at certain microenvironments in non-dividing cells could hypothetically serve as a reservoir of soluble functional polymer ready to assemble into a ring when required. The preferential distribution of FtsZ would also have implications for the differential molecular recognition of other biomolecules, favouring the complexes with species/elements accumulated within the same regions over those involving molecules excluded from them. Indeed, there are evidences of FtsZ persisting as patches upon Z-ring disassembly that may act as precursors for its reassembly, also suggested to be involved in the formation of mobile complexes by recruitment of other binding partners (Rowlett and Margolin 2014). It can be reasonably expected, therefore, that the joint action of phase transitions and assembly/disassembly triggering signals deeply influence the reactivity of FtsZ.

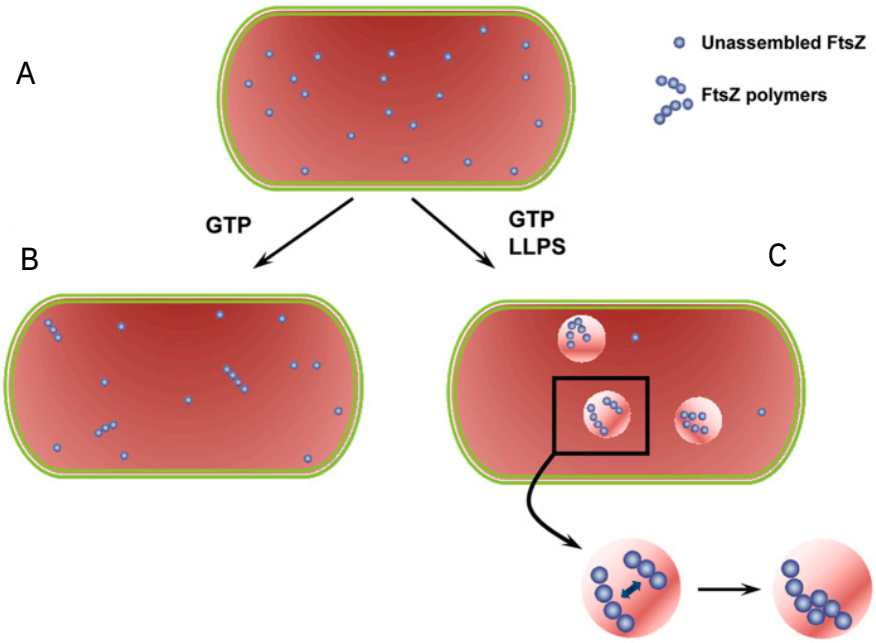

Figure 3.13. Scheme of the behaviour of FtsZ in LLPS systems. (A) In homogeneous media, the FtsZ monomers and small oligomers formed in the presence of GDP would, in principle, distribute randomly. (B) GTP triggers the polymerization of FtsZ molecules above the critical concentration. Thus, in these homogeneous media, at low total FtsZ concentration, the protein would largely remain unassembled, even in the presence of GTP. (C) Homogeneous crowding reduces the critical concentration of assembly and favours lateral interactions between the filaments. Changes in the local concentration of background molecules may produce phase transitions, and FtsZ molecules would likely distribute preferentially in certain microenvironments, being excluded from others. Under these circumstances, the local increase of FtsZ concentration would further favour its polymerization (overcoming the critical concentration threshold) and bundling. The accumulation of polymers in certain areas may also act as a polymer reservoir under non-division conditions. Besides, this asymmetric distribution would deeply impact the differential molecular recognition of FtsZ modulators and hence FtsZ function.

Bacterial division is a process tightly regulated in space and time. The accurate division of a bacterium into two cells of equivalent size and identical genomic material requires the formation of a division ring attached to the membrane and precisely located in the middle of the cell. Bacteria have developed a number of well-known mechanisms for this purpose, most of which operate through the positive or negative regulation of FtsZ polymerization at certain locations (Haeusser and Margolin 2016, Ortiz *et al.* 2016). Recent studies show that, in addition to the mechanisms so far identified, additional factors might contribute to site selection that remain to be determined (Bailey *et al.* 2014). Our results suggest that the formation of membrane-free microcompartments as a result of crowding-induced phase transitions may be among those unknown factors affecting the positioning and assembly of the division machinery through modulation of the localisation and distribution of assembled and unassembled FtsZ species.

The behaviour in PEG/DNA is remarkably different from that in the other LLPS studied, being the FtsZ polymers repelled from the interface and their distribution in the DNA phase largely anisotropic. This is probably due to the charged and non-inert nature of DNA, and maybe to its preferential hydration, meaning that it interacts with water molecules stronger than with cosolutes, providing a driving force for their exclusion (Hultgren and Rau 2004, Stanley and Rau 2006). Localisation of the condensed FtsZ bundles in the DNA-rich phase may seem, in principle, unexpected since the divisome assembles at nucleoid free regions to divide the cell without severing the chromosome. However, it has been shown that, under certain conditions, Z-ring assembly can initiate over the centre of the nucleoid (Bailey *et al.* 2014), indicating that the nucleoid and FtsZ polymers can share the same spatial region or, at least, are not mutually repelled. Indeed, we have previously shown that the polymerization of FtsZ is dramatically increased in the presence of DNA, likely due to the electrostatic repulsion between both species derived from their negative net charges (Monterroso *et al.* 2016). Although condensed in the DNA-rich phase, depolymerization with time proves FtsZ polymers remain dynamic, indicating they retain the capability of hydrolysing GTP. The formation of condensed assemblies instead of discrete arrangements of polymers in the DNA phase may prevent formation of a functional constriction ring to protect the chromosome from scission, while the protein remains active to polymerize into a proper ring in locations devoid of DNA. The behaviour of FtsZ polymers found here may be different from that in the areas occupied by the nucleoid due to the different size, structure and compactness of the DNA used

compared to the chromosome. In addition, the nucleoid occlusion protein SlmA and other DNA binding proteins may interfere with the formation of condensed FtsZ polymers in the DNA microdomains.

An important fraction of the FtsZ polymers tend to localise at the liquid/liquid interface in the mixtures composed of dextrans, particularly with dextran 500. Interfacial location of large particles has been previously demonstrated (Albertsson 1986, Cabral 2007) and, although the mere exclusion of particles from the phases can, at least in part, drive them towards the interface, it seems to be favoured because of the concomitant reduction of surface tension at the aqueous/aqueous interface (Keating 2012). In contrast to the PEG/dextran mixtures, FtsZ polymers do not have a particular preference for the interface in the LLPS systems containing Ficoll and they even seem to be expelled from the PEG/DNA interfaces. Along the same line, differences in the fraction of cells and nanoparticles at the LLPS system interfaces have been reported, depending on the specific properties of the particle surface and the type and concentration of the crowders forming the phases system (as composition also impacts interfacial tension) (Atefi *et al.* 2015, Helfrich *et al.* 2005). In the case of FtsZ polymers, we may speculate that the final distribution is also possibly related with the partition of FtsZ into the two phases in each of the LLPS systems. Thus, although FtsZ is generally excluded from the PEG phase, it distributes more evenly in the PEG/dextran mixtures compared to the Ficoll or DNA LLPS systems in which most of the protein is located in the non-PEG phase. The larger repulsion from the dextran phase may further favour its larger location at the interface whereas the preference of FtsZ molecules for the Ficoll or DNA phases may disfavour their interfacial positioning. Localisation of FtsZ polymers at the interface may serve to concentrate them within a defined region, which might enhance or hinder interactions with other division elements. Interfacial assembly favours arrangement of the FtsZ polymers in two rather than three dimensions, which might render a relative orientation more appropriate for constriction.

Lipid encapsulated LLPS systems provide a better platform to evaluate the impact of microenvironments on protein function compared with two-phase emulsions, since the lipid layer limits the size of the systems, bringing them closer to the cellular scale. It also maintains a stable LLPS composition, allowing the study of confinement effects and facilitating the tracking of time-dependent processes. The simultaneous encapsulation of two phases within a lipid container is experimentally challenging though, only attained so far using giant unilamellar vesicles (GUVs) and a single phase

formed by two polymers where separation was afterwards induced by physical methods (Helfrich *et al.* 2005, Li *et al.* 2008, Long *et al.* 2005). The approach we propose here allows overcoming some of the difficulties associated to these procedures, including the low yield of encapsulation, the limited amount of vesicles, the restriction to certain compositions, and the need for changes in conditions to separate the phases after encapsulation that may be incompatible when including biomolecules. Encapsulation of phases within water in oil droplets has been previously achieved using surfactants to stabilize them (Torre *et al.* 2014) but, to the best of our knowledge, not with lipids as the boundary material, that have been however used for single phase encapsulation in droplets (Mellouli *et al.* 2013, Yanagisawa *et al.* 2014). Although our model system is not exactly the same as a living bacterial cell, it captures many of its key features as it contains crowding, compartments, microscale volume and a lipid boundary.

Using LLPS systems with controllable composition we have shown that microenvironments driven by phase transitions dynamically modulate FtsZ assembly and localisation. The preference of FtsZ for some compartments may enhance the local concentration of the protein favouring FtsZ assembly at certain locations but not in others from which the protein is excluded. Clearly, the asymmetric distribution of FtsZ between phases can determine its interactions with other molecules involved in division depending on their particular distribution. As phase transitions can occur locally and in a reversible manner, we propose that they may contribute to the fine tuning of bacterial division, likely acting jointly with other specific mechanisms designed for the control of this essential process.

CHAPTER 4

Encapsulation of a compartmentalized cytoplasm mimic within a lipid membrane by microfluidics

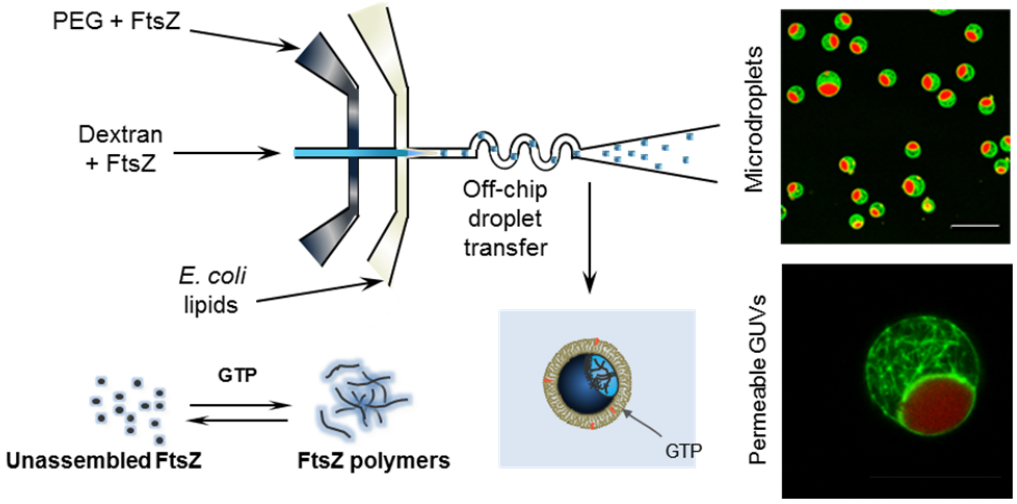

There is growing interest in analyzing the effect of microenvironments, which may be mimicked through liquid–liquid phase separation (LLPS), on the reactivity of biological macromolecules. We report the encapsulation by microfluidics of the division protein FtsZ and a LLPS system inside microdroplets and their conversion into permeable vesicles (allowing ligand uptake), with higher yield, homogeneity and biomolecular compatibility than those previously described.

RESULTS AND DISCUSSION

Microfluidic methods have been recently used for the generation of compartmentalized structures as two-droplet multisomes (Elani *et al.* 2016), nested liposomes (Deng *et al.* 2017) and for surfactant stabilized single-phase droplets where separation was subsequently induced (Yuan 2017). In this chapter we report a microfluidics based method for the direct encapsulation of two aqueous phases together with a protein and a physiological ligand inside droplets stabilized by a lipid monolayer. In addition, we have produced GUVs from these droplets containing the two-phase system and the protein by a modified droplet transfer method. Finally, the incorporation of small molecules into the permeable GUVs is shown. To optimize the procedures we have selected a LLPS system widely used in previous studies, PEG 8/dextran 500, and the central bacterial division protein FtsZ, the behaviour of which was studied in bulk LLPS systems in the previous chapter. We have triggered FtsZ polymerization with GTP either immediately before droplet formation or by external addition of the nucleotide to the permeable vesicles. This method could aid in the generation of artificial cells more faithfully resembling functionalities, as it enables the inclusion of some of the features vital for living systems (Buddingh and van Hest 2017). The semipermeable boundary allows the exchange of molecules, and can be used as the basis for developments in tunable permeability promoting adaptivity. Membraneless phase separated systems modulate macromolecules' dynamic localization. The tight control of the concentrations of all reagents (and hence in the generation of synthetic compartments) is of utmost importance for the control of reaction networks.

4.1 Encapsulation and behaviour of FtsZ in microdroplets containing PEG/dextran LLPS systems

Water in oil droplets containing the LLPS system stabilized by the *E. coli* lipid mixture (EcL) were produced in flow focusing microfluidic chips (Mellouli *et al.* 2013) (Figure 4.1). Two streams of dispersed aqueous phases were mixed in an approximately 1:1 ratio prior to the droplet formation junction, one stream containing dextran 500 and the other one PEG 8, prepared as described in Materials and Methods. Encapsulation of both aqueous phases was verified by fluorescence microscopy including Alexa 647 labelled PEG. FtsZ, added to the two aqueous phases,

was monitored by including a tracer amount labelled with Alexa 488. No difference was observed when adding the protein in either phase. The third stream delivered the EcL mixture in mineral oil. The typical flow rates were 120 µL h^{-1} for the continuous phase and 5 and 7 µL h^{-1} for the dextran and PEG aqueous phases, respectively, controlled by automated syringe pumps rendering uniform droplets (~2 pL). Production of droplets was more laborious than when a single phase is encapsulated (i.e. when both aqueous solutions have the same composition), likely due to the different viscosities of the two crowding solutions.

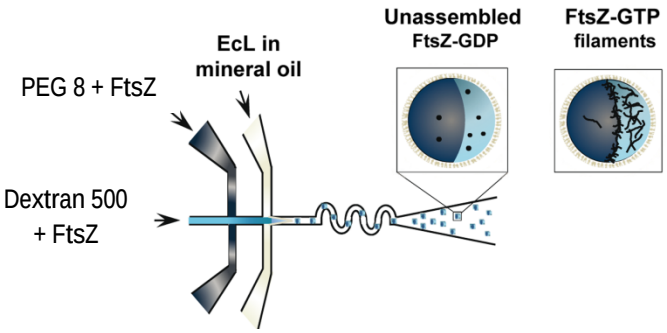

Figure 4.1. Scheme of the junction in the microfluidic chip. Water-in-oil droplets containing the LLPS system with FtsZ stabilized by *E. coli* lipids mixture were produced in the microfluidic chip. Black dots and lines inside the droplets represent the unassembled and assembled form of FtsZ, respectively, distributed in both phases.

To analyse the resulting droplets, we imaged them directly in the chip. Despite some polydispersity in droplets size due to the poor surfactant capacity of *E. coli* lipids (Mellouli *et al.* 2013), the formation of a large number of droplets narrowly distributed in size, virtually all of them containing in similar proportion the two aqueous phases, was observed (Figure 4.2). The distribution of diameters for a representative population of over 100 droplets from 3 independent experiments is shown in Figure 4.2B, with an average diameter for the main population of ~16 µm. Slight variations in the size were found depending on the flows tested. The overlap between the intensity profiles in the red and green channels for different microdroplets, reflecting the distribution of PEG-Alexa 647 and of FtsZ-Alexa 488, evidenced the uniform distribution in the encapsulation of the two phases and in the protein partition among the droplet population (Figure 4.2C). FtsZ was found preferentially in the dextran phase (Figure 4.2A), in good agreement with previous observations (see Chapter 3).

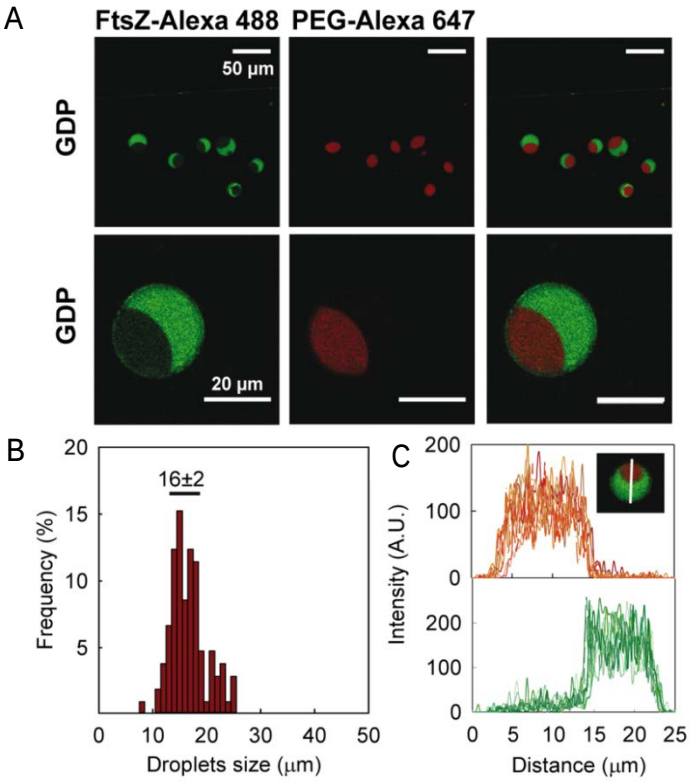

Figure 4.2. Microfluidic encapsulation of FtsZ in a LLPS system inside microdroplets. (A) Representative confocal images of the distribution of unassembled FtsZ in the biphasic PEG/dextran mixture inside the microdroplets stabilized by the *E. coli* lipid mixture. (B) Size distribution of the microdroplets (N = 105). Average size corresponds to the mean value (±SD) of the most populated sizes, indicated by the horizontal line. (C) Intensity profiles of the red (PEG-Alexa 647, up) and green (FtsZ-Alexa 488, down) channels for several droplets containing unpolymerized FtsZ, obtained across lines drawn as exemplified in the inset.

4.2 Coencapsulation of FtsZ and GTP inside microdroplets

In order to test the performance of the method for the coencapsulation of a protein and one of its physiological ligands, we encapsulated the LLPS system with FtsZ and GTP, which triggered the polymerization of the protein just before droplet formation (Figure 4.3). To this aim we included FtsZ with FtsZ-Alexa 488 in one aqueous solution and GTP in the other, with similar results irrespective of their individual addition to either the PEG or dextran solutions. Imaging of the chip revealed the formation of droplets of similar sizes, containing comparable amounts of phases and FtsZ polymers. The distribution of FtsZ polymers, preferentially located in the dextran phase and at the interface, was compatible with prior work (see Chapter 3). The microfluidics based method we report here allows the generation of a high number of virtually equal microdroplets containing LLPS together with a protein, with or without physiological ligands, enabling to perform studies of protein reactivity and distribution.

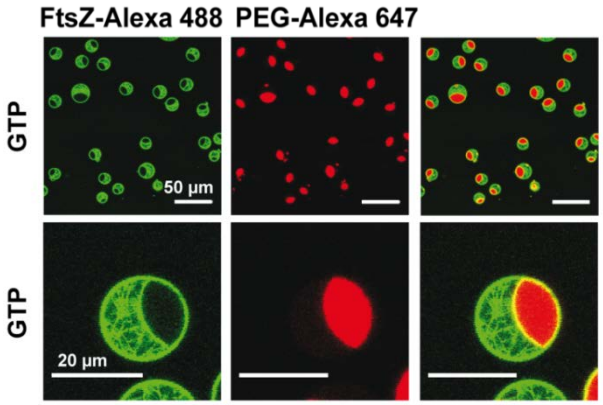

Figure 4.3. Polymeric FtsZ in a LLPS system encapsulated inside microfluidics microdroplets. Representative confocal images of the distribution of FtsZ filaments in the biphasic PEG/dextran mixture inside the microdroplets stabilized by the *E. coli* lipid mixture.

4.3 Generation of GUVs from FtsZ microfluidics microdroplets

Once we achieved the microfluidics encapsulation of the LLPS system with the protein of interest inside the microdroplets, we optimized a method to convert them into GUVs, as the bilayer boundary provides both a better cell-like system and the possibility of external addition of small ligands. The procedure was based on the droplet transfer method in which the droplets acquire the bilayer upon transition from an oil phase to an aqueous solution when the interface between them is coated with oriented lipids (Carrara *et al.* 2012) (see Introduction). The first step was the collection of the droplets by introducing the outlet tubing from the microfluidic chip into oil phase lying on top the outer solution (Figure 4.4). Different outer solutions were assayed and the composition was chosen to be the same as that of the inner buffer with a sucrose concentration rendering an osmolarity slightly above the highest osmolarity of the encapsulated solutions, which we found enhanced vesicle integrity. It should be noted that, to avoid any possible influence on FtsZ polymerization (Monterroso *et al.* 2016), we removed the sucrose usually contained in the encapsulated solution in the original method. Different droplet collection times were tried and 30 minutes was chosen to improve the yield of the procedure.

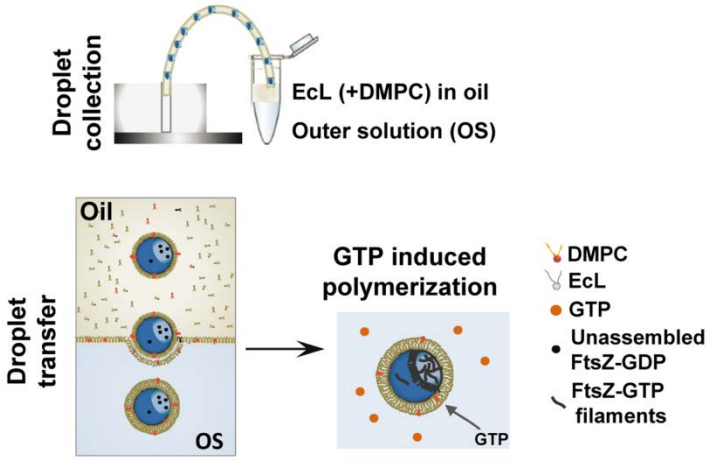

Figure 4.4. Generation of GUVs from microfluidics microdroplets. Schematic illustration of the procedure for collection of droplets and subsequent formation of permeable vesicles.

The formed GUVs, in which the two aqueous phases are surrounded by a lipid bilayer, were relatively homogeneous in size and composition (Figure 4.5A). However, the yield of GUV production among experiments was more variable than that of the microdroplets because it involves many more steps, some of which cannot be as tightly controlled as the production of microdroplets in microfluidics, like the bilayer acquisition step and vesicle washing. The size estimation proved to be harder due to the smaller number of replicates amenable to be measured, attributable to factors occurring upon the centrifugation of the droplets as rupture, and fusion and/or segregation of composing phases into individual droplets rendering a somehow wider size distribution. Also, small differences derived from measurements of non-circular shaped vesicles (see, for instance, bottom images in Figure 4.5A) cannot be discarded. The distribution of diameters was determined for 60 vesicles obtained in 2 different experiments (Figure 4.5B), with an average diameter for the main population of ~18 µm. Noteworthily, the observed dependence of the average size of droplets with the final flows was maintained in GUVs, *i.e.* the most abundant population of vesicles within an experiment, representative of the microdroplets produced, is that corresponding to the same average size. As expected, the uniform distribution of the encapsulated phases and partition of the protein, determined by the microdroplet production step, were maintained in the GUVs generated from them, as reflected by the overlapped intensity profiles of PEG-Alexa 647 and FtsZ-Alexa 488 across the GUV population (Figure 4.5C).

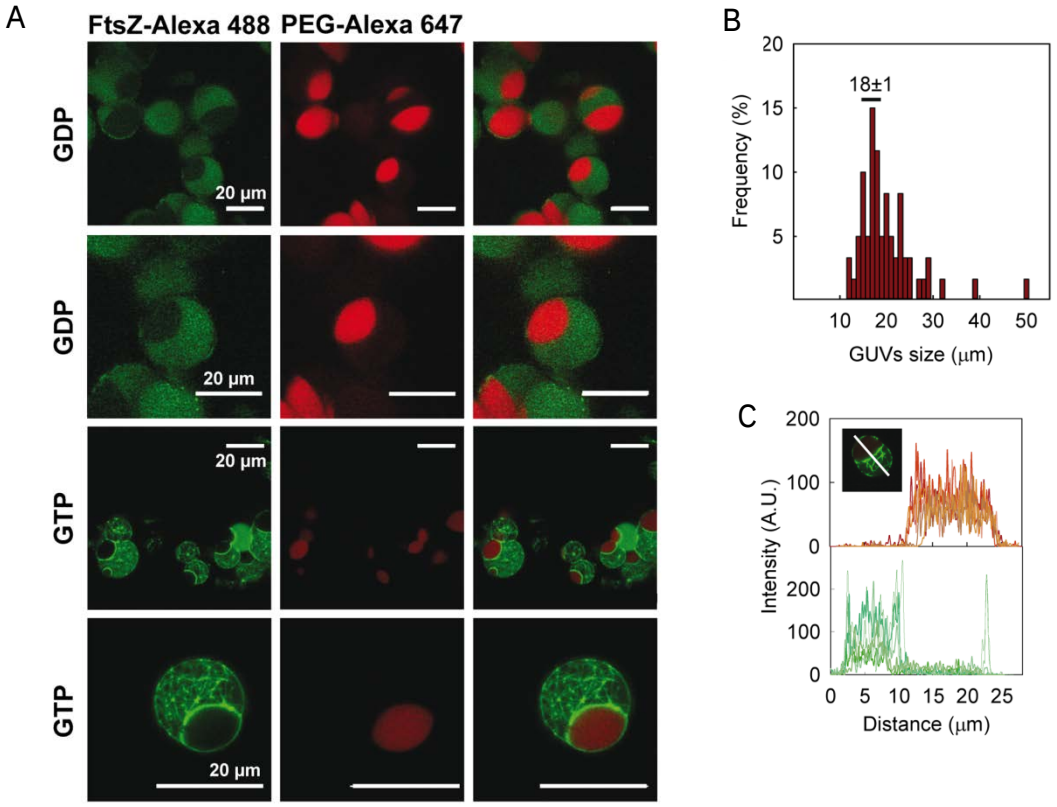

Figure 4.5. Encapsulation of FtsZ in a LLPS system inside GUVs generated from microfluidics microdroplets and triggering of assembly. (A) Representative confocal images of the GUVs containing the LLPS system and unassembled FtsZ or FtsZ filaments triggered by diffusion of GTP through the DMPC in the *E. coli* lipid bilayer. PEG is labelled in red (PEG-Alexa 647) and FtsZ in green (FtsZ-Alexa 488). (B) Size distribution of the generated vesicles (N = 60). Average size corresponds to the mean value (±SD) of the most populated sizes, indicated by the horizontal line. (C) Intensity profiles of the red (PEG-Alexa 647, up) and green (FtsZ-Alexa 488, down) channels for several vesicles (disregarding polymerization was triggered or not), obtained across lines drawn as exemplified in the inset.

Using our method the final size of the generated vesicles is significantly reduced, at least by 30%, compared with those fully produced on chips and so far applied for a single aqueous phase (Arriaga *et al.* 2014, Karamdad *et al.* 2015, Matosevic and Paegel 2011), a feature that can be of utmost importance depending on the process under study, as with cellular systems. Besides, the ability to work with two aqueous streams enables the encapsulation of not only two different phases, but also of several species, as for instance proteins with binding partners or inhibitors, with the obvious applications for the study of biological systems. This is, however, at the expense of reducing the number of comparable GUVs obtained per experiment.

4.4 Triggering of FtsZ polymerization from outside the vesicles

As in many instances the introduction of small ligands after encapsulation of the LLPS systems may improve the experimental design, for example for the analysis of time dependent processes, we tested our procedure for the formation of permeable GUVs. To this end, we produced vesicles containing the two phases and FtsZ, following the adapted droplet transfer method described earlier but including DMPC in the lipid mixture. To probe the permeability of the vesicles, FtsZ polymerization was triggered by external addition of GTP. Polymers inside vesicles were always observed (Figure 4.5A), but the number of vesicles in which polymerization was triggered somehow varied among experiments and was found to increase with time. In any case, the appearance of FtsZ polymers, again with the expected distribution within phases (Figure 4.5A), proved the permeability of the bilayer as well as the formation of the bilayer itself and the active state of the protein after encapsulation.

CONCLUSIONS

The procedures presented allowed the microfluidics based encapsulation of LLPS systems and active protein into microdroplets stabilized by lipids and the production of permeable vesicles from them, notably increasing the yield when compared with the established bulk methods. Moreover, by these methods, the formation of droplets and vesicles stabilized by the *E. coli* lipid mixture is feasible, and the avoidance of the need for an osmolyte inside them rules out possible uncontrolled effects. Advantages and drawbacks can be named for both procedures. If all elements participating in the studied process can be simultaneously encapsulated, microdroplets by microfluidics is probably the LLPS encapsulation strategy of choice, as it brings about improvements to the simpler, and faster, encapsulation in bulk emulsion: (1) tight control over the size and content of the droplets, (2) minimal contact of the protein with the oil, and (3) elimination of vortexing prior to protein addition to improve the encapsulation of both phases. GUVs produced from microdroplets, when a lipid bilayer is needed to more closely resemble the physiological conditions and/or a subsequent addition of a metabolite is required, obviously maintain these features, although a loss of material is unavoidable. This procedure also overcomes the necessity to modify experimental conditions to induce phase separation after encapsulation, thus avoiding possible damage to susceptible biomolecules.

CONCLUDING REMARKS AND FUTURE PERSPECTIVES

In the first part of this thesis, ZipA-FtsZ interaction was reconstituted in minimal membrane systems and analysed by a combination of biochemical and biophysical techniques:

- The amount of FtsZ bound to surface-immobilized ZipA can greatly exceed a stoichiometric ratio of unity due to the oligomerization of FtsZ. In the case of FtsZ-GDP, the ability of linear surface-associated FtsZ oligomers to continue to grow leads to receptor unsaturability. FtsZ-GTP forms narrowly-sized polymers compatible with cyclic structures that cannot further grow, and so receptors saturate.
- Binding of FtsZ-GMPCPP polymers to ZipA-containing bilayers was also saturable and occurred in two phases, the first one corresponding to a 2D growth of polymers at the immediate vicinity of the membrane and a second phase corresponding to their 3D extension into the bulk solution. This 3D growth might actually be related to the exposure of FtsZ central hub to integrate signals that modulate divisome assembly.
- ZipA surface density modulates both the binding stoichiometry of FtsZ-GMPCPP to ZipA and the organization of the polymer film at the membrane.

In the second part, the influence of macromolecular crowding and compartmentalization induced by phase separation on the essential protein FtsZ was analysed.

- FtsZ tends to accumulate in one of the phases and/or at the interface, depending on the system composition and on the oligomerization state of the protein. The existence of dynamic compartments driven by phase transition can alter the local composition and reactivity of FtsZ during its life cycle acting as a nonspecific modulating factor of cell function.
- Microfluidics allows the encapsulation of LLPS systems and active FtsZ into microdroplets stabilized by lipids and the production of permeable vesicles from them, allowing GTP incorporation and subsequent FtsZ polymerization.

FUTURE PERSPECTIVES

In this thesis, the activity, interactions and assembly properties of FtsZ have been studied in minimal reconstructions of the proto-ring structured in membrane systems, in solutions mimicking crowding and microenvironments in the cytoplasm and in cell-like containers.

The results of the **first part of the thesis** have shed light on the recognition between FtsZ and the *E. coli* proto-ring protein ZipA through reconstitution of the complexes in biomimetic membrane systems. It was found that the ability of FtsZ to self-assemble according to different mechanisms, depending on the nucleotide present (GDP or GTP), dramatically determines the mode of interaction with immobilized ZipA. In both cases several FtsZ subunits can be recruited by a single receptor. However, the interaction of FtsZ with the membrane largely depends on receptor density in the case of the relatively short linear indefinitely growing GDP oligomers, whereas this dependence is much less pronounced for the large cyclic GTP-triggered fibers.

It would be interesting to extend these studies to determine how other positive and negative modulators of ring stability impact the interactions between FtsZ and ZipA in membrane systems. This is a challenge as several multiple protein-protein interactions occur simultaneously and most of them through the C-terminal region of FtsZ, which acts as a central hub integrating signals to drive divisome assembly. In addition, to study the effect of mutations at key regions of FtsZ on these interactions will be very informative to unravel the mechanistic insights of these complex interactions.

In the **second part of this thesis,** the impact of phase transitions and microenvironments related with natural crowding on FtsZ distribution, localization and reactivity has been analyzed. Furthermore, cell models have been generated through encapsulation of biphasic aqueous systems inside lipid-stabilized microdroplets or vesicles by using microfluidics technology. The results described show that FtsZ accumulates in a specific phase, at the interface between the two aqueous phases or at the interface with the lipids depending on the size of the FtsZ oligomers and on the nature of the liquid-liquid phase separation system. Moreover, obtained data suggest that the protein is able of migrating from one microenvironment to another in response to changes in its association state. From these results it is proposed that microenvironments may have a strong influence on the polymerization of FtsZ and on

the recognition of other elements participating in division, depending on their accumulation in or exclusion from the preferred locations of FtsZ.

To test these hypothesis, similar experiments to the ones conducted here can be designed incorporating other division proteins like negative or positive regulators of FtsZ polymerization or by co-reconstructing the membrane anchoring proteins together with FtsZ inside the lipid-stabilized microdroplets or vesicles encasing the aqueous phases. The cell-like containers produced in this thesis, in which FtsZ oligomers and polymers have been reconstructed as a proof of concept, incorporate features like crowding, microcompartments, a membrane boundary and a small size. In order to reproduce more faithfully the bacterial interior in which these reactions occur, it would be relevant to incorporate other elements of the intracellular complexity, for example, the addition of ribosomes and polyamines which contribute to the polyelectrolyte character of the cytosplasm. In this case, exploring the properties of FtsZ in polyelectrolyte-rich intracellular droplets (coacervates) will be very informative. Finally, the study of the impact of geometry of the containers in which these self-organization reactions occur can be analyzed by microfluidic approaches.

PUBLICATIONS

Publications derived from this thesis:

- Begoña Monterroso, Silvia Zorrilla, **Marta Sobrinos-Sanguino**, Christine D Keating, Germán Rivas. Microenvironments created by liquid-liquid phase transition control the dynamic distribution of bacterial division FtsZ protein. *Scientific Reports*, 2016, 6: 35140.

- **Marta Sobrinos-Sanguino**, Silvia Zorrilla, Christine D Keating, Begoña Monterroso, Germán Rivas. Encapsulation of a compartmentalized cytoplasm mimic within a lipid membrane by microfluidics. *Chemical Communications*, 2017, 53(35): 4775-4778.

- **Marta Sobrinos-Sanguino**, Silvia Zorrilla, Begoña Monterroso, Allen P Minton, Germán Rivas. Nucleotide and receptor density modulate binding of bacterial FtsZ protein to ZipA containing lipid-coated microbeads. *Scientific Reports*, 2017, 7(1): 13707.

Other publications:

- Marcin Krupka, **Marta Sobrinos-Sanguino**, Mercedes Jiménez, Germán Rivas, William Margolin. *Escherichia coli* organizes FtsZ polymers into dynamic ring-like structures containing single protofilaments. *Accepted*.

- Begoña Monterroso, Silvia Zorrilla, **Marta Sobrinos-Sanguino**, Miguel A Robles-Ramos, Marina López-Álvarez, Christine D Keating, Germán Rivas. Bacterial division FtsZ forms liquid condensates with nucleoid-associated Z-ring inhibitor SlmA. *Submitted*.

REFERENCES

REFERENCES

Adams DW and Errington J. Bacterial cell division: assembly, maintenance and disassembly of the Z ring. *Nat Rev Microbiol*, 2009, **7**, 642-53.

Ahijado-Guzmán R, Alfonso C, Reija B, Salvarelli E, Mingorance J, Zorrilla S, Monterroso B and Rivas G. Control by potassium of the size distribution of *Escherichia coli* FtsZ polymers is independent of GTPase activity. *J Biol Chem*, 2013, **288**, 27358-65.

Ahijado-Guzmán R, Gómez-Puertas P, Álvarez-Puebla RA, Rivas G and Liz-Marzán LM. Surface-Enhanced Raman scattering-based detection of the interactions between the essential cell division FtsZ protein and bacterial membrane elements. *ACS Nano*, 2012, **6**, 7514-20.

Ahmed S and Wunder SL. Effect of high surface curvature on the main phase transition of supported phospholipid bilayers on SiO2 nanoparticles. *Langmuir*, 2009, **25**, 3682-91.

Amster-Choder O. The compartmentalized vessel: The bacterial cell as a model for subcellular organization (a tale of two studies). *Cell Logist*, 2011, **1**, 77-81.

Andes-Koback M and Keating CD. Complete budding and asymmetric division of primitive model cells to produce daughter vesicles with different interior and membrane compositions. *J Am Chem Soc*, 2011, **133**, 9545-55.

Arriaga LR, Datta SS, Kim SH, Amstad E, Kodger TE, Monroy F and Weitz DA. Ultrathin shell double emulsion templated giant unilamellar lipid vesicles with controlled microdomain formation. *Small*, 2014, **10**, 950-6.

Arumugam S, Chwastek G, Fischer-Friedrich E, Ehrig C, Monch I and Schwille P. Surface topology engineering of membranes for the mechanical investigation of the tubulin homologue FtsZ. *Angew Chem Int Ed Engl*, 2012, **51**, 11858-62.

Atefi E, Joshi R, Mann JA, Jr. and Tavana H. Interfacial tension effect on cell partition in aqueous two-phase systems. *ACS Appl Mater Interfaces*, 2015, **7**, 21305-14.

Bailey MW, Bisicchia P, Warren BT, Sherratt DJ and Mannik J. Evidence for divisome localization mechanisms independent of the Min system and SlmA in *Escherichia coli*. *PLoS Genet*, 2014, **10**, e1004504.

Balakrishnan G, Nicolai T, Benyahia L and Durand D. Particles trapped at the droplet interface in water-in-water emulsions. *Langmuir*, 2012, **28**, 5921-6.

Bayburt TH and Sligar SG. Membrane protein assembly into nanodiscs. *FEBS Lett*, 2010, **584**, 1721-7.

Bernhardt TG and de Boer PA. SlmA, a nucleoid-associated, FtsZ binding protein required for blocking septal ring assembly over Chromosomes in *E. coli. Mol Cell*, 2005, **18**, 555-64.

Beutel O, Nikolaus J, Birkholz O, You C, Schmidt T, Herrmann A and Piehler J. High-fidelity protein targeting into membrane lipid microdomains in living cells. *Angew Chem Int Ed Engl*, 2014, **53**, 1311-5.

Bi EF and Lutkenhaus J. FtsZ ring structure associated with division in *Escherichia coli. Nature*, 1991, **354**, 161-4.

Biswas N, Ichikawa M, Datta A, Sato YT, Yanagisawa M and Yoshikawa K. Phase separation in crowded micro-spheroids: DNA–PEG system. *Chemical Physics Letters*, 2012, **539-540**, 157-162.

Biswas Nea. Phase separation in crowded micro-spheroids: DNA-PEG system. *Chemical PhysicsLetters*, 2012, **539-540**, 157-162.

Brangwynne CP. Phase transitions and size scaling of membrane-less organelles. *J Cell Biol*, 2013, **203**, 875-81.

Brian AA and McConnell HM. Allogeneic stimulation of cytotoxic T cells by supported planar membranes. *Proc Natl Acad Sci U S A*, 1984, **81**, 6159-63.

Buddingh BC and van Hest JCM. Artificial Cells: Synthetic compartments with life-like functionality and adaptivity. *Acc Chem Res*, 2017, **50**, 769-777.

Cabral JM. Cell partitioning in aqueous two-phase polymer systems. *Adv Biochem Eng Biotechnol*, 2007, **106**, 151-71.

Cabré EJ, Sánchez-Gorostiaga A, Carrara P, Ropero N, Casanova M, Palacios P, Stano P, Jiménez M, Rivas G and Vicente M. Bacterial division proteins FtsZ and ZipA induce vesicle shrinkage and cell membrane invagination. *J Biol Chem*, 2013, **288**, 26625-34.

Cacace DN, Rowland AT, Stapleton JJ, Dewey DC and Keating CD. Aqueous emulsion droplets stabilized by lipid vesicles as microcompartments for biomimetic mineralization. *Langmuir*, 2015, **31**, 11329-38.

Carrara P, Stano P and Luisi PL. Giant vesicles "colonies": a model for primitive cell communities. *Chembiochem*, 2012, **13**, 1497-502.

Carton I, Brisson AR and Richter RP. Label-free detection of clustering of membrane-bound proteins. *Anal Chem*, 2010, **82**, 9275-81.

Cisse I, Okumus B, Joo C and Ha T. Fueling protein DNA interactions inside porous nanocontainers. *Proc Natl Acad Sci U S A*, 2007, **104**, 12646-50.

Cordell SC, Robinson EJ and Lowe J. Crystal structure of the SOS cell division inhibitor SulA and in complex with FtsZ. *Proc Natl Acad Sci U S A*, 2003, **100**, 7889-94.

Cunha S, Woldringh CL and Odijk T. Polymer-mediated compaction and internal dynamics of isolated *Escherichia coli* nucleoids. *J Struct Biol*, 2001, **136**, 53-66.

Chatelier RC and Minton AP. Adsorption of globular proteins on locally planar surfaces: models for the effect of excluded surface area and aggregation of adsorbed protein on adsorption equilibria. *Biophys J*, 1996, **71**, 2367-74.

Cheng S, Liu Y, Crowley CS, Yeates TO and Bobik TA. Bacterial microcompartments: their properties and paradoxes. *Bioessays*, 2008, **30**, 1084-95.

de Boer P, Crossley R and Rothfield L. The essential bacterial cell-division protein FtsZ is a GTPase. *Nature*, 1992, **359**, 254-6.

De Feijter JA, Benjamins J and Veer FA. Ellipsometry as a tool to study the adsorption behavior of synthetic and biopolymers at the air-water interface. *Biopolymers*, 1978, **17**, 1759-1772.

de Pereda JM, Leynadier D, Evangelio JA, Chacon P and Andreu JM. Tubulin secondary structure analysis, limited proteolysis sites, and homology to FtsZ. *Biochemistry*, 1996, **35**, 14203-15.

de Vries R. DNA condensation in bacteria: Interplay between macromolecular crowding and nucleoid proteins. *Biochimie*, 2010, **92**, 1715-21.

Den Blaauwen T, Andreu JM and Monasterio O. Bacterial cell division proteins as antibiotic targets. *Bioorg Chem*, 2014,

Deng NN, Yelleswarapu M, Zheng L and Huck WT. Microfluidic assembly of monodisperse vesosomes as artificial cell models. *J Am Chem Soc*, 2017, **139**, 587-590.

Dewey DC, Strulson CA, Cacace DN, Bevilacqua PC and Keating CD. Bioreactor droplets from liposome-stabilized all-aqueous emulsions. *Nat Commun*, 2014, **5**, 4670.

Dominak LM, Gundermann EL and Keating CD. Microcompartmentation in artificial cells: pH-induced conformational changes alter protein localization. *Langmuir*, 2010, **26**, 5697-705.

Du S, Park KT and Lutkenhaus J. Oligomerization of FtsZ converts the FtsZ tail motif (conserved carboxy-terminal peptide) into a multivalent ligand with high avidity for partners ZipA and SlmA. *Mol Microbiol*, 2015, **95**, 173-88.

Eisele NB, Frey S, Piehler J, Gorlich D and Richter RP. Ultrathin nucleoporin phenylalanine-glycine repeat films and their interaction with nuclear transport receptors. *EMBO Rep*, 2010, **11**, 366-72.

Elani Y, Solvas XC, Edel JB, Law RV and Ces O. Microfluidic generation of encapsulated droplet interface bilayer networks (multisomes) and their use as cell-like reactors. *Chem Commun (Camb)*, 2016, **52**, 5961-4.

Ellis RJ. Macromolecular crowding: obvious but underappreciated. *Trends Biochem Sci*, 2001, **26**, 597-604.

Erickson HP. The FtsZ protofilament and attachment of ZipA--structural constraints on the FtsZ power stroke. *Curr Opin Cell Biol*, 2001, **13**, 55-60.

Erickson HP. FtsZ, a prokaryotic homolog of tubulin? *Cell*, 1995, **80**, 367-70.

Erickson HP, Anderson DE and Osawa M. FtsZ in bacterial cytokinesis: cytoskeleton and force generator all in one. *Microbiol Mol Biol Rev*, 2010, **74**, 504-28.

Erickson HP, Taylor DW, Taylor KA and Bramhill D. Bacterial cell division protein FtsZ assembles into protofilament sheets and minirings, structural homologs of tubulin polymers. *Proc Natl Acad Sci U S A*, 1996, **93**, 519-23.

Ferreira LA, Madeira PP, Breydo L, Reichardt C, Uversky VN and Zaslavsky BY. Role of solvent properties of aqueous media in macromolecular crowding effects. *J Biomol Struct Dyn*, 2016, **34**, 92-103.

Fodeke AA and Minton AP. Quantitative characterization of polymer-polymer, protein-protein, and polymer-protein interaction via tracer sedimentation equilibrium. *J Phys Chem B*, 2010, **114**, 10876-80.

Fu G, Huang T, Buss J, Coltharp C, Hensel Z and Xiao J. *In vivo* structure of the *E. coli* FtsZ-ring revealed by photoactivated localization microscopy (PALM). *PLoS One*, 2010, **5**, e12682.

Galush WJ, Shelby SA, Mulvihill MJ, Tao A, Yang P and Groves JT. A nanocube plasmonic sensor for molecular binding on membrane surfaces. *Nano Lett*, 2009, **9**, 2077-82.

Geissler B, Elraheb D and Margolin W. A gain-of-function mutation in ftsA bypasses the requirement for the essential cell division gene zipA in *Escherichia coli. Proc Natl Acad Sci U S A*, 2003, **100**, 4197-202.

González JM, Jiménez M, Vélez M, Mingorance J, Andreu JM, Vicente M and Rivas G. Essential cell division protein FtsZ assembles into one monomer-thick ribbons under conditions resembling the crowded intracellular environment. *J Biol Chem*, 2003, **278**, 37664-71.

González JM, Vélez M, Jiménez M, Alfonso C, Schuck P, Mingorance J, Vicente M, Minton AP and Rivas G. Cooperative behavior of *Escherichia coli* cell-division protein FtsZ assembly involves the preferential cyclization of long single-stranded fibrils. *Proc Natl Acad Sci U S A*, 2005, **102**, 1895-900.

Gopalakrishnan G, Rouiller I, Colman DR and Lennox RB. Supported bilayers formed from different phospholipids on spherical silica substrates. *Langmuir*, 2009, **25**, 5455-8.

Haeusser DP and Margolin W. Splitsville: structural and functional insights into the dynamic bacterial Z ring. *Nat Rev Microbiol*, 2016, **14**, 305-19.

Hale CA and de Boer PA. Direct binding of FtsZ to ZipA, an essential component of the septal ring structure that mediates cell division in *E. coli*. *Cell*, 1997, **88**, 175-85.

Hale CA and de Boer PA. Recruitment of ZipA to the septal ring of *Escherichia coli* is dependent on FtsZ and independent of FtsA. *J Bacteriol*, 1999, **181**, 167-76.

Hauser H. Short-chain phospholipids as detergents. *Biochim Biophys Acta*, 2000, **1508**, 164-81.

Helfrich MR, El-Kouedi M, Etherton MR and Keating CD. Partitioning and assembly of metal particles and their bioconjugates in aqueous two-phase systems. *Langmuir*, 2005, **21**, 8478-86.

Hernández-Rocamora VM, García-Montañés C, Rivas G and Llorca O. Reconstitution of the *Escherichia coli* cell division ZipA-FtsZ complexes in nanodiscs as revealed by electron microscopy. *J Struct Biol*, 2012, **180**, 531-8.

Hernández-Rocamora VM, Reija B, García C, Natale P, Alfonso C, Minton AP, Zorrilla S, Rivas G and Vicente M. Dynamic interaction of the *Escherichia coli* cell division ZipA and FtsZ proteins evidenced in nanodiscs. *J Biol Chem*, 2012, **287**, 30097-104.

Herrig A, Janke M, Austermann J, Gerke V, Janshoff A and Steinem C. Cooperative adsorption of ezrin on PIP2-containing membranes. *Biochemistry*, 2006, **45**, 13025-34.

Herzfeld J. Crowding-induced organization in cells: spontaneous alignment and sorting of filaments with physiological control points. *J Mol Recognit*, 2004, **17**, 376-81.

Holthuis JC and Ungermann C. Cellular microcompartments constitute general suborganellar functional units in cells. *Biol Chem*, 2013, **394**, 151-61.

Hultgren A and Rau DC. Exclusion of alcohols from spermidine-DNA assemblies: probing the physical basis of preferential hydration. *Biochemistry*, 2004, **43**, 8272-80.

Hurley KA, Santos TM, Nepomuceno GM, Huynh V, Shaw JT and Weibel DB. Targeting the Bacterial Division Protein FtsZ. *J Med Chem*, 2016, **59**, 6975-98.

Hyman AA and Simons K. Cell biology. Beyond oil and water--phase transitions in cells. *Science*, 2012, **337**, 1047-9.

Jaffe A, Boye E and D'Ari R. Rule governing the division pattern in *Escherichia coli* minB and wild-type filaments. *J Bacteriol*, 1990, **172**, 3500-2.

Jiménez M, Martos A, Cabré EJ, Raso A and Rivas G. Giant vesicles: a powerful tool to reconstruct bacterial division assemblies in cell-like compartments. *Environ Microbiol*, 2013, **15**, 3158-68.

Jiménez M, Martos A, Vicente M and Rivas G. Reconstitution and organization of *Escherichia coli* proto-ring elements (FtsZ and FtsA) inside giant unilamellar vesicles obtained from bacterial inner membranes. *J Biol Chem*, 2011, **286**, 11236-41.

Johannsmann D, Reviakine I and Richter RP. Dissipation in films of adsorbed nanospheres studied by quartz crystal microbalance (QCM). *Anal Chem*, 2009, **81**, 8167-76.

Karamdad K, Law RV, Seddon JM, Brooks NJ and Ces O. Preparation and mechanical characterisation of giant unilamellar vesicles by a microfluidic method. *Lab Chip*, 2015, **15**, 557-562.

Keating CD. Aqueous phase separation as a possible route to compartmentalization of biological molecules. *Acc Chem Res*, 2012, **45**, 2114-24.

Koets P. Phase separation in aqueous colloidal systems. *Reports on Progress in Physics*, 1944, **10**, 129-140.

Koga S, Williams DS, Perriman AW and Mann S. Peptide-nucleotide microdroplets as a step towards a membrane-free protocell model. *Nat Chem*, 2011, **3**, 720-4.

Laurent TC and Granath KA. Fractionation of dextran and Ficoll by chromatography on Sephadex G-200. *Biochim Biophys Acta*, 1967, **136**, 191-8.

Leung AK, Lucile White E, Ross LJ, Reynolds RC, DeVito JA and Borhani DW. Structure of Mycobacterium tuberculosis FtsZ reveals unexpected, G protein-like conformational switches. *J Mol Biol*, 2004, **342**, 953-70.

Li Y, Lipowsky R and Dimova R. Membrane nanotubes induced by aqueous phase separation and stabilized by spontaneous curvature. *Proc Natl Acad Sci U S A*, 2011, **108**, 4731-6.

Li Y, Lipowsky R and Dimova R. Transition from complete to partial wetting within membrane compartments. *J Am Chem Soc*, 2008, **130**, 12252-3.

Lim YT, Lee KY, Lee K and Chung BH. Immobilization of histidine-tagged proteins by magnetic nanoparticles encapsulated with nitrilotriacetic acid (NTA)-phospholipids micelle. *Biochem Biophys Res Commun*, 2006, **344**, 926-30.

Linseisen FM, Hetzer M, Brumm T and Bayerl TM. Differences in the physical properties of lipid monolayers and bilayers on a spherical solid support. *Biophys J*, 1997, **72**, 1659-67.

Liu Y, Lipowsky R and Dimova R. Concentration dependence of the interfacial tension for aqueous two-phase polymer solutions of dextran and polyethylene glycol. *Langmuir*, 2012, **28**, 3831-9.

Long MS, Cans AS and Keating CD. Budding and asymmetric protein microcompartmentation in giant vesicles containing two aqueous phases. *J Am Chem Soc*, 2008, **130**, 756-62.

Long MS, Jones CD, Helfrich MR, Mangeney-Slavin LK and Keating CD. Dynamic microcompartmentation in synthetic cells. *Proc Natl Acad Sci U S A*, 2005, **102**, 5920-5.

Loose M and Mitchison TJ. The bacterial cell division proteins FtsA and FtsZ self-organize into dynamic cytoskeletal patterns. *Nat Cell Biol*, 2014, **16**, 38-46.

Loose M and Schwille P. Biomimetic membrane systems to study cellular organization. *J Struct Biol*, 2009, **168**, 143-51.

López-Montero I, López-Navajas P, Mingorance J, Vélez M, Vicente M and Monroy F. Membrane reconstitution of FtsZ-ZipA complex inside giant spherical vesicles made of *E. coli* lipids: large membrane dilation and analysis of membrane plasticity. *Biochim Biophys Acta*, 2013, **1828**, 687-98.

Lowe J. Crystal structure determination of FtsZ from *Methanococcus jannaschii. J Struct Biol*, 1998, **124**, 235-43.

Lowe J and Amos LA. Crystal structure of the bacterial cell-division protein FtsZ. *Nature*, 1998, **391**, 203-6.

Lowe J and Amos LA. Erratum to: Prokaryotic cytoskeletons : Filamentous protein polymers active in the cytoplasm of bacterial and archaeal cells. *Subcell Biochem*, 2017, **84**, E1.

Lowe J and Amos LA. Helical tubes of FtsZ from *Methanococcus jannaschii*. *Biol Chem*, 2000, **381**, 993-9.

Lu C and Erickson HP. Purification and assembly of FtsZ. *Methods Enzymol*, 1998, **298**, 305-13.

Lutkenhaus J. The regulation of bacterial cell division: a time and place for it. *Curr Opin Microbiol*, 1998, **1**, 210-5.

Madeira PP, Reis CA, Rodrigues AE, Mikheeva LM, Chait A and Zaslavsky BY. Solvent properties governing protein partitioning in polymer/polymer aqueous two-phase systems. *J Chromatogr A*, 2011, **1218**, 1379-84.

Madeira PP, Teixeira JA, Macedo EA, Mikheeva LM and Zaslavsky BY. "On the Collander equation": protein partitioning in polymer/polymer aqueous two-phase systems. *J Chromatogr A*, 2008, **1190**, 39-43.

Mannik J and Bailey MW. Spatial coordination between chromosomes and cell division proteins in *Escherichia coli*. *Front Microbiol*, 2015, **6**, 306.

Margolin W. Bacterial division: another way to box in the ring. *Curr Biol*, 2006, **16**, R881-4.

Martos A, Alfonso C, López-Navajas P, Ahijado-Guzmán R, Mingorance J, Minton AP and Rivas G. Characterization of self-association and heteroassociation of bacterial cell division proteins FtsZ and ZipA in solution by composition gradient-static light scattering. *Biochemistry*, 2010, **49**, 10780-7.

Martos A, Jiménez M, Rivas G and Schwille P. Towards a bottom-up reconstitution of bacterial cell division. *Trends Cell Biol*, 2012, **22**, 634-43.

Martos A, Monterroso B, Zorrilla S, Reija B, Alfonso C, Mingorance J, Rivas G and Jiménez M. Isolation, characterization and lipid-binding properties of the recalcitrant FtsA division protein from *Escherichia coli*. *PLoS One*, 2012, **7**, e39829.

Martos A, Raso A, Jiménez M, Petrasek Z, Rivas G and Schwille P. FtsZ polymers tethered to the membrane by ZipA are susceptible to spatial regulation by Min waves. *Biophys J*, 2015, **108**, 2371-83.

Mateos-Gil P, Marquez I, Lopez-Navajas P, Jimenez M, Vicente M, Mingorance J, Rivas G and Velez M. FtsZ polymers bound to lipid bilayers through ZipA form dynamic two dimensional networks. *Biochim Biophys Acta*, 2012, **1818**, 806-13.

Mateos-Gil P, Márquez I, López-Navajas P, Jiménez M, Vicente M, Mingorance J, Rivas G and Vélez M. FtsZ polymers bound to lipid bilayers through ZipA form dynamic two dimensional networks. *Biochim Biophys Acta*, 2012, **1818**, 806-13.

Mateos-Gil P, Páez A, Horger I, Rivas G, Vicente M, Tarazona P and Vélez M. Depolymerization dynamics of individual filaments of bacterial cytoskeletal protein FtsZ. *Proc Natl Acad Sci U S A*, 2012, **109**, 8133-8.

Matosevic S and Paegel BM. Stepwise synthesis of giant unilamellar vesicles on a microfluidic assembly line. *J Am Chem Soc*, 2011, **133**, 2798-800.

Mellouli S, Monterroso B, Vutukuri HR, te Brinke E, Chokkalingam V, Rivas G and Huck WTS. Self-organization of the bacterial cell-division protein FtsZ in confined environments. *Soft Matter*, 2013, **9**, 10493-10500.

Mingorance J, Rivas G, Vélez M, Gómez-Puertas P and Vicente M. Strong FtsZ is with the force: mechanisms to constrict bacteria. *Trends Microbiol*, 2010, **18**, 348-56.

Mingorance J, Tadros M, Vicente M, González JM, Rivas G and Vélez M. Visualization of single *Escherichia coli* FtsZ filament dynamics with atomic force microscopy. *J Biol Chem*, 2005, **280**, 20909-14.

Minton AP. Adsorption of globular proteins on locally planar surfaces. II. Models for the effect of multiple adsorbate conformations on adsorption equilibria and kinetics. *Biophys J*, 1999, **76**, 176-87.

Minton AP. Implications of macromolecular crowding for protein assembly. *Curr Opin Struct Biol*, 2000, **10**, 34-9.

Minton AP. The influence of macromolecular crowding and macromolecular confinement on biochemical reactions in physiological media. *J Biol Chem*, 2001, **276**, 10577-80.

Monterroso B, Ahijado-Guzmán R, Reija B, Alfonso C, Zorrilla S, Minton AP and Rivas G. $Mg^{(2+)}$-linked self-assembly of FtsZ in the presence of GTP or a GTP analogue involves the concerted formation of a narrow size distribution of oligomeric species. *Biochemistry*, 2012, **51**, 4541-50.

Monterroso B, Reija B, Jiménez M, Zorrilla S and Rivas G. Charged molecules modulate the volume exclusion effects exerted by crowders on FtsZ polymerization. *PLoS One*, 2016, **11**, e0149060.

Monterroso B, Rivas G and Minton AP. An equilibrium model for the Mg(2+)-linked self-assembly of FtsZ in the presence of GTP or a GTP analogue. *Biochemistry*, 2012, **51**, 6108-13.

Mosyak L, Zhang Y, Glasfeld E, Haney S, Stahl M, Seehra J and Somers WS. The bacterial cell-division protein ZipA and its interaction with an FtsZ fragment revealed by X-ray crystallography. *EMBO J*, 2000, **19**, 3179-91.

Mukherjee A, Dai K and Lutkenhaus J. *Escherichia coli* cell division protein FtsZ is a guanine nucleotide binding protein. *Proc Natl Acad Sci U S A*, 1993, **90**, 1053-7.

Mukherjee A and Lutkenhaus J. Dynamic assembly of FtsZ regulated by GTP hydrolysis. *EMBO J*, 1998, **17**, 462-9.

Nath A, Atkins WM and Sligar SG. Applications of phospholipid bilayer nanodiscs in the study of membranes and membrane proteins. *Biochemistry*, 2007, **46**, 2059-69.

Nguyen BT, Nicolai T and Benyahia L. Stabilization of water-in-water emulsions by addition of protein particles. *Langmuir*, 2013, **29**, 10658-64.

Nollert P, Kiefer H and Jahnig F. Lipid vesicle adsorption versus formation of planar bilayers on solid surfaces. *Biophys J*, 1995, **69**, 1447-55.

Ohashi T, Hale CA, de Boer PA and Erickson HP. Structural evidence that the P/Q domain of ZipA is an unstructured, flexible tether between the membrane and the C-terminal FtsZ-binding domain. *J Bacteriol*, 2002, **184**, 4313-5.

Oliva MA, Cordell SC and Lowe J. Structural insights into FtsZ protofilament formation. *Nat Struct Mol Biol*, 2004, **11**, 1243-50.

Oliva MA, Huecas S, Palacios JM, Martín-Benito J, Valpuesta JM and Andreu JM. Assembly of archaeal cell division protein FtsZ and a GTPase-inactive mutant into double-stranded filaments. *J Biol Chem*, 2003, **278**, 33562-70.

Ortiz C, Kureisaite-Ciziene D, Schmitz F, McLaughlin SH, Vicente M and Lowe J. Crystal structure of the Z-ring associated cell division protein ZapC from *Escherichia coli*. *FEBS Lett*, 2015, **589**, 3822-8.

Ortiz C, Natale P, Cueto L and Vicente M. The keepers of the ring: regulators of FtsZ assembly. *FEMS Microbiol Rev*, 2016, **40**, 57-67.

Osawa M, Anderson DE and Erickson HP. Reconstitution of contractile FtsZ rings in liposomes. *Science*, 2008, **320**, 792-4.

Osawa M and Erickson HP. Inside-out Z rings--constriction with and without GTP hydrolysis. *Mol Microbiol*, 2011, **81**, 571-9.

Parsons JB, Frank S, Bhella D, Liang M, Prentice MB, Mulvihill DP and Warren MJ. Synthesis of empty bacterial microcompartments, directed organelle protein incorporation, and evidence of filament-associated organelle movement. *Mol Cell*, 2010, **38**, 305-15.

Pautot S, Frisken BJ and Weitz DA. Production of unilamellar vesicles using an inverted emulsion. *Langmuir*, 2003, **19**, 2870-2879.

Pazos M, Natale P and Vicente M. A specific role for the ZipA protein in cell division: stabilization of the FtsZ protein. *J Biol Chem*, 2013, **288**, 3219-26.

Pelletier J, Halvorsen K, Ha BY, Paparcone R, Sandler SJ, Woldringh CL, Wong WP and Jun S. Physical manipulation of the *Escherichia coli* chromosome reveals its soft nature. *Proc Natl Acad Sci U S A*, 2012, **109**, E2649-56.

Pichoff S and Lutkenhaus J. Tethering the Z ring to the membrane through a conserved membrane targeting sequence in FtsA. *Mol Microbiol*, 2005, **55**, 1722-34.

Pichoff S and Lutkenhaus J. Unique and overlapping roles for ZipA and FtsA in septal ring assembly in *Escherichia coli*. *EMBO J*, 2002, **21**, 685-93.

Pichoff S, Shen B, Sullivan B and Lutkenhaus J. FtsA mutants impaired for self-interaction bypass ZipA suggesting a model in which FtsA's self-interaction competes with its ability to recruit downstream division proteins. *Mol Microbiol*, 2012, **83**, 151-67.

Pla J, Sánchez M, Palacios P, Vicente M and Aldea M. Preferential cytoplasmic location of FtsZ, a protein essential for *Escherichia coli* septation. *Mol Microbiol*, 1991, **5**, 1681-6.

Popp D, Iwasa M, Narita A, Erickson HP and Maeda Y. FtsZ condensates: an *in vitro* electron microscopy study. *Biopolymers*, 2009, **91**, 340-50.

Ramírez D, García-Soriano DA, Raso A, Feingold M, Rivas G and Schwille P. Chiral vortex dynamics on membranes is an intrinsic property of FtsZ, driven by GTP hydrolysis. *bioRxiv*, 2016.

Reija B, Monterroso B, Jiménez M, Vicente M, Rivas G and Zorrilla S. Development of a homogeneous fluorescence anisotropy assay to monitor and measure FtsZ assembly in solution. *Anal Biochem*, 2011, **418**, 89-96.

Reviakine I, Johannsmann D and Richter RP. Hearing what you cannot see and visualizing what you hear: interpreting quartz crystal microbalance data from solvated interfaces. *Anal Chem*, 2011, **83**, 8838-48.

Rico AI, Krupka M and Vicente M. In the beginning, *Escherichia coli* assembled the proto-ring: an initial phase of division. *J Biol Chem*, 2013, **288**, 20830-6.

Richter RP, Berat R and Brisson AR. Formation of solid-supported lipid bilayers: an integrated view. *Langmuir*, 2006, **22**, 3497-505.

Rivas G, Alfonso C, Jiménez M, Monterroso B and Zorrilla S. Macromolecular interactions of the bacterial division FtsZ protein: from quantitative biochemistry and crowding to reconstructing minimal divisomes in the test tube. *Biophys Rev*, 2013, **5**, 63-77.

Rivas G, Fernández JA and Minton AP. Direct observation of the enhancement of noncooperative protein self-assembly by macromolecular crowding: indefinite linear self-association of bacterial cell division protein FtsZ. *Proc Natl Acad Sci U S A*, 2001, **98**, 3150-5.

Rivas G, López A, Mingorance J, Ferrandiz MJ, Zorrilla S, Minton AP, Vicente M and Andreu JM. Magnesium-induced linear self-association of the FtsZ bacterial cell division protein monomer. The primary steps for FtsZ assembly. *J Biol Chem*, 2000, **275**, 11740-9.

Rivas G and Minton AP. Macromolecular crowding *in vitro*, *in vivo*, and in between. *Trends Biochem Sci*, 2016, **41**, 970-981.

Rivas G, Vogel SK and Schwille P. Reconstitution of cytoskeletal protein assemblies for large-scale membrane transformation. *Curr Opin Chem Biol*, 2014, **22**, 18-26.

Romberg L and Levin PA. Assembly dynamics of the bacterial cell division protein FtsZ: poised at the edge of stability. *Annu Rev Microbiol*, 2003, **57**, 125-54.

Rowlett VW and Margolin W. 3D-SIM super-resolution of FtsZ and its membrane tethers in *Escherichia coli* cells. *Biophys J*, 2014, **107**, L17-20.

Rueda S, Vicente M and Mingorance J. Concentration and assembly of the division ring proteins FtsZ, FtsA, and ZipA during the *Escherichia coli* cell cycle. *J Bacteriol*, 2003, **185**, 3344-51.

Salvarelli E, Krupka M, Rivas G, Vicente M and Mingorance J. Independence between GTPase active sites in the *Escherichia coli* cell division protein FtsZ. *FEBS Lett*, 2011, **585**, 3880-3.

Saroff HA. Evaluation of uncertainties for parameters in binding studies: the sum-of-squares profile and Monte Carlo estimation. *Anal Biochem*, 1989, **176**, 161-9.

Scheffers DJ, de Wit JG, den Blaauwen T and Driessen AJ. GTP hydrolysis of cell division protein FtsZ: evidence that the active site is formed by the association of monomers. *Biochemistry*, 2002, **41**, 521-9.

Sezgin E and Schwille P. Model membrane platforms to study protein-membrane interactions. *Mol Membr Biol*, 2012, **29**, 144-54.

Skoog K and Daley DO. The *Escherichia coli* cell division protein ZipA forms homodimers prior to association with FtsZ. *Biochemistry*, 2012, **51**, 1407-15.

Small E and Addinall SG. Dynamic FtsZ polymerization is sensitive to the GTP to GDP ratio and can be maintained at steady state using a GTP-regeneration system. *Microbiology*, 2003, **149**, 2235-42.

Sokolova E, Spruijt E, Hansen MM, Dubuc E, Groen J, Chokkalingam V, Piruska A, Heus HA and Huck WT. Enhanced transcription rates in membrane-free protocells formed by coacervation of cell lysate. *Proc Natl Acad Sci U S A*, 2013, **110**, 11692-7.

Stanley C and Rau DC. Preferential hydration of DNA: the magnitude and distance dependence of alcohol and polyol interactions. *Biophys J*, 2006, **91**, 912-20.

Stricker J, Maddox P, Salmon ED and Erickson HP. Rapid assembly dynamics of the *Escherichia coli* FtsZ-ring demonstrated by fluorescence recovery after photobleaching. *Proc Natl Acad Sci U S A*, 2002, **99**, 3171-5.

Strulson CA, Molden RC, Keating CD and Bevilacqua PC. RNA catalysis through compartmentalization. *Nat Chem*, 2012, **4**, 941-6.

Torre P, Keating CD and Mansy SS. Multiphase water-in-oil emulsion droplets for cell-free transcription-translation. *Langmuir*, 2014, **30**, 5695-9.

Tsuda K, Furuta N, Inaba H, Kawai S, Hanada K, Yoshimori T and Amano A. Functional analysis of alpha5beta1 integrin and lipid rafts in invasion of epithelial cells

by Porphyromonas gingivalis using fluorescent beads coated with bacterial membrane vesicles. *Cell Struct Funct*, 2008, **33**, 123-32.

Vendeville A, Lariviere D and Fourmentin E. An inventory of the bacterial macromolecular components and their spatial organization. *FEMS Microbiol Rev*, 2011, **35**, 395-414.

Vicente M and Rico AI. The order of the ring: assembly of *Escherichia coli* cell division components. *Mol Microbiol*, 2006, **61**, 5-8.

Vogel SK and Schwille P. Minimal systems to study membrane-cytoskeleton interactions. *Curr Opin Biotechnol*, 2012, **23**, 758-65.

Walde P, Cosentino K, Engel H and Stano P. Giant vesicles: preparations and applications. *Chembiochem*, 2010, **11**, 848-65.

Walter H and Brooks DE. Phase separation in cytoplasm, due to macromolecular crowding, is the basis for microcompartmentation. *FEBS Lett*, 1995, **361**, 135-9.

Wang JD and Levin PA. Metabolism, cell growth and the bacterial cell cycle. *Nat Rev Microbiol*, 2009, **7**, 822-7.

Wirth AJ and Gruebele M. Quinary protein structure and the consequences of crowding in living cells: leaving the test-tube behind. *Bioessays*, 2013, **35**, 984-93.

Woldringh CL, Mulder E, Huls PG and Vischer N. Toporegulation of bacterial division according to the nucleoid occlusion model. *Res Microbiol*, 1991, **142**, 309-20.

Yanagisawa M, Nigorikawa S, Sakaue T, Fujiwara K and Tokita M. Multiple patterns of polymer gels in microspheres due to the interplay among phase separation, wetting, and gelation. *Proc Natl Acad Sci U S A*, 2014, **111**, 15894-9.

Yeates TO, Kerfeld CA, Heinhorst S, Cannon GC and Shively JM. Protein-based organelles in bacteria: carboxysomes and related microcompartments. *Nat Rev Microbiol*, 2008, **6**, 681-91.

Yu XC and Margolin W. Ca2+-mediated GTP-dependent dynamic assembly of bacterial cell division protein FtsZ into asters and polymer networks in vitro. *EMBO J*, 1997, **16**, 5455-63.

Yuan H, Ma, Q., Song, Y., Tang, M.Y.H., Chan, Y.K. & Shum, H.C. Phase-separation-induced formation of janus droplets based on aqueous two-phase systems. *Macromol. Chem. Phys.*, 2017, **218**,

Zaslavsky B. Aqueous two phase partitioning: physical chemistry and bioanalytical applications. 1994,

Zaslavsky BY, Miheeva LM, Mestechkina NM, Pogorelov VM and Rogozhin SV. General rule of partition behaviour of cells and soluble substances in aqueous two-phase polymeric systems. *FEBS Lett*, 1978, **94**, 77-80.

Zhou HX. Effect of mixed macromolecular crowding agents on protein folding. *Proteins*, 2008, **72**, 1109-13.